UNIVERSITY OF OKLAHOMA

GRADUATE COLLEGE

FISCHER-TROPSCH SYNTHESIS ON HYDROPHOBIC CATALYSTS IN BIPHASIC MEDIA

A DISSERTATION

SUBMITTED TO THE GRADUATE FACULTY

in partial fulfillment of the requirements for the

Degree of

DOCTOR OF PHILOSOPHY

By

JUAN FELIPE ANAYA SALTARIN
Norman, Oklahoma
2018

FISCHER-TROPSCH SYNTHESIS ON HYDROPHOBIC CATALYSTS IN BIPHASIC MEDIA

A DISSERTATION APPROVED FOR THE
SCHOOL OF CHEMICAL, BIOLOGICAL AND MATERIALS ENGINEERING

BY

Dr. Daniel E. Resasco, Chair

Dr. Lance L. Lobban

Dr. Steven P. Crossley

Dr. Bin Wang

Dr. David Sabatini

To my wife Kayleigh and to my son.

Acknowledgements

First, I thank God Almighty from whom all things flow, including this dissertation. Thanks to my wife Kayleigh for her unconditional support and love, especially through the writing stages of this dissertation.

I would like to thank my advisor Dr. Daniel Resasco for the immense opportunity of working under his guidance, for his support and trust, as he challenged me during the last several years to work hard, think critically, learn fundamentals well, and be a leader. Thank you for believing in me and for inspiring me to be a better person, researcher, and Chemical Engineer.

I would like to thank Dr. Steven Crossley, Dr. Bin Wang, and Dr. Lance Lobban for serving on my PhD committee, for their input, comments, questions, and challenges, and for their support throughout the development of this dissertation work. Thanks to Dr. Robert Thomson for serving as my outside committee member throughout the majority of my PhD and thanks to Dr. David Sabatini for stepping in as my outside committee member for my dissertation defense.

Special thanks to Daniela Santos and Nabi Rahman for their invaluable help with experimental work included in this dissertation, especially in chapters 3 and 4. Thanks to Lawrence Barrett for his assistance with TGA analysis, to Brent Johnson from the OSU Microscopy Laboratory and Greg Strout from the Sam Noble microscopy lab for their assistance with transmission electron microscopy imaging, and thanks to Valeria Herrera for her assistance with ethylene hydrogenation experiments. Thanks also to Alan Miles and his assistants at the shop for all their help for most of my dissertation work and Dennis McAlister in most recent years after Alan's retirement. Their

mechanical and electrical expertise proved extremely useful numerous times in allowing the research to continue with the least amount of interruptions.

A big, heartful thank you to all CBME staff that have provided all the administrative support to allow us graduate students to focus on our classes and research work, especially Donna King, Vernita Farrow, Terri Colliver, Madena McGinnis, Wanda Gress, Ginger Murray, Melyssa Smith. Their diligence in assisting us with necessary paperwork requirements, travel arrangements, payroll, ordering research supplies, etc. was only matched by their kindness and patience. Simply, this dissertation work could not have happened without them.

Special thanks to all my friends and lab mates who accompanied me at some point during my time as graduate student, especially Miguel, Lei, Taiwo, Gap, Nhung, Tuong, Reda, Lawrence, Rajiv, Alejandra, Santiago, Valeria, Tania, Daniela, Nabi, Danny, Zheng, Abhishek, Nick, Monica, Qiaohua, Lu, and everyone else in the biofuels research group. Their friendship and company made graduate school a much more rewarding experience even during challenging times. Thanks also to my friends and FOCUS teammates Louis, Rae, and Nicole; their love, support, and patience in the last few months of dissertation writing have truly been a blessing from God.

Thanks to the US Department of Energy for providing funding sources for this research and thanks to all scholarship donors for the scholarships I received during my studies.

Last but not least, I would like to thank my father Carlos, my mother Ana Maria, my brother Carlos, and my sister Anita. Despite the distance, they have remained so close to me in my heart and in my thoughts and encouraged me to continue growing and working towards the completion of this PhD.

Table of Contents

List of Tables

List of Figures

Abstract

Fischer-Tropsch (FT) synthesis stands out as a relevant alternative technology for the production of liquid fuels. Natural gas, coal, biomass and other carbon-containing raw materials can be converted to syngas (CO and H_2), that in turn is fed to Fischer-Tropsch reactors, to produce a wide range of hydrocarbon products. Various reactor systems have been developed and tested successfully for their utilization in Fischer-Tropsch synthesis. High-temperature reactors are typically designed to obtain high concentrations of branched hydrocarbons and alcohols while low-temperature reactors primarily produce high concentrations of linear alkanes and alkenes. Low-temperature reactors, typically slurry bubble column or multi-tubular, have shown great promise for further developments in industrial applications due to advantages such as efficient heat transfer, uniform temperatures, reduced diffusion limitations, high catalyst productivity, ease of catalyst regeneration, and low costs. At conditions of low temperature, FT products are present in the liquid phase. Therefore, it is of interest to investigate the effects of liquid media on the activity and selectivity of these FT reactors. Fischer-Tropsch in biphasic media benefits from the present of liquid water that enhances FT rates and the organic phase that solubilizes hydrocarbon products facilitating product separation. Moreover, effects of organic phases on FT rates have not been discussed extensively. From the findings of the present dissertation, it is apparent that catalyst hydrophobicity plays a crucial role in bringing about the positive effects of organic solvents on FT in single organic and biphasic aqueous/organic systems which may explain why the positive effects by organic solvents have not been discussed significantly in the literature before. Moreover, a systematic study of catalyst

hydrophobicity on FT rates and selectivity reveals that a minimum degree of surface hydrophobicity is required to enable the positive effects of organic solvents in FT rates. The combined effect of the aqueous and organic solvents on highly hydrophobic catalysts results in unprecedented FT rates and selectivities compared to aqueous or biphasic FT results reported before.

In Chapter 1, the fundamentals of Fischer-Tropsch synthesis are presented as way of introduction. In Chapter 2, the effect of biphasic media on the rate of Fischer-Tropsch is studied on Ru catalysts supported on carbon nanotubes. As expected, FT rates were significantly higher in pure water compared to pure decalin solvents. Interestingly, rates were yet higher in biphasic decalin/water when hydrophobic particles were used. A cooperative effect of decalin and water at the decalin/water interface is observed when hydrophobic catalysts are used. In Chapter 3, a systematic study of the effect of hydrophobicity on the activity and selectivity of Fischer-Tropsch in emulsions was carried out. Ru supported on SiO_2 catalysts with varying hydrophobicity were prepared by surface functionalization with organosilanes of different hydrocarbon chain lengths. Highly hydrophobic Ru/SiO_2 catalysts led to high FT rates without significant changes in selectivity. Finally, in Chapter 4, a preliminary study of the effect of Ru metal particle size on biphasic Fischer-Tropsch using hydrophobic catalysts is presented. In Chapter 2 through 4, the effect of organic and aqueous solvents on FT activity and selectivity, in the presence catalysts of varying hydrophobicity, is discussed in light of mechanistic insights recently discussed in the literature.

Chapter 1: Introduction

1.1. The Fischer-Tropsch Synthesis

1.1.1. Fundamentals

Fischer-Tropsch (FT) synthesis is the reaction of carbon monoxide (CO) and hydrogen (H_2) at high pressures and temperatures in the presence of Fe, Co, or Ru to produce mainly straight-chain aliphatic hydrocarbons, water and carbon dioxide[1]. Depending on reaction conditions and catalyst, other products like alcohols or branched hydrocarbons may also form. FT is highly exothermic [2–4] and requires temperatures between 200 – 350 °C and pressures of 10-60 bar [2] to achieve relevant rates of reaction, even in the presence of catalysts. Equation (1) and (2) show the general FT reactions that produce alkanes and alkenes, respectively.

$$nCO + (2n + 1)H_2 \longrightarrow C_nH_{(2n+2)} + nH_2O \quad (1)$$

$$nCO + 2nH_2 \longrightarrow C_nH_{2n} + nH_2O \quad (2)$$

The main reaction that produces alkanes (Equation 1) has a heat of reaction of -150 kJ/mol [2–4]. Some undesirable side reactions include the formation of alcohols (equation 3), water/gas shift (Equation 4) and the Boudouard reaction (Equation 5)

$$nCO + 2nH_2 \longrightarrow C_nH_{2n+1}OH + (n-1)H_2O \quad (3)$$

$$CO + H_2O \longrightarrow CO_2 + H_2 \quad (4)$$

$$CO + CO \longrightarrow C + CO_2 \quad (5)$$

Commercially FT is carried out by two alternative types of processes: high-temperature processes, where the products are in the gas phase, and low-temperature processes, where some products are also in the liquid phase and three phases are present at reaction

conditions (Gas-liquid-solid) [5]. Multi-tubular and slurry bubble columns are the typical industrial reactors used for low-temperature processes. Current multiphase reactor technologies show important advantages, namely, good heat transfer, high catalyst efficiency, convenience for catalyst reloading/regeneration, and low costs [6,7]. Therefore, they are also considered promising for further development of FT technologies[2]. Thus it is of practical interest to investigate the properties of liquid reaction media that can further improve the performance of FT reactors.

Among the group VIII transition metals that catalyze FT mentioned above (Fe, Co, Ru), iron shows a high selectivity to alcohols and branched hydrocarbons and it requires elevated temperatures to achieve significant rates. Therefore, this catalyst is used preferentially in high-temperature technologies. Promoters like alkali or Cu are added to improve the activity [8,9]. Fe is susceptible to oxidation by water [10], and catalyst life is short compared to the other metals. Cobalt, on the other hand, shows higher resistance to oxidation by water and has the advantage of producing high yields and higher selectivity to high-molecular weight, straight-chain, hydrocarbons [11,12]. Thus, it is a desirable catalyst in low-temperature technologies. Ruthenium metal is known to be the most active catalyst for FT [9]. It shows the highest selectivity to higher-molecular-weight hydrocarbons, the lowest deactivation rate, and the lowest susceptibility to oxidation by water [13]. Therefore, it is a great catalyst to study the fundamentals of FT without the effects of side reactions and significant catalyst deactivation.

Rates of CO consumption over FT catalysts decrease strongly with decreasing dispersion at particle sizes lower than 10 nm [14–16]. Various explanations have been

given for the structure sensitivity of FT. Van Santen's research group in the Netherlands proposes that special low coordination sites, located in the "open corners" of larger metal clusters, are responsible for the activity on these catalysts [17–19]. Conversely, Iglesia's group at UC Berkeley argue that, in agreement with trends of decreasing rates with smaller particle size, the active sites for FT are highly coordinated surfaces prevalent on larger metal clusters [20–22]. The nature of the presumed active site determines also the mechanism that operates during FT. It is generally agreed that FT in high-coordination planes follows H-assisted CO dissociation paths, whereas in low coordination sites unassisted CO dissociation is the preferred path [17,18,20,22].

1.1.2. Mechanism

Fischer-Tropsch is a polymerization-type reaction in which CO-derived monomers react on the surface of a catalyst to form higher-molecular-weight hydrocarbons [23]. It is generally accepted that Fischer-Tropsch polymerization reaction proceeds via an initiation step, followed by chain propagation, and ends with chain termination [24,25]. Much progress has been made to understand how each of these steps occurs, and both theoretical and experimental studies have provided support for different mechanisms proposed. However, the exact nature of the elementary steps and their active sites are still a matter of debate [20,26]. Next we give a brief summary of the most relevant FT mechanisms presented in the literature in recent years.

Two main types of mechanisms are discussed in the recent FT literature for activation of CO on metal surfaces (Initiation): the carbide or direct CO dissociation mechanisms, and the H-assisted CO dissociation mechanisms. The first carbide-type mechanism was proposed by Fischer and Tropsch in their original publication [27] as they suggested

that the first step of FT is the dissociation of CO and subsequent hydrogenation of adsorbed carbon (C*) to form CH_x that initiates a chain. Later on, Storch, Golumbic, and Anderson proposed that chains were initiated by hydrogenation of the CO to form oxygen-containing intermediates on the surface (HCOH*) [28]. Many other proposals have been made since and they can be grouped within the two types of mechanisms [20]: those involving direct CO dissociation [29–35] and those that involve hydrogenation of adsorbed CO before C-O bond cleavage [35–38].

Recent work from Enrique Iglesia's research group at the University of California, Berkeley suggests that H-assisted CO dissociation on highly coordinated metal planes, prevalent on large metal clusters, is the kinetically-dominant path at conditions relevant for industrial FT [20–22,39]. Meanwhile, work from Rutger Van Santen's research group in the Netherlands agrees that H-assisted paths dominate on highly coordinated sites. However, they suggest that direct CO dissociation on low-coordination sites (Step-edge sites) is the dominant path during practical FT [17–19,26]. These step-edge sites, the group suggests, are not stable on smaller particles but are stable in "open corners" in larger particles [40].

The second step in FT involves the formation of C-C bonds during chain-growth (propagation). This step can occur via CO insertion or CH_2 insertion. In CO insertion, carbon monoxide reacts with the growing alkyl chain on the surface to form a C-C bond followed by C-O bond breaking and hydrogenation to form a C_xH_y species that can repeat the cycle and react with a new CO molecule [24,39]. The CHx insertion mechanism involves the dissociation and hydrogenation of CO, by the same mechanism as the initiation step, to form surface CHx species that act as monomers in chain growth

[41]. CHx insertion is the most accepted mechanism for chain-growth because there is significant evidence to support it. However, CO insertion cannot be ruled out [24]. Finally, the third step in FT is chain termination. The mechanism of chain termination determines the nature of the FT products. It is generally accepted that a chain can be terminated via hydrogen addition to form alkanes, hydrogen abstraction to form olefins, or CO insertion to form oxygenated species [24].

1.1.3. Product distribution

Since Fischer-Tropsch synthesis is a surface polymerization reaction [23], product distribution can be predicted using polymerization kinetics. Anderson [23] was the first to apply this concept to Fischer-Tropsch and, in 1951, developed an equation that predicts the distribution of products as a function of a parameter known as the chain-growth probability (α). The chain-growth probability is the probability of adding one additional monomer to the growing chain instead of desorbing the hydrocarbon molecule from the surface. The equation assumes that the chain-growth probability is constant and independent of the size of the molecule on the surface. Flory [42] and Schulz [43] independently developed the same equation 15 years before Anderson. However, it was done as a general equation to predict the selectivity of polymerization reactions and not specifically for FT. In 1976, Olive [44] applied for the first time the Schulz-Flory equation to FT, and, after this, the equation came to be known as the Anderson-Schulz-Flory equation (ASF). The ASF equation that describes the weight fraction distribution of hydrocarbon products as a function of the chain-growth probability is given by

$$W_n = n\alpha^{n-1}(1-\alpha)^2 \qquad (6)$$

where n is the number of carbons in the molecule, W_n is the weight fraction of the hydrocarbon with n carbons, and α is the chain-growth probability as defined above. Figure 1 shows the weight fraction of hydrocarbons as a function of carbon number for α = 0.8 and Figure 2 shows the expected hydrocarbon distribution as a function of α. As expected, the higher "α", the higher the selectivity to higher-molecular-weight hydrocarbons (Figure 2). A common strategy in commercial gas-to-liquids technologies is to design reactors to give products with high "α" to produce high content of waxes and then feed the product to a hydrocracking unit to convert them to desired carbon ranges. In practice, real distributions deviate from the ideal ASF equation. Typically, methane weight fractions are much greater than expected, and ethane/ethylene selectivities are much smaller than predicted [2].

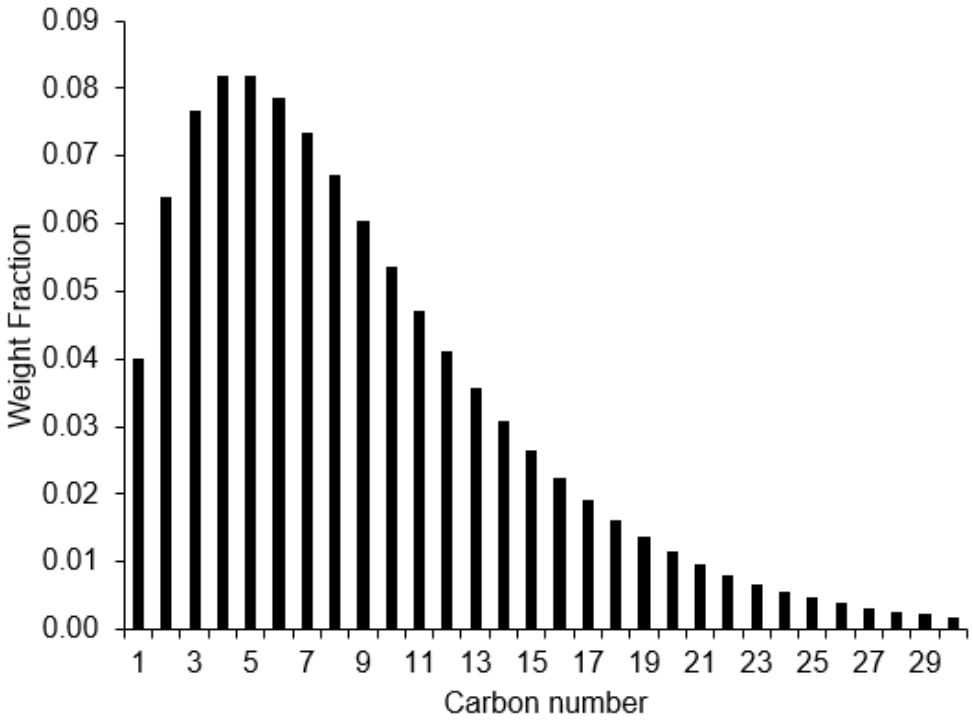

Figure 1. Theoretical Anderson-Schulz-Flory (ASF) distribution for chain-growth probability (α) of 0.8.

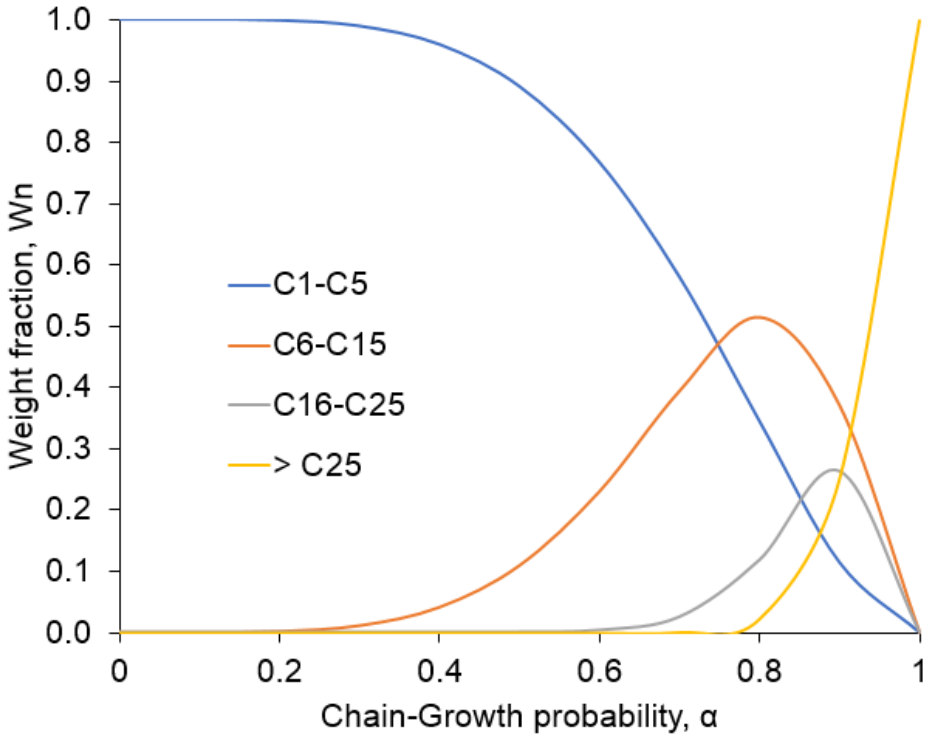

Figure 2. Theoretical Anderson-Schulz-Flory distribution as a function of chain-growth probability (α).

1.1.4. The effect of water

Depending on the catalyst properties, water may increase [39,45–47], decrease [24,48], or not affect [10,49] the activity of FT. Water can enhance intrinsic reaction rates [39] and can also deactivate catalysts by modifying metal surfaces [48]. Thus, observed water effects depend on the balance of several contributions. For example, iron catalysts are readily oxidized by water, and, therefore, the impact of water on activity is negative [24]. The influence of water on Co-based catalysts depends on metal loading, support identity and preparation method [46,50], leading to more complex water effects. For example, in a study using Co supported on Al_2O_3, low H_2O partial pressures increased CO consumption rates, but high ratios of H_2O/H_2 inhibited rates, presumably, by

increasing O* coverages on the surface [48]. Inhibition on ruthenium metal requires higher H_2O/H_2 ratio than cobalt, making Ru stable even in liquid phase water during FT [51]. Thus, the positive effects of water on FT can be easily observed and studied on Ru catalysts.

It was proposed that water can enhance the rate of CO consumption on high-coordination metal surfaces during vapor phase FT, especially on Ru and Co, by enhancing the rate of H-assisted CO dissociation via H_2O-mediated H-transport [39]. Therefore, water molecules near surfaces decrease the activation energy to form *HCOH* surface intermediates by mediating the addition of H* to adsorbed CO molecules [39]. To the best of our knowledge, a parallel path for the enhancement of FT rates by H_2O on low-coordination metal sites has not been proposed. During liquid-phase FT in a batch reactor, co-feeding water increased CO turnover rates on Ru catalysts [52]. In batch reactors, adding small volumes of water increases water partial pressures in the gas phase until the saturation pressure is reached. Thus, when partial pressures increased, water chemical potential also increased which enhanced CO consumption rates in agreement with results previously observed in the vapor phase [39]. Adding water beyond the saturation pressure will form a liquid phase without further increasing the water chemical potential. Nevertheless, adding increasing volumes of liquid water further improved FT activity and selectivity consistent with more pronounced H-shuttling effects in the much-less-restricted liquid water phase [52,53].

Chapter 2: Enhanced Rates of Fischer-Tropsch Synthesis by the Combined Effect of Aqueous and Organic Solvents in Biphasic Media

Abstract

Biphasic decalin/water solvent media led to higher Fischer-Tropsch (FT) rates than pure decalin or pure water during liquid-phase experiments on Ru supported on multiwall carbon nanotubes. Ru supported on multiwall carbon nanotubes of varying wettability were prepared, characterized, and tested in liquid phase Fischer-Tropsch (FT) in a batch reactor (H_2:CO = 4:1, 220 °C, 55 Bar). Both the aqueous and organic phases improved FT rates while water also improved selectivity to long-chain hydrocarbons in single and biphasic media. FT rate enhancements by the organic solvent were more substantial on catalysts with higher oil wettability and at higher oil/water ratios. This suggests that the interaction of catalyst surfaces with organic solvents at decalin/water interfaces plays a key role in enabling higher rates. These important results show that catalysts with high oil-wettability bring about the positive effects of organic solvents. Therefore, highly hydrophobic catalysts in biphasic media are a promising system for obtaining high FT turnover rates. Finally, the positive effect of biphasic decalin/water solvents on activity and selectivity is discussed in light of mechanistic insights recently proposed in the literature.

2.1. Introduction

Fischer-Tropsch synthesis (FT) is a family of reactions that convert synthesis gas mixtures (CO and H_2) to hydrocarbons on Fe, Co, and Ru catalysts [27]. Commercial low-temperature Fischer-Tropsch synthesis is carried out in multiphase reactors containing liquid organic solvents [54]. Water, a primary product of the reaction, is

always present in the reactor [27]. Recent studies have shown that water/oil emulsions stabilized by catalyst nanohybrids significantly enhance the FT activity and selectivity to long-chain hydrocarbons compared to pure organic solvents [52,53]. The emulsion phase also showed improved catalyst stability compared to pure water solvent; this was ascribed to the presence of the organic phase that facilitates the removal of hydrocarbon products that otherwise would be trapped on the surface of the catalyst when surrounded only by a water phase due to the low solubility of the hydrocarbon chains in water.

In FT, hydrocarbon chains are initiated by CO activation on metal surface sites. These chains propagate by rapid incorporation of CO-derived monomers and terminate by hydrogen addition or abstraction to form alkanes or alkenes, respectively [50,55,56]. Oxygenates may also form by termination of chains with CO followed by hydrogenation [50,55,56]. On Ru catalysts, vapor H_2O enhances CO-consumption turnover rates, improves C5+ selectivity, and decreases methane selectivity [52,53]. For example, Claeys and Van Steen [47] used a Ru catalyst to study the effect of water on FT in a slurry reactor and found that CO conversion increased with increasing water partial pressures. The promotion of FT by H_2O may be a result of enhanced transport of H_2 and CO within pores containing H_2O-rich liquids which would otherwise be mass-transport-limited [50]. However, water effects on Ru catalysts have been observed even under conditions of strict kinetic control suggesting that an intrinsic kinetic effect must be present [39].

Computational and kinetic studies have shown that CO dissociation via H-assisted paths has lower energy barriers than direct C-O bond cleavage on high-coordination metal

surfaces on Co and Ru catalysts [20]. Therefore, it was proposed that water further decreases the barrier of the kinetically-relevant CO dissociation steps by acting as a H-shuttle. In this mechanism, water picks up H from the surface forming a short-lived $H_3O^{\delta+}$ that transfers the H to CO* and forms CH*O* and CH*OH* before C-O bond cleavage [39]. CH*OH dissociation forms CH* and OH*; OH* results in H_2O co-products while CH* hydrogenates to form CH_x species that react with CO-derived monomers to form C-C bonds during chain-propagation. Finally, chains are terminated by desorption as alkane, alkene, or oxygenate in a series of quasi-equilibrated steps that do not contribute to the overall rate of CO consumption [20].

Recent studies have revealed that FT in liquid water shows higher CO rates compared to vapor water at the same water chemical potential [52,53]. Increasing volumes of liquid water in a batch reactor continually increased the rate of CO consumption and decreased the selectivity to CH_4 even though the chemical potential of the water was unchanged. These results indicate that water acts as a more effective H-shuttle in the less-restricted liquid phase because of greater mobility, larger number of degrees of freedom, and greater connectivity of the H_2O molecules in the H-bonded liquid phase network that make H-shuttling more effective by a mechanism that resembles the Grotthuss mechanism [52]. Alternatively, the effect of water on FT rates on low-coordination metal sites has not been discussed.

Here we show that Fischer-Tropsch in biphasic decalin/water on Ru-doped multiwall carbon nanotubes results in higher CO turnover rates compared to Fischer-Tropsch in pure decalin (water-free) or pure water solvent. Moreover, varying the wettability of the carbon nanotubes influences the interaction of catalyst surfaces with the aqueous and

organic phases at decalin/water interfaces which had a direct effect on catalyst performance. The catalytic trends observed are discussed in light of CO dissociation and chain growth mechanisms recently proposed in the literature.

2.2. Experimental

2.2.1. Catalyst preparation and Characterization

Purified pristine multiwall carbon nanotubes (SMW200), kindly provided by Southwest Nanotechnologies (SWeNT), were used as received and labeled "CNT". SMW200 nanotubes have reported outer diameters of 10 ± 1 nm, inner diameters of 4.5 ± 0.5 nm, and lengths of 3 - 6 μm per the manufacturer. Surface oxidized carbon nanotubes, labeled "CNT-Ox", were prepared by treating 5 g of CNT with a mixture of Nitric Acid 70% (75 ml) and sulfuric acid 98% (40 ml) in a reflux system at 80 °C for 12 hours. After acid treatment, the carbon nanotubes were filtered in vacuum using a 0.2 μm PTFE filter and thoroughly rinsed with 18 MΩ water to remove residual nitric and sulfuric acids until neutral pH was achieved. 18 MΩ water was obtained from an in-house filtration system.

Ruthenium supported on multiwall carbon nanotubes (CNT and CNT-Ox) was prepared by Incipient Wetness Impregnation (IWI). Ruthenium (III) Nitrosyl Nitrate solution (SIGMA-ALDRICH) was used as Ruthenium precursor for metal deposition. In a typical preparation procedure 5 g of multiwall carbon nanotubes (CNT or CNT-O) were added to a mortar and the appropriate volume of Ruthenium Nitrosyl Nitrate solution was added dropwise. Next, the catalyst was dried, first at room temperature for 6 hours, then at 80 ºC for 12 hours in a vacuum oven. Following preparation, the catalyst was treated in flowing hydrogen to eliminate nitrosyl nitrate ions and reduce ruthenium

cations to their metal form. The temperature was first increased at 2 ºC/min from room temperature to 120 °C and held for 1 hour, then ramped at 2 ºC/min to the final 400 ºC and held for 3 hours before cooling down to room temperature.

Hydrophilic groups on the surface of CNT and CNT-Ox were estimated by temperature programmed desorption (TPD) and thermogravimetric analysis (TGA). For TPD experiments, 50 mg of CNT or CNT-O were placed in a quartz micro-reactor under flowing N_2. The temperature was ramped at 10 °C/min from room temperature to 800 °C and held at 800 °C for 30 min. The carbon desorbed as CO_2 was converted to methane in a methanation reactor with a nickel catalyst at 400 °C. The signal was recorded by an FID detector, and the amount of carbon desorbed was quantified by calibrating the area under the curve with a known amount of carbon. TGA was evaluated using a Netzsch STA-449 F1 Jupiter. In a typical experiment, CNT or CNT-Ox (30mg) was placed in a crucible with a constant flow of Ar (40 ml/min). The cell was preheated to 50°C, then increased to 800°C with a ramping rate of 3°C/min. The desorbed carbon-containing gases (CO, CO_2) were analyzed with an on-line mass chromatograph Aeolos QMS 403C.

Pickering emulsions stabilized by CNT and CNT-Ox were prepared to evaluate the hydrophilicity of the carbon nanotubes. The total volume of solvents was 25 ml for all the emulsions prepared. For the preparation, 5 mg of carbon nanotubes were added to the appropriate volume of decalin (5-20 ml) and dispersed by horn sonication (1/4-inch tip) at 50% amplitude for 1 hour with a Fischer-Scientific Model 505C Sonic dismembrator. Then, the appropriate volume of 18 MΩ water (5-20 ml) was added and the emulsion formed by horn sonication (1/4-inch tip) at 50% amplitude for 1 hour.

Emulsion type was determined 24 h after emulsion preparation by taking droplets of the emulsion and adding it to pure decalin and pure water. If the continuous phase of the emulsion was decalin, droplets dispersed readily in decalin; however, when added to water the drop stayed together and sunk to the bottom of the beaker. Similarly, if the continuous phase of the emulsion was water, droplets dispersed readily in water; however, in decalin the emulsion droplet was preserved and sunk visibly to the bottom of the beaker.

Ruthenium weight percent on Ru/CNT and Ru/CNT-Ox catalysts was confirmed by Inductively Coupled Plasma (Galbraith laboratories). Surface area was determined by N_2 physisorption using a micromeritics ASAP 2000 unit. Prior to analysis, the samples were degassed in situ at 180°C for 6 h. Transmission electron microscopy (TEM) images were obtained on a JEOL 2100 field emission system operated at 200 kV. For sample preparation, the catalyst was pre-reduced at 400 ºC in flowing H_2 for 3 hours, then a few milligrams of the solid were dispersed in 2-propanol and sonicated at 40% amplitude for 30 minutes by horn sonicator (Fischer Scientific Model 505C) before deposition onto a lacey carbon coated copper grid. Average particle size and particle size distribution were estimated from TEM by measuring the particle diameter of over 100 particles.

Exposed Ru surface area was probed using the structure-insensitive ethylene hydrogenation reaction at low temperature (40 °C, 1 atm) in a flow reactor. In a typical experiment, the catalyst sample was reduced in H_2 flow (100 ml/min) at 400 °C for 3 h and then cooled down to 40 °C before introduction of the ethylene and hydrogen feed

gases at a molar ratio of 1:50. An online gas chromatograph system equipped with a Poraplot U column (27.5 m, 250 μm) was used for product analysis.

2.2.2. Catalytic activity measurements

The FT reaction was carried out in a 300-mL stainless steel Parr autoclave reactor, operating in batch mode. The temperature inside the reactor was controlled with a CAL 9500P controller (CAL Controls Ltd.). The pressure was monitored with an Ashcroft 2074 digital industrial pressure gauge. In a typical run, 50 mg of catalyst sample were added to the reactor vessel and dispersed in 40 ml of decalin (mix. cis + trans, anhydrous ≥99.9%, Sigma-Aldrich) by horn sonicator (50% amp, 1 h). Then, 40 ml of deionized water (18 MΩ) were added and the mixture emulsified by horn sonicator (50% amp, 1 h). The reactor was sealed, purged, and pressurized with H_2 to 500 psi for a reduction period at 250 °C for 1 h, while stirring at 300 rpm. After the reduction, the reactor was cooled down to room temperature, purged, and pressurized with H_2/CO (ratio 4/1) to 800 psi for reaction. After equilibration of the pressure reading, the reactor was heated to 220 °C and held for the desired reaction time while stirring at 300 rpm. The zero reaction time was taken as the moment when the specified reaction temperature was reached.

At the end of the reaction period the reactor was quickly cooled down to room temperature and a high-pressure gas sample was taken before depressurizing. The compositions of H_2, CO and CO_2 in the gas phase were analyzed by gas chromatography-thermal conductivity detector (GC-TCD, Carle 400 AGC). Light hydrocarbon (C1-C7) gas-phase products were analyzed by gas chromatography-mass spectrometry (GC-MS, Agilent 7820A, MS 5975 Series MSD) equipped with a

capillary, bonded polystyrene-divinylbenzene (DVB) column (HP-PLOT/Q) of 30 m x 0.320 mm x 20.0 μm. The liquid-phase products were separated from the solid catalyst by centrifugation followed by filtration with a 0.22 μm PTFE filter forming two immiscible layers of clear liquid. These two phases were analyzed separately by gas chromatography (GC-FID and GC-MS). An Agilent GC-FID 7890B equipped with a capillary, low-polarity column (Phenomenex ZB-5) of 60.0 m x 0.25 mm x 0.25 μm was used for product quantification, while a Shimadzu QP2010 GC–MS equipped with a mid-polarity (Phenomenex ZB-1701) capillary column, 60.0 m x 0.25 mm x 0.25 μm nominal, was used for product identification. The reaction results were analyzed by calculating turnover frequency (TOF) based on CO consumption, and yields and selectivity based on moles of C, as given by the following expressions,

$$TOF\ (h^{-1}) = \frac{mol\ CO\ reacted}{mol\ Ru\ exposed \cdot h}$$

$$\%\ Yield = \frac{Total\ mol\ C\ in\ product}{mol\ of\ C\ in\ CO\ (initial)}\ x\ 100$$

$$\%\ Selectivity = \frac{mol\ of\ C\ in\ product}{Total\ mol\ of\ C\ in\ all\ products} \times 100$$

2.3. Results

2.3.1. Catalyst characterization

Pristine multiwall carbon nanotubes (MWNT) are intrinsically hydrophobic, and oxidization with strong acids is a common method to increase their hydrophilicity by creating surface hydrophilic groups such as carboxylic acids and alcohols [57–61]. It has been shown that unmodified MWNT are capable of stabilizing oil-in-water

Pickering emulsions due to their hydrophobic nature [60,61]; after treatment with acids, the increased hydrophilicity modifies the wettability of the carbon nanotubes and allows catastrophic emulsion inversion at low oil/water ratios [60,61]. In this study, two samples of Ru-doped multiwall carbon nanotubes with different wettability were prepared. The more hydrophobic sample was the untreated, as-received, pristine multiwall carbon nanotubes acquired commercially (CNT), and the more hydrophilic sample (CNT-Ox) was prepared by treating the pristine multiwall carbon nanotubes in a mixture of nitric and sulfuric acid.

The content of hydrophilic groups on the surface of CNT and CNT-Ox was determined using TPD methods. Figure 3 shows temperature programmed desorption (TPD) profiles for pristine (CNT) and acid-treated (CNT-Ox) multiwall carbon nanotubes in N_2 flow. Integration of the area under the curve of the TPD profiles shows a lower content of hydrophilic groups in CNT (2.1%) compared to CNT-Ox (5.1%). Thermogravimetric Analysis (TGA) profiles under flowing argon were also measured (Figure 4). The CNT-Ox TGA profile shows greater unstable carbon content (~9%) compared to the TPD experiments, while CNT shows similar carbon content (~1.8%) to the TPD. Both the TPD and the TGA results are consistent with CNT-Ox having greater content of defective carbon. Thus, CNT-Ox is expected to be more hydrophilic than CNT [60,61].

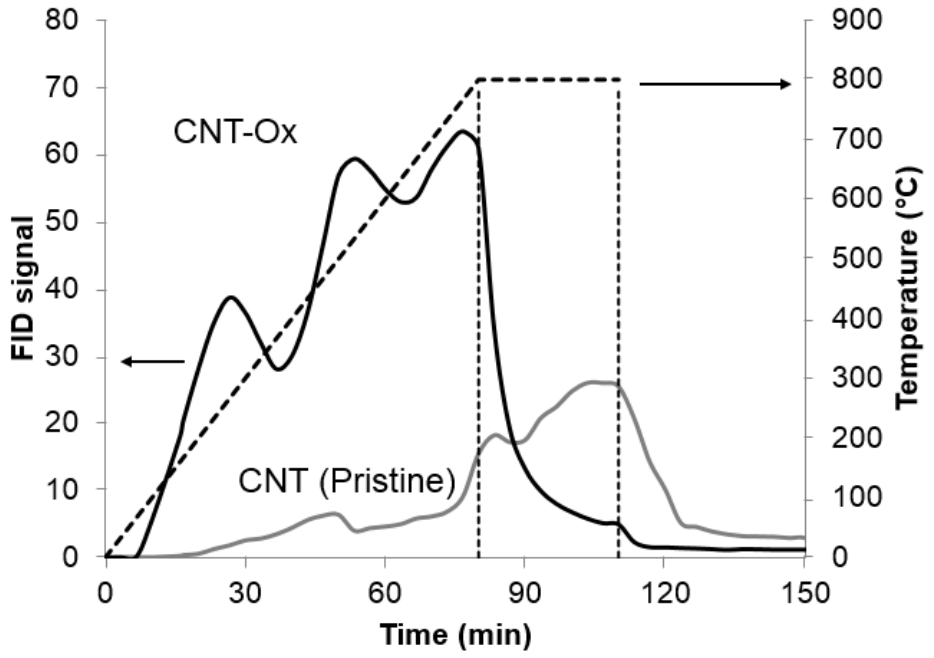

Figure 3. Temperature programmed desorption (TPD) profile as a function of time for pristine carbon nanotubes (Gray) and surface oxidized carbon nanotubes (Black) under N_2 flow. (N_2 flow 50 cm^3/min, heating rate 10 °C/min to 800 °C, hold at 800 °C for 0.5 h)

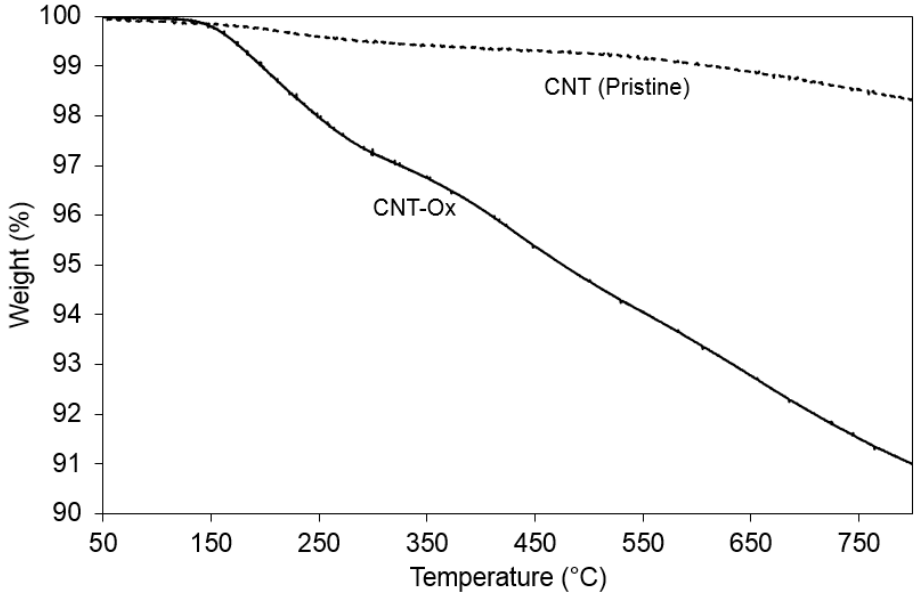

Figure 4. TGA-TPD profiles for pristine carbon nanotubes (dashed) and surface oxidized carbon nanotubes (solid) under Ar flow (heating rate 3 °C/min to 1000 °C).

Further evidence of different wettability of the modified and unmodified carbon nanotubes was found from the type of Pickering emulsions stabilized with varying water/oil ratios [61]. Table 1 shows the types of emulsion stabilized by CNT and CNT-Ox as a function of the ratio of organic (decalin) to aqueous phase. Hydrophobic CNTs formed water-in-oil (W/O) emulsions regardless of the ratio of aqueous and organic phase, while the less hydrophobic CNT-Ox formed W/O emulsions at high ratios of decalin/water but at ratios of 1/1 and lower, oil-in-water (O/W) emulsions were formed. These results are consistent with increased water wettability of CNT-Ox that favors emulsion inversion at lower decalin/water ratios than CNT [61].

Table 1. Emulsion type as a function of Decalin/Water ratio for pristine carbon nanotubes (CNT) and surface oxidized carbon nanotubes (CNT-Ox).

O:W† Ratio	Sample	
	CNT	CNT-Ox
7:1	W/O‡	W/O
3:1	W/O	W/O
1:1	W/O	O/W*
1:3	W/O	O/W

† Oil/water ratio
‡ Water-in-oil emulsion
* Oil-in-water emulsion

Table 2 shows a summary of average particle size, dispersion, and ruthenium weight percent for Ru/CNT and Ru/CNT-Ox. Average particle size and dispersion were determined from TEM images (Figure 5) and from ethylene hydrogenation experiments (Appendix A). Ru metal average particle sizes for Ru/CNT estimated from TEM (2.8 nm) and ethylene hydrogenation (2.84 nm) were essentially the same while Ru metal

average particle size for Ru/CNT-Ox estimated from ethylene hydrogenation (2.98 nm) was higher than from TEM (2.3 nm). Transmission Electron Microscopy imaging captures a very small area of the catalyst sample while ethylene hydrogenation probes the entire surface of the sample catalyst sample (20 mg). Therefore, ethylene hydrogenation may be a more suitable method to characterize the active surface area of the catalyst. Reaction turnover frequencies reported hereafter are based on the average particle size and dispersion estimated from ethylene hydrogenation experiments.

Table 2. Summary of Ru metal loading, average metal particle size, and metal dispersion for Ru/CNT and Ru/CNT-Ox.

Catalyst	% Ru by ICP	TEM		Ethylene Hydrogenation	
		Particle Size (nm)	Dispersion	Particle Size (nm)	Dispersion
Ru/CNT-Ox	8.66	2.3 +/- 0.5	0.62	2.98	0.48
Ru/CNT	9.03	2.8 +/- 1.0	0.51	2.84	0.50

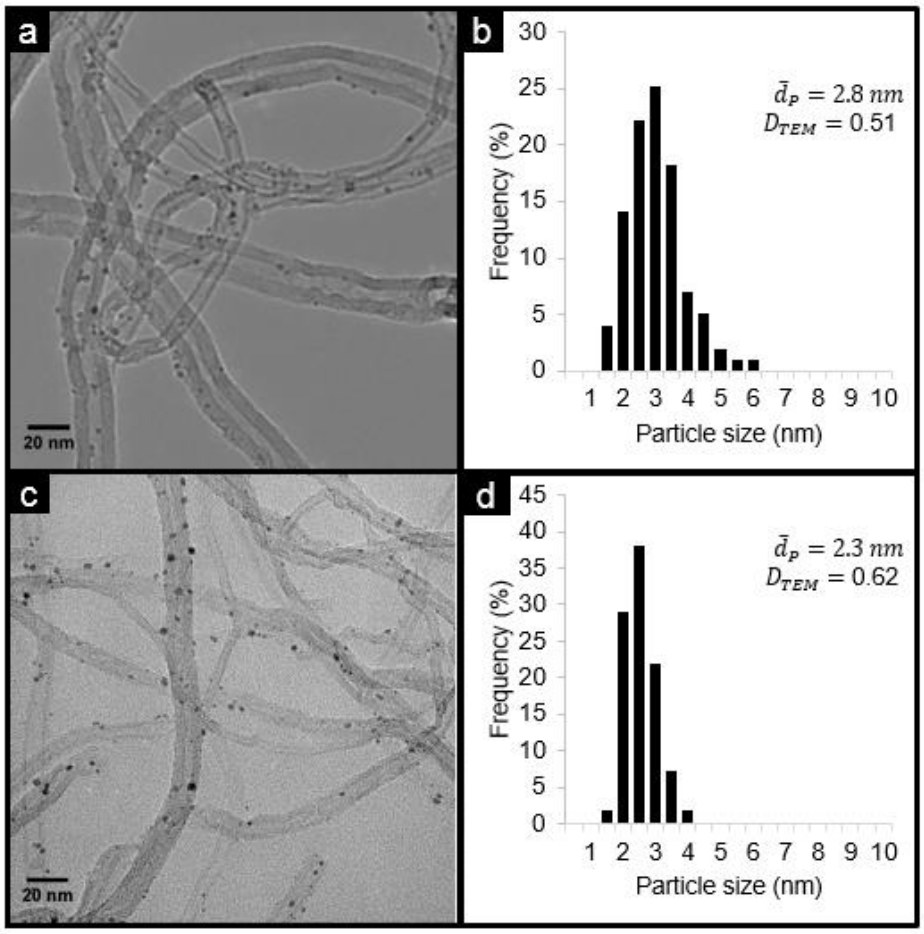

Figure 5. TEM images of Ru/CNT (a) and Ru/CNT-Ox (c) and their respective particle size distribution histograms, Ru/CNT (b) and Ru/CNT-O (d).

Table 3 shows N_2 physisorption results before and after depositing Ru metal on the surface of CNT. The BET surface area for CNT (274.3 m^2/g) was close to typical values reported by the manufacturer (280- 350 m^2/g) and remained essentially unchanged (275.4 m^2/g) after depositing Ru on the surface. BET surface area for CNT-Ox (284.3 m^2/g) was slightly higher than CNT. Slight increase in surface area after acid treatment of pristine carbon nanotubes has been observed before [61] and is generally attributed to improved accessibility to the inner surface area of nanotubes by breaking of the

nanotubes into shorter lengths and by removing catalyst particles left from carbon nanotube synthesis [61].

Table 3. BET surface area and pore volume of pristine (CNT) and oxidized (CNT-Ox) multiwall carbon nanotubes before and after Ru loading.

	BET Surface Area, m^2/g		BJH Pore Volume cm^3/g		BET Pore diameter Å	
Sample	Bare	Ru/	Bare	Ru/	Bare	Ru/
CNT	274	275	1.5	1.3	131	151
CNT-Ox	284	NA	1.4	NA	131	NA

2.3.2. FT activity in single phase and biphasic liquid mixtures

Figure 6a and b compare Fischer-Tropsch (FT) activity and selectivity on Ru/CNT catalyst varying the solvent media at constant reaction conditions. Pure water, pure decalin, and biphasic decalin/water (7% water) were used as solvents in separate experiments and tested under practical low-T FT reaction conditions. The catalytic activity was recorded as the hydrocarbon yield as a function of time (Figure 6a), and selectivity to hydrocarbons is presented as a function of hydrocarbon yield (Figure 6b). Experiments in pure decalin solvent showed the poorest results. Hydrocarbon yield was lowest at all reaction times studied. Selectivity to long-chain hydrocarbons (C6+) was significantly lower while selectivity to undesirable CH_4 was significantly higher. Reactions in pure water solvent showed higher yields to hydrocarbons and higher selectivity to desired long-chain hydrocarbon (C6+) products. For example, at 3 hours of reaction the hydrocarbon yield was ~22% in pure decalin and ~57% in pure water, and at 20% hydrocarbon yield the selectivity to C6+ was ~75% in pure water and ~52% in pure decalin.

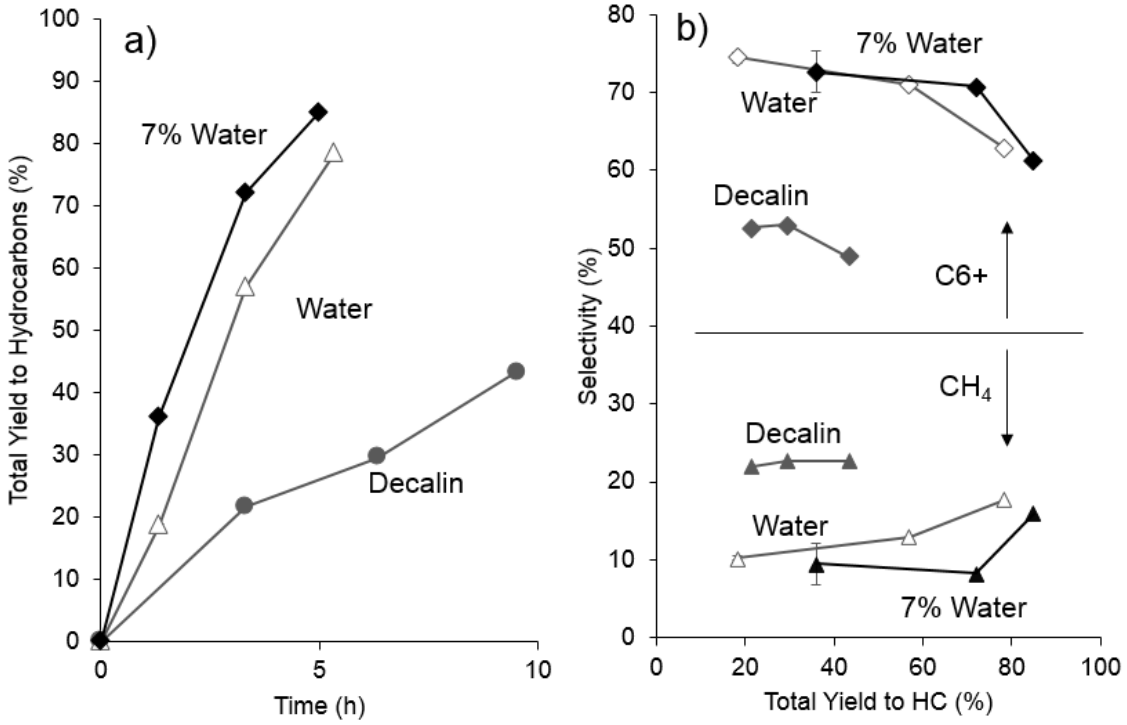

Figure 6. a) FT hydrocarbon total yield as a function of time for Ru /CNT in decalin/water (7% H_2O) (◆), pure water (△), pure decalin (●). b) Selectivity to CH_4 (Triangles) and C6+ (Diamonds) in pure decalin (▲,◆), pure water (△,◇), and decalin/water (7% H_2O) (▲,◆), as a function of hydrocarbon total yield. Reaction conditions: 220 C, 800 psi H_2/CO (4/1), 300rpm, 100mg of catalyst.

Interestingly, experiments in biphasic decalin/water (7% water) showed the best catalytic performance (Figure 6a and b). Hydrocarbon yield was highest at all reaction times with high selectivity to long-chain hydrocarbons (C6+) and low selectivity to undesirable CH_4. Water clearly had a positive effect on Fischer-Tropsch as evidenced by higher rates observed in pure water compared to pure decalin. On the other hand, positive effects on activity by decalin were not apparent from pure decalin experiments since there is not a point of comparison for activity in the absence of decalin. However, biphasic decalin/water results suggest that both the water and decalin may have positive effects on rates when they are present together during Fischer-Tropsch reactions since water/decalin experiments showed higher activity than pure water.

2.3.3. FT on catalysts of different hydrophobicity

Figure 7a and b compare FT activity and selectivity on Ru supported on carbon nanotubes of different hydrophobicity in biphasic decalin/water (7% Water). Hydrocarbon yield as a function of time (Figure 7a) was higher for Ru/CNT than Ru/CNT-Ox at all reaction times while product selectivity was similar for both catalysts at all conversions studied (Figure 7b). Further, the activity of Ru/CNT and Ru/CNT-Ox was tested in pure water, pure decalin and biphasic decalin/water (7% water), and the initial turnover frequencies (TOF) were measured (Figure 8). For Ru/CNT-Ox, initial TOFs were lowest for decalin (~51 h^{-1}), increased almost 10 times in pure water (~427 h^{-1}), and remained approximately constant in biphasic decalin/water (~417 h^{-1}). Ru/CNT showed a significant increase in TOF from pure decalin (~139 h^{-1}) to pure water (~335 h^{-1}) similar to Ru/CNT-Ox, but, most interestingly, Ru/CNT in biphasic water/decalin showed the highest rate enhancement (~607 h^{-1}). Based on these results, high catalyst hydrophobicity seems to be required to observe rate enhancements in biphasic decalin/water. If the catalysts were not hydrophobic enough, rates in biphasic decalin/water would be similar to rates in pure water as was the case for Ru/CNT-Ox.

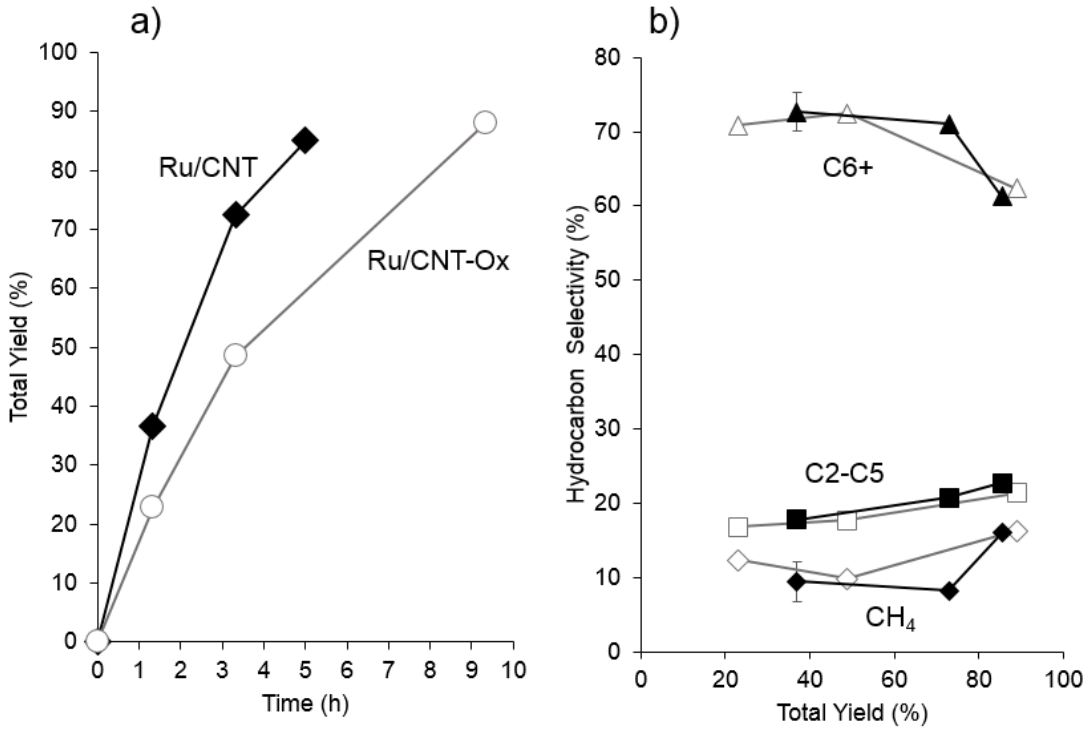

Figure 7. FT in biphasic water/decalin (7% H2O) in a batch reactor. a) FT hydrocarbon total yield as a function of time for Ru/CNT (◆) and Ru/CNT-Ox (○). b) Selectivity to CH_4 (◆, ◇), C2-C5 (■, □), and C6+ (▲, △) as a function of hydrocarbon total yield for Ru/CNT (Full) and Ru/CNT-Ox (Open). Reaction conditions: 220 C, 800 psi H_2/CO (4/1), 300rpm, 100mg of catalyst.

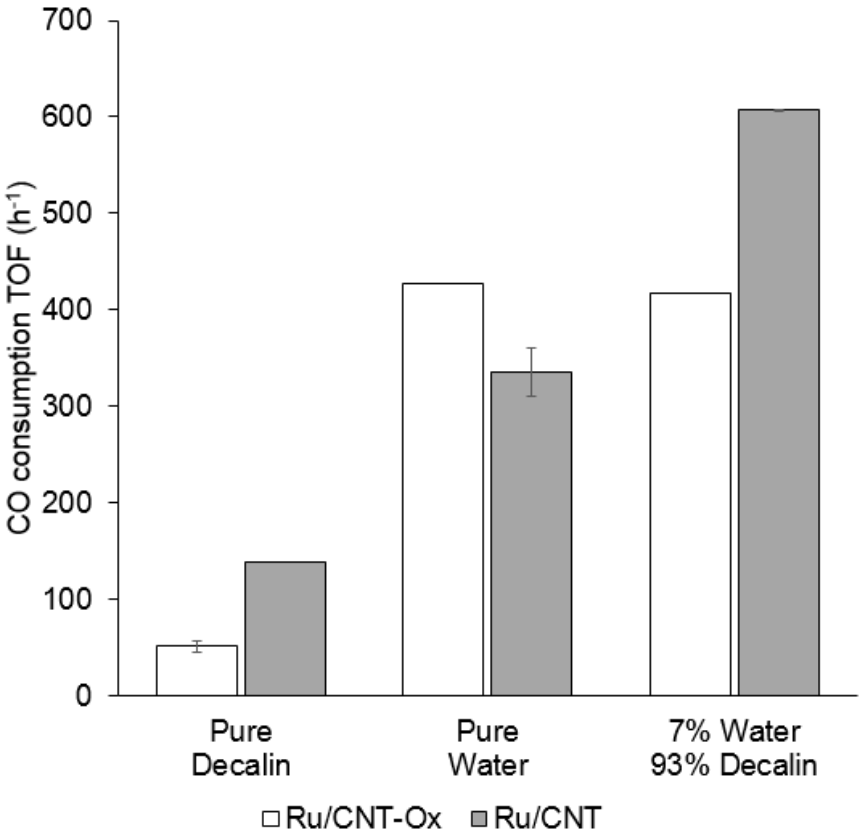

Figure 8. Initial FT CO consumption turnover rates for Ru/CNT and Ru/CNT-Ox in a batch reactor in pure decalin, pure water, and biphasic decalin/water (7% water). Reaction conditions: 220 C, 800 psi H2/CO (4/1), 300rpm.

Figure 9 shows hydrocarbon selectivity for reactions on Ru/CNT and Ru/CNT-Ox in different solvents at relatively low conversions (~20%). For both Ru/CNT and Ru/CNT-Ox, the selectivity to C6+ increased while the selectivity to C2-C5 and CH_4 decreased whenever water was present in the system compared to the water-free case. Also, the selectivity to hydrocarbons was very similar for pure water and biphasic decalin/water regardless of the catalyst used. Thus, while the rate of reaction was significantly higher on Ru/CNT in biphasic decalin/water (Figure 8), the product selectivity did not change significantly. While water enhances both the rates and selectivity of Fischer-Tropsch,

decalin seems to have a positive effect on rates only, without significant change in product selectivity.

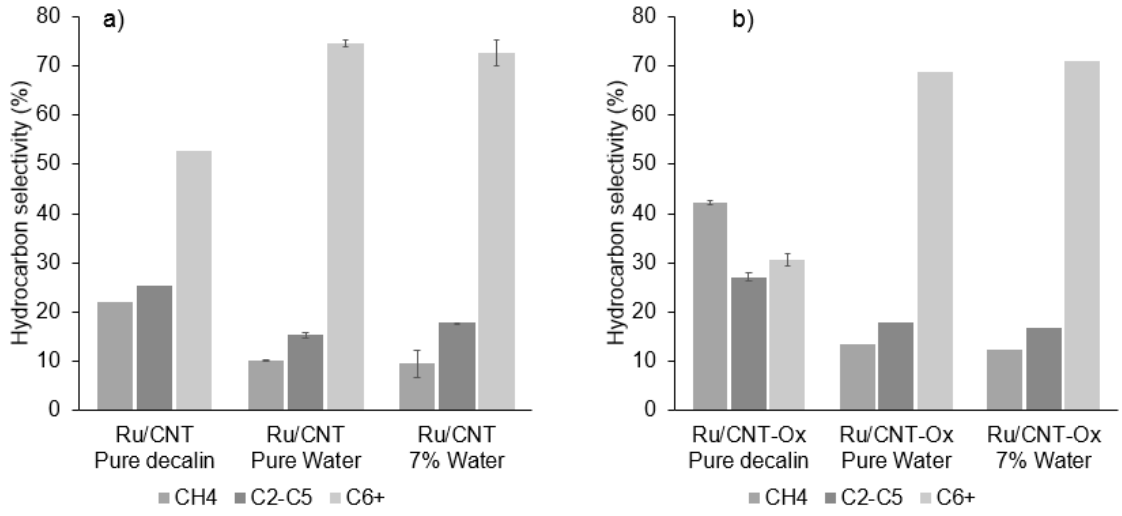

Figure 9. Hydrocarbon selectivity in pure decalin, pure water, and biphasic decalin/water (7% water, 93% Decalin) on a) Ru/CNT and b) Ru/CNT-Ox. Conditions: 220 C, 800 psi H_2/CO (4/1), 300rpm, Conversion ~20%.

2.3.4. FT activity and selectivity as a function of water volume % in emulsions

The effect of water volume percent on FT activity and selectivity was studied by varying the oil water ratio. Figure 10 shows initial CO consumption TOF as a function of water volume percent in biphasic decalin/water. The dotted line at 2.9% volume outlines the minimum amount of water required to form a liquid phase in the batch reactor at the present reaction conditions. Below 2.9% water volume, there are not enough water molecules to saturate the gas phase at the reaction temperature (220 °C), therefore, all the water will be present in the vapor phase and no liquid water will form. At 2.9% water volume, the amount of water present will be just enough to saturate the gas phase at 220 °C. Any water present beyond 2.9% volume will be in liquid state, and,

since the gas phase is already saturated with water, the water partial pressure in the gas phase will not increase any further.

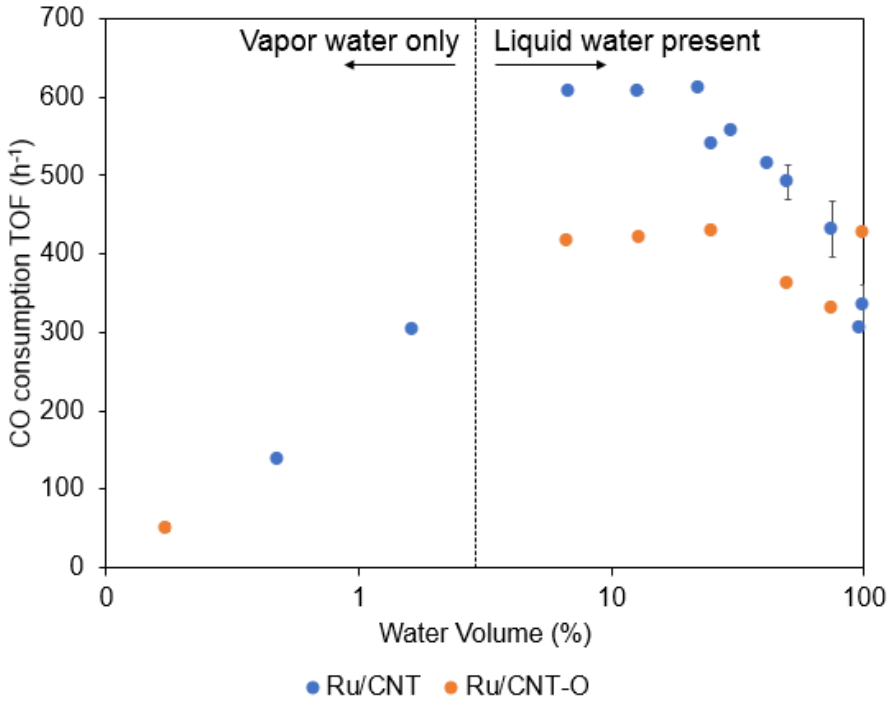

Figure 10. Rates of CO consumption for Ru/CNT and Ru/CNT-O as a function of H_2O volume (220 C, 800 psi H_2/CO (4/1), 300rpm, conversion ~20%)

Below the saturation line, increasing the initial volume of water increases the partial pressure in the gas phase and therefore its chemical potential. As a result, turnover rates doubled for Ru/CNT when water volume percent was increased from 0.5% to 1.6% (Figure 10). Increasing the amount of water beyond saturation further increased the turnover rate to a maximum value between 7 and 22% water (~607 h^{-1}) even though the chemical potential of the water remains constant. Beyond 22% water the turnover frequency decreased continually reaching the minimum value at 100% water (~335 h^{-1}). For Ru/CNT-Ox, a similar initial trend was observed. Turnover frequencies increased initially with increasing partial pressure of water when the water volume percent was

below 2.9%. Beyond 2.9% water volume the TOF continued to increase, even though the chemical potential of water was not increasing, up to a maximum between 7 and 22% water (~420 h^{-1}). The highest rates reached in biphasic Ru/CNT-Ox were similar to rates in pure water for the same catalyst (~428 h^{-1}). This result confirms that rate enhancements due to the presence of biphasic water/decalin were not evident in Ru/CNT-Ox. CO consumption rates in biphasic water/decalin were clearly higher for Ru/CNT than Ru/CNT-Ox at all ratios of water/decalin investigated (Figure 10) which is consistent with the observation that high hydrophobicity is required to observe the rate enhancements in the presence of biphasic decalin/water.

Figure 11 and Figure 12 show selectivity to CH_4, C2-C5, and C6+ products as a function of water on Ru/CNT and Ru/CNT-Ox, respectively. For Ru/CNT (Figure 11) at low water volume concentration, C6+ selectivity increased from 52% to 73% when the water concentration changed from 0.5 to 7%. This was the largest increase in selectivity observed and shows that the presence of water greatly enhances the selectivity to longer-chain hydrocarbons. Moreover, when the concentration of water was increased beyond 7%, C6+ selectivity increased only slightly to 76% (30% water) before decreasing to 50% (97.5% water). Interestingly, pure water showed higher selectivity to C6+ than emulsions with water concentrations higher than 41%.

Selectivities for Ru/CNT-Ox (Figure 12) follow a trend similar to Ru/CNT. C6+ selectivity increased from 30% to 71% when water concentrations changed from 0.2 to 7%. Beyond 7% water, C6+ selectivity decreased steadily to 59% (at 75% water). Pure water showed higher C6+ selectivity than biphasic experiments with water

concentrations higher than 25%. For both Ru/CNT and Ru/CNT-Ox, selectivity to CH_4 and C2-C5 decreased whenever selectivity to C6+ increased and vice versa.

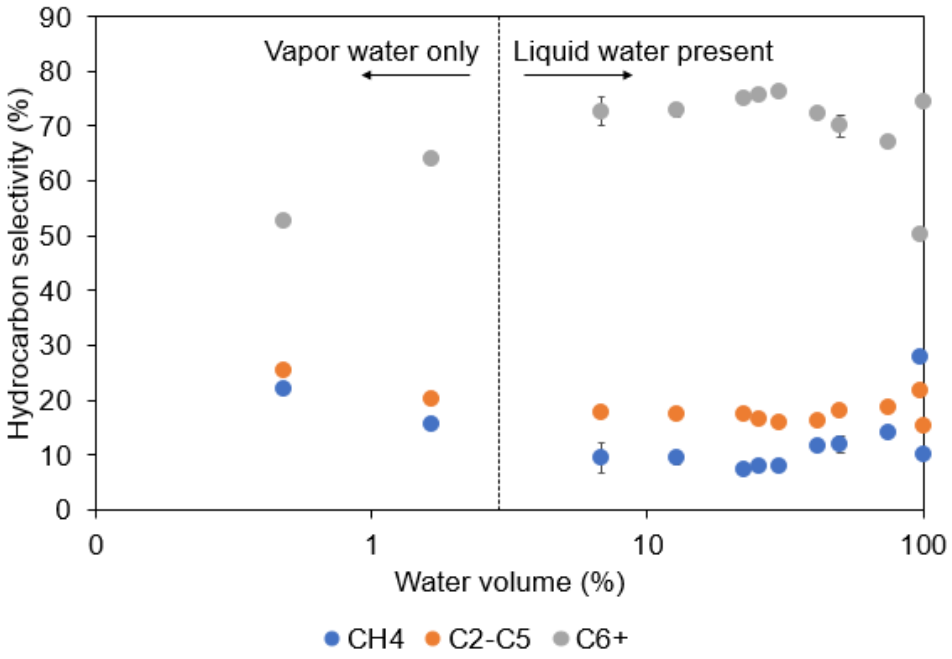

Figure 11. Hydrocarbon selectivity Ru/CNT as a function of water volume fraction. Reaction conditions: 220 C, 800 psi H_2/CO (4/1), 300rpm, conversion ~20%.

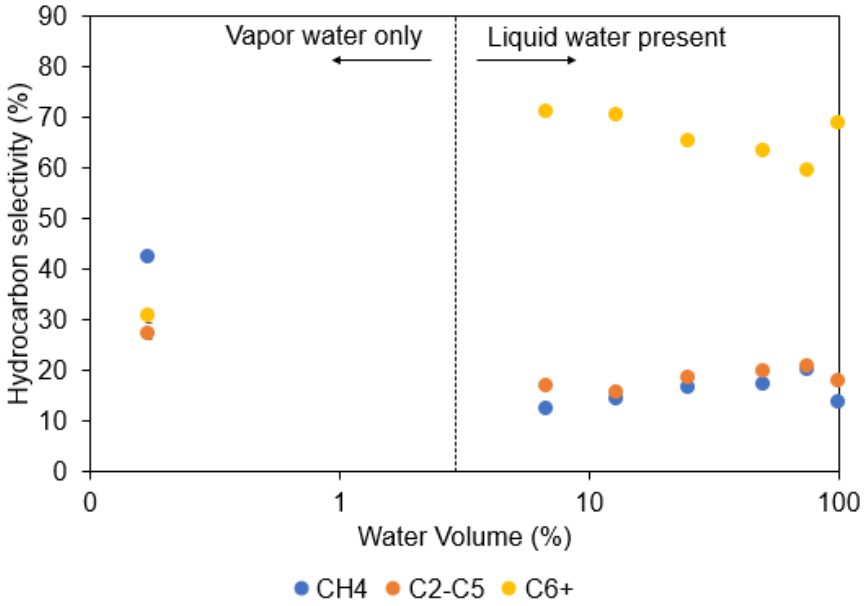

Figure 12. Hydrocarbon selectivity to hydrocarbons for Ru/CNT-Ox as a function of water volume fraction. Reaction conditions: 220 C, 800 psi H_2/CO (4/1), 300rpm, conversion ~20%.

2.3.5. Mass transfer limitations.

Important concerns about mass-transfer limitations may be raised in this reaction system where reactants are in the gas phase and the solvent media is biphasic (decalin/water). To rule out the presence of external mass transfer limitations, the stirring rate was varied, and the rate of reaction was measured in independent experiments for pure decalin, pure water and biphasic decalin/water (Figure 13). When the stirring speed was varied from 200 to 400 rpm the CO consumption TOF did not vary significantly for any of the solvent systems studied, suggesting that external mass transfer limitations through a stagnant film are not significant under the conditions of these tests. Internal mass transfer limitations are not likely to play a role under the conditions of the present experiments because Ru metal nanoparticles are likely located

preferentially on the external surface of the carbon nanotubes. Therefore, reactants do not need to travel to inner pores of the catalyst support in order to reach the active site.

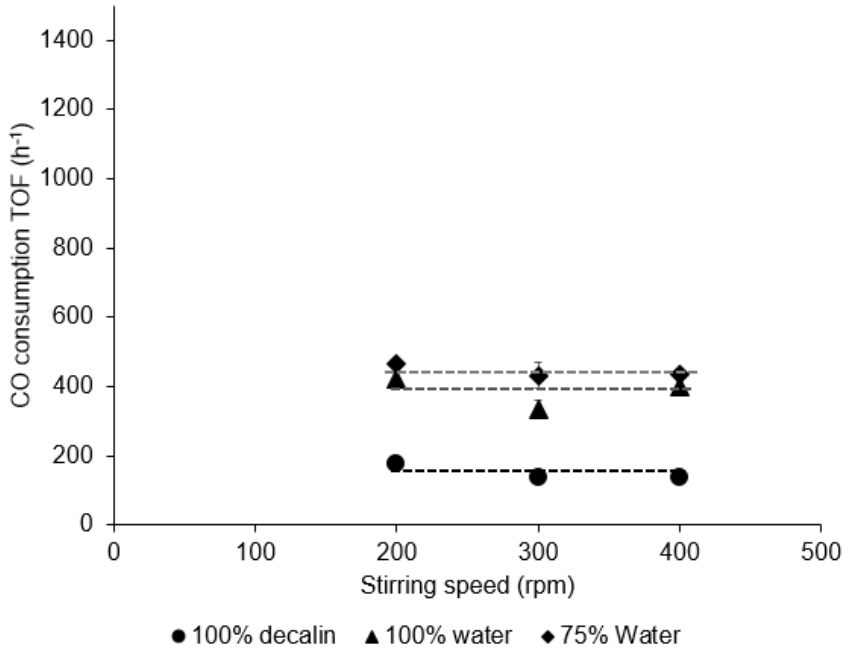

Figure 13. External mass transfer test for Ru/CNT (220 C, 800 psi H_2/CO (4/1)).

Activity enhancement from pure water to biphasic decalin/water (Figure 10) cannot be explained by improved reactant diffusion. Diffusivity of H_2 and CO is greater in water than in common hydrocarbon liquids [62,63], thus replacing some of the water solvent with decalin, as in the case of biphasic experiments, would decrease the rate and not increase it (Figure 8). Additional evidence for the absence of mass transfer limitations comes from the order of magnitude of CO consumption turnover frequencies recorded in the present study. Comparison with FT turnover frequencies reported in the literature (Appendix A, Table A3) confirms that values reported in this work are in the higher end for both vapor and liquid phase experiments at similar conditions and metal particle size.

As final confirmation that the reaction is not controlled by mass transfer, a catalyst with higher activity was prepared and the activity tested at the conditions of the most active Ru/CNT catalyst. Ru supported on hydrophobic SiO_2 was tested at 13% water volume (Appendix A, Table A4) at the same conditions for all experiments in Figure 10. The rate of CO consumption per gram of FT on Ru/SiO_2-OTS (0.40 mol CO/ h·g cat) was higher than Ru/CNT at the same conditions (0.27 molecule CO/ h·g cat). This suggests that reactions on Ru/CNT are not limited by transport even at the highest rate observed because Ru/SiO_2-OTS shows that the intrinsic rate of reaction can be increased further. If the reaction was mass transport-limited the activity would not be increased with a more active catalyst because it would be determined by the transport of reactants and products and not by the intrinsic activity of the catalyst.

2.4. Discussion

2.4.1. FT rate enhancement in emulsions

Positive effects of water on Fischer-Tropsch activity and selectivity on Ru catalysts (Figure 8) are consistent with previous reports [39,52,53,47,64]. Work by Iglesia's research group has suggested that under conditions of intrinsic kinetic control, H_2O molecules decrease the barrier for H-assisted CO dissociation via H_2O mediated H-shuttling which results in higher FT rates [39]. Moreover, liquid water can act as a more effective H-shuttle than vapor water due to the high mobility and interconnectivity of the hydrogen-bonded liquid water network (Figure 10) [52,53]. Under the conditions of this study, positive effects on activity of the organic solvents were also observed. Previous reports have also shown the positive effect of organic solvents on CO

consumption rates during liquid-phase Fischer-Tropsch [51,65,66]. For example, Xiao et al studied the effect of solvents on low-temperature FT on Ru catalysts [51]. While they observed the highest rates in aqueous phase, they also observed increasingly higher FT rates in ethanol, dioxane, and cyclohexane. It is possible that rates may increase due to improved diffusion of reactants or products as long as the system is under mass transport limitations. However, under strict kinetic control a different effect must be the cause of increased rates.

In order to evaluate the effect of organic solvents at the mass-transport-free conditions of this study, a different solvent (heptane) was selected and tested at similar conditions in single phase and biphasic solvents. As shown in Figure 14, measured turnover frequencies were 3 times higher in pure decalin (124 h^{-1}) than in pure heptane (38.4 h^{-1}). In biphasic experiments (13% water), FT rates were greater in decalin/water (725 h^{-1}) than heptane/water (472 h^{-1}). Two important observations can be made from these results. First, the choice of organic solvent had a direct effect on reaction rates. FT rates in the presence of decalin were greater than in heptane for both single phase and biphasic experiments. Second, biphasic experiments (13% water) showed rate enhancements compared to pure water (316 h^{-1}) for both heptane and decalin but to different extents. This shows that heptane also increases FT rates but not as much as decalin.

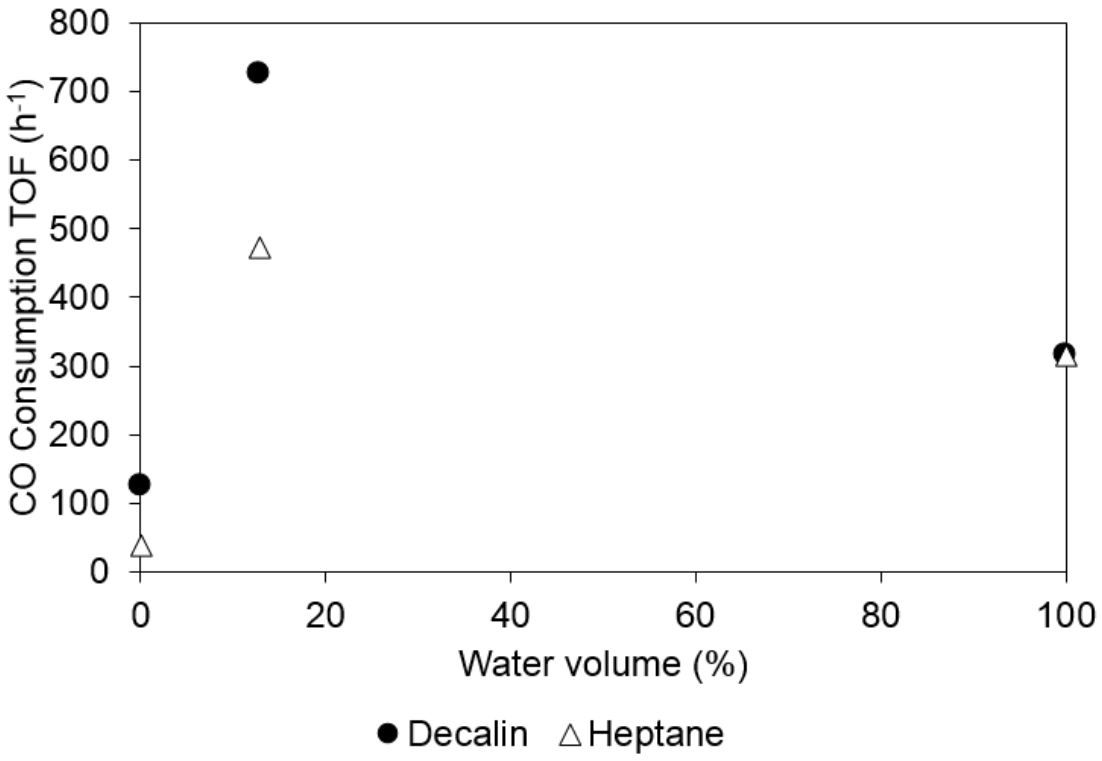

Figure 14. Rates of CO consumption for Ru/CNT as a function of water volume using decalin or heptane as the organic solvent. Reaction conditions: 220 C, 500 psi H_2/CO (4/1), 300rpm, conversion ~20%.

These results are consistent with enhancements in FT rates in biphasic media due to the presence of the organic phase. Figure 15 shows hydrocarbon selectivity for experiments in decalin and heptane. While reaction rates in the presence of decalin were higher than in heptane, Figure 15 shows that hydrocarbon selectivity was very similar regardless of the organic solvent used. Thus, organic solvents seem to increase FT rates without significantly changing product distributions. Next, the positive effect of organic solvents on the activity of Fischer-Tropsch is discussed in light of mechanistic insights recently discussed in the literature.

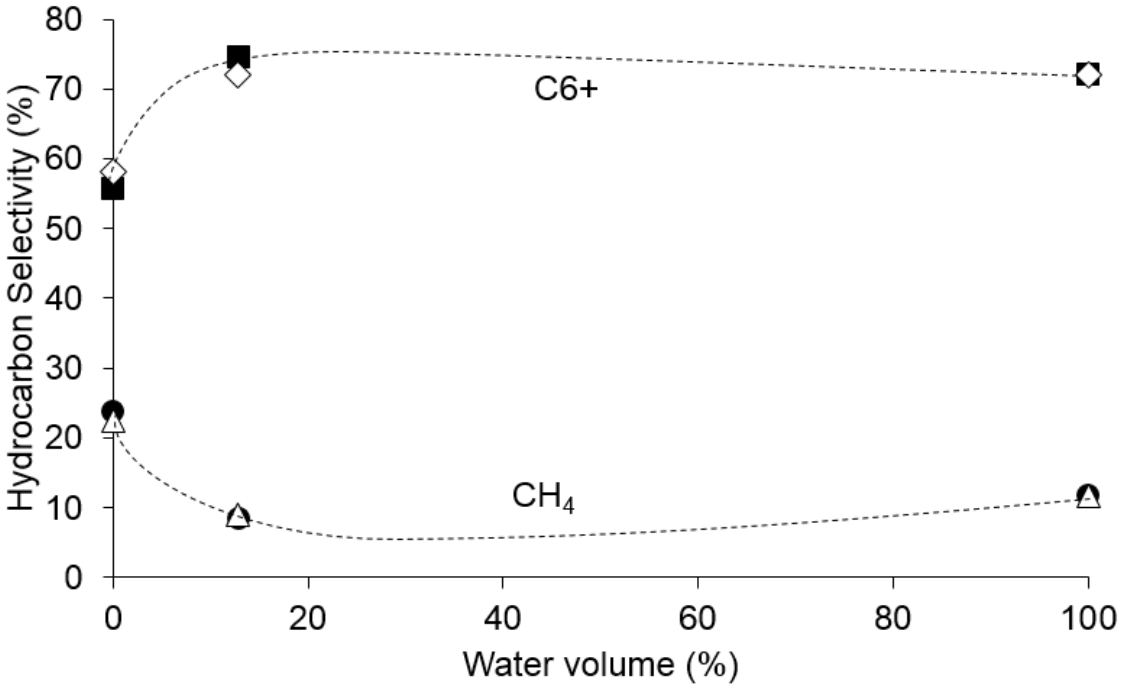

Figure 15. Selectivity to CH_4 and C6+ hydrocarbons as a function of water volume percent using decalin (Full symbols) or heptane (Open symbols) as the organic solvent. CH_4 in decalin (●) and heptane (△); C6+ in decalin (■) and heptane (◇). Reaction conditions: 220 C, 500 psi H_2/CO (4/1), 300rpm, conversion ~20%. Dashed lines are drawn to help the eye.

It has been proposed that the Fischer-Tropsch reaction proceeds via H-assisted paths on high coordination surfaces [20,22,67]. In this proposal both CO dissociation and chain growth occur on a single type of active site. Work from Iglesia's research group has recently pointed out the prevalence of high CO coverages during practical FT under high pressures of CO and H_2 [22,67,68]. According to these authors, under these high coverages, CO dissociation via H-assisted paths requires an adjacent empty site to anchor "O" atoms [20]. Therefore, desorbing an adjacent CO molecule is required and constitutes an energy penalty that increases the overall barrier of CO dissociation [68]. Interestingly, it was proposed that growing hydrocarbon chains on CO-saturated surfaces can disrupt the dense CO adlayers and generate empty sites near growing

chains without the need for desorption of CO molecules. As a result, CO dissociation has a lower barrier near growing hydrocarbon chains[68].

During liquid phase FT, solvent molecules adsorb on the surface of the catalyst. In the absence of mass transfer limitations, the adsorption of solvent molecules will equilibrate with the bulk liquid phase as determined by the adsorption equilibrium constant. If catalyst surfaces are completely covered with CO, adsorbed solvent molecules may disrupt these dense CO adlayers, similar to growing hydrocarbon chains, lowering the barrier for CO dissociation [68]. The effectiveness of a molecule to disrupt the layers of adsorbed CO on Ru surfaces may depend on several factors such as heat of adsorption and adsorption configuration. Higher heat of adsorption would increase the equilibrium constant and the coverage of the solvent molecule at a given temperature, while the adsorption configuration would affect the area of the surface covered by the molecule. For example, decalin has been shown to have higher heat of adsorption than heptane on transition state metals[69], therefore, higher surface coverages of decalin would be expected at similar conditions. Additionally, it is reasonable to expect that the more bulky, bicyclic decalin molecule would cover more surface area on Ru surfaces and disrupt the CO monolayer more effectively. Therefore, under the conditions of this study, adsorbed decalin molecules may disrupt CO adlayers more effectively, resulting in higher rate enhancements than heptane (Figure 14).

This requires, of course, that surfaces be saturated with CO under reaction conditions. Vapor phase kinetic studies have shown that the kinetics of Fischer-Tropsch can be described by the following kinetic expression [20]

$$r_{FT} = \frac{k' P_{H_2} P_{CO}}{(1 + K_{CO} P_{CO})^2}$$

And, when surfaces are saturated with CO the expression becomes:

$$r_{FT} = \frac{k'}{{K_{CO}}^2}\frac{P_{H_2}}{P_{CO}}$$

Therefore, when surfaces are covered with CO, further increase in CO pressure will decrease the overall rate of Fischer-Tropsch. Figure 16 shows the results of increasing the CO pressure while keeping the H_2 pressure and reaction conditions constant. When CO pressure was increased from 100 to 200 psi, the overall rate of Fischer-Tropsch decreased from 724 h^{-1} to 491h^{-1}, suggesting that at 100 psi CO, surfaces are already saturated with CO.

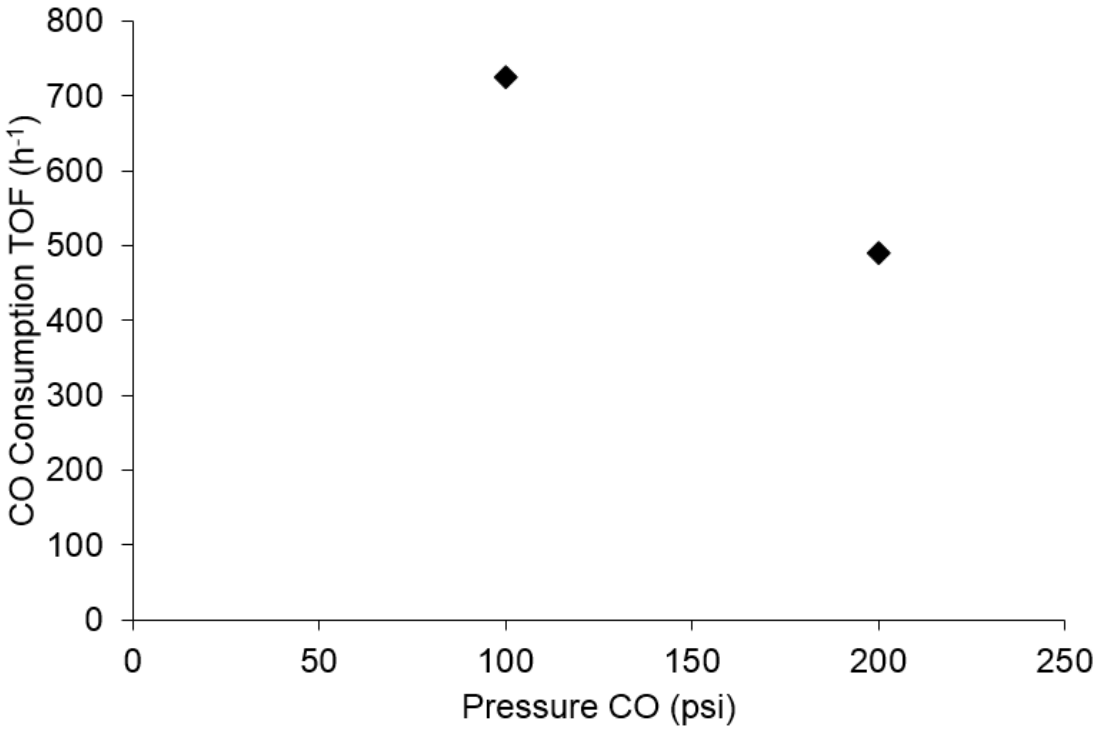

Figure 16. Rates of CO consumption for Ru/CNT as a function of CO pressure at constant H_2 pressure. Reaction conditions: 220 C, 400 psi H_2, 300rpm, H_2/CO (4/1) conversion ~20%.

FT hydrocarbon product selectivity depends on the relative rates of chain growth to chain termination. Largely unchanged FT hydrocarbon selectivity in biphasic

decalin/water compared to pure water (Figure 11 and Figure 15) suggests that the relative rates of chain growth to chain termination remained unchanged even though the overall rate of reaction increased (Figure 10 and Figure 14). If the effect of the organic solvent is disruption of CO adlayers that decrease the CO dissociation barrier, then it is expected that this effect will primarily reduce the dissociation of a CO molecule that initiates a chain. After a chain is initiated and starts chain-growth, the growing chain itself will disrupt the dense CO monolayer. Therefore, adsorbed organic molecules are not expected to increase chain growth rates via CO adlayer disruption near growing chains. Therefore, the effect of the organic solvent is to increase the number of chains that are initiated without significantly changing the chain-growth rate.

In short, higher rates in biphasic decalin/water compared to pure water or pure decalin is consistent with the organic solvent and water both playing a role in enhancing the intrinsic rate of FT. It is apparent that water shows the greatest positive enhancement by decreasing the overall barrier of CO dissociation via H_2O mediated H-shuttling [39]. Additionally, the organic solvent may further enhance the rate by disrupting the monolayer of CO and generating vacant sites for the dissociation of CO [68]. This further decreases the overall barrier of CO dissociation because it eliminates the need to desorb CO molecules to make sites available which increases energy barriers. This effect is especially important for the dissociation of CO molecules that initiate a new hydrocarbon chain. Therefore, in the presence of both organic and aqueous solvents, a combined effect of H-shuttling and disruption of the CO monolayer is observed which results in higher CO rates.

An alternative Fischer-Tropsch reaction mechanism that consists of dual reaction centers has also been proposed [70–72]. In this mechanism, CO dissociation occurs preferentially via direct cleavage of the C-O bond on low-coordination Ru(1121) step-edge sites [70]. After dissociation and hydrogenation, formed CH species migrate quickly from four-fold hollow sites to the three-fold hollow site vacating the first active site for further CO-dissociation. The next CO molecule dissociates and hydrogenates forming a new CH species that migrates to a neighboring three-fold hollow site. Two CH intermediates located on neighboring three-fold hollow sites undergo C-C coupling forming CH-CH that initiates chain-growth [70]. The rate determining step was proposed to be chain termination. Therefore, synchronized CO dissociation and C-C coupling in a different active site was proposed to explain the high activity and high selectivity to high-molecular weight hydrocarbons [70].

Positive effects of organic solvents observed in the present work might also be consistent with the dual-site mechanism. In light of this mechanism, organic solvents may play a role in keeping Ru surfaces clean by removing hydrocarbon molecules that otherwise would block chain-growth active sites [52]. In single-water phase experiments (Figure 8), hydrocarbon chains formed on chain-growth sites would not be efficiently removed from Ru surfaces because of their low solubility in water. This would decrease the overall rate of FT since chain-termination is considered the rate determining step. In biphasic decalin/water, the organic solvent in contact with catalyst particles facilitates the removal of hydrocarbon chains from the surface. The removal of these hydrocarbon chains keeps a greater fraction of chain-growth active sites clean and

available for hydrocarbon formation which increases the overall rate of Fischer-Tropsch.

It is important to note that in a typical case of site blocking by reaction products one would expect to observe catalyst deactivation rather than a drop in initial reaction rates. Nevertheless, blocking of active sites can also affect initial rates if the concentration of sites blocked by hydrocarbon products reaches quasi-equilibrium at early reaction times. In other words, the number of available active sites for FT turnovers decreases quickly early on in the reaction, due to blocking by hydrocarbon products, and remains constant afterwards as it reaches quasi-equilibrium. In the presence of organic solvents in biphasic decalin/water hydrocarbon molecules are more efficiently solubilized and the quasi-equilibrated number of available active sites may increase.

2.4.2. Enhancement in FT activity in hydrophobic catalysts

In the presence of decalin, FT reactions on the more hydrophobic Ru/CNT catalyst showed greater rate enhancements than the less hydrophobic Ru/CNT-Ox (Figure 10). For example, at 13% water volume, rates on Ru/CNT were higher (~608 h^{-1}) than on Ru/CNT-Ox (~421 h^{-1}). This suggests that the hydrophobic nature of the support affects the interactions of the organic solvent with Ru surfaces that enhance the rates of FT. These important results show that the positive effect of organic solvents on FT rates can be improved by increasing the hydrophobicity of the catalyst support. Similar results were observed on SiO_2-supported Ru catalysts with varying wettability where FT rates were higher for catalysts with greater hydrophobicity [73]. Table A4 (Appendix A) shows that FT rates for a Ru catalyst supported on hydrophobic silica (Ru/SiO_2-OTS)

were higher (841.4 h^{-1}) than the highest rates observed in Ru/CNT (608.4 h^{-1}) at similar conditions.

Higher FT rates of Ru/CNT in biphasic decalin/water seems to correlate with oil particle wettability. The high hydrophobicity of Ru/CNT leads to more efficient wetting by the organic phases at decalin/water interfaces that in turn enhanced FT rates. Conversely, lower organic phase wettability in Ru/CNT-Ox resulted in lower rate enhancements at similar reaction conditions. Based on both the single-site and dual-site mechanism, molecules of the organic solvent must come near Ru surfaces to enhance the rate of Fischer-Tropsch. In the single-site mechanism, solvent molecules adsorb on Ru surfaces and disrupt CO monolayers [68], while in dual-site mechanistic paths decalin molecules help remove hydrocarbon chains from Ru surfaces [70]. Thus, increased oil wettability seems to facilitate the interaction of organic phases with Ru surfaces that enhanced FT rates.

Contact of the catalyst particles with the organic phase at the decalin/water interface may also be enhanced by increasing oil/water ratios [61]. Briggs *et al*. [61] showed that, for water-in-oil emulsions stabilized by multiwall carbon nanotubes, increasing the oil/water ratios decreased emulsion droplet size regardless of the wettability of the particles. For amphiphilic particles, increasing oil/water ratios in oil-in-water emulsions caused catastrophic emulsion inversion. This behavior is consistent with enhanced contact of the carbon nanotubes with the organic phase as oil/water ratios increased. Figure 10 shows FT rates as a function of water volume percent (balance decalin). Increasing water volume percent is equivalent to decreasing the oil/water ratio. Data for Ru/CNT and Ru/CNT-Ox in Figure 7 show that as water volume percent was increased

beyond 22.5%, FT rates decreased steadily until 100% water concentration. This trend is consistent with lessened contact of the catalyst particles with the organic phase at the decalin/water interface as the oil/water ratio decreased.

Positive effects of organic solvents on FT rates seem to improve with increased contact of catalyst particles with the organic phase at the decalin/water interface. This statement seems to suggest that the system is limited by mass transfer of the decalin and that changing the fraction wetted by decalin overcomes this limitation. In the absence of mass transfer limitations, the chemical potential of decalin should be the same in the water phase and on Ru surfaces regardless of what fraction of the catalyst particle is wetted by the organic or aqueous phase. Therefore, the fraction of the catalyst wetted by decalin should not affect the positive effects of decalin on FT rates. Thus some important future work should aim to address the reason for these inconsistencies. Alternatively in light of the dual site mechanism, hydrophobic catalysts are wetted more efficiently by the organic phase in biphasic decalin/water which facilitates the removal of hydrocarbon chains from Ru surfaces and, as a result, FT rates increased (Figure 10).

2.5. Conclusions

FT rates on Ru/CNT in biphasic decalin/water showed greater CO consumption rates than pure water or pure decalin experiments because of the combined positive effects of water and decalin solvents. Water increased rates and improved C6+ selectivity while decalin improved reaction rates without significant changes in selectivity. The positive effects of organic phases on rates were observed in single-phase and biphasic experiments. Replacing decalin for heptane as the organic phase in FT experiments

resulted in lower rates suggesting that decalin enhances activity more than heptane in both single-phase and biphasic systems. FT rates enhancements by organic phases were more pronounced in catalysts with higher oil wettability and at higher oil/water ratios. Therefore, high contact of decalin with Ru surfaces in biphasic systems seems to be required to observe rate enhancements by the organic phase.

Increased rates in biphasic systems cannot be explained by improved mass transfer of reactants or products since reaction systems were under strict kinetic control. Positive impact of water and decalin on FT rates must stem from changes in rates of kinetically relevant steps. As recently proposed, water might improve FT rates by acting as a H-shuttle, which decreases energy barriers for kinetically relevant CO dissociation via H-assisted paths. As a result, CO dissociation and chain-growth rates increase which led to higher overall FT rates and higher selectivities to desired long-chain hydrocarbons. Recent kinetic and spectroscopic studies pointed out the prevalence of high CO coverages under practical FT conditions at high CO pressures. Disruption of these dense CO adlayers by growing hydrocarbon chains was proposed to reduce CO barriers near growing chains. In this study, organic solvent molecules may adsorb on Ru surfaces and disturb CO-saturated surfaces, enhancing FT rates. Organic solvent molecules reduce the energy barrier for dissociation of CO molecules that initiate a hydrocarbon chain. After chain initiation, growing chains are able to self-disrupt CO monolayers so that there is no added effect of the decalin solvent during chain-growth steps. As a result, decalin increases FT rates without significantly changing product distributions.

The positive effect of organic solvents on rates may also be understood in light of the two-site FT model. Based on this mechanism, organic solvents may play a role in

facilitating the removal of hydrocarbons from chain-growth active sites. In pure water, hydrocarbon products formed may not leave Ru surfaces because of their low solubility in water thus carbonaceous deposits may form block chain-growth active sites. Therefore, organic solvents in biphasic systems increase the overall rate of reaction by helping maintain chain-growth sites active by efficiently removing hydrocarbon products from Ru surfaces.

Chapter 3: Enhanced Fischer-Tropsch Synthesis Rates on hydrophobic Ru/SiO_2 in biphasic decalin/water.

Abstract

Enhanced interaction of hydrophobic Ru/SiO_2 surfaces with organic phases during single-phase and biphasic decalin/water led to higher Fischer-Tropsch (FT) rates. Ru/SiO_2 catalysts of varying hydrophobicity were prepared by surface silylation and tested in liquid-phase FT in biphasic decalin/water (H_2:CO = 4:1, 220 °C, 800 psi). Hydrophobic catalysts showed up to two times higher FT rates than hydrophilic catalysts while selectivities improved only slightly consistent with positive effects of organic solvents on FT. Hydrogenation of oil-soluble and water-soluble molecules showed that hydrophobic catalysts are wetted preferentially by organic solvents while hydrophilic catalysts are wetted preferentially by water phases during biphasic reactions. Interestingly, a minimum degree of surface hydrophobicity, as measured by water-air contact angles, was required to trigger significant positive effects on FT rates. It was proposed that strong van der Waals interactions between surface-anchored organosilanes and organic solvent molecules might increase catalyst oil wettability which facilitates rate enhancements by the organic phase.

3.1. Introduction

Fischer-Tropsch (FT) synthesis converts CO and H_2 to long-chain hydrocarbons at high pressure and temperature on Fe, Co, or Ru catalysts and it is the heart of gas-to-liquids and coal-to-liquids technologies. Historically, FT has drawn intermittent industrial attention to offset low availability and high costs of petroleum-based fuels. In recent decades, increasing concern for the environment has gained FT additional interest for

production of liquid fuels from biomass sources. At conditions of Low-Temperature Fischer Tropsch (LTFT), reaction media and hydrocarbon products are in the liquid phase, therefore, the effect of solvents can be explored to optimize reaction conditions to improve rates and selectivities.

As shown in chapter 2 of this dissertation, organic solvents increase FT rates. Decalin showed greater FT rate enhancements than heptane in both single phase and biphasic experiments. These observations are consistent with previous reports that showed increasingly higher FT rates in ethanol, dioxane and cyclohexane solvents [51]. On the other hand, aqueous phase FT rates are greater than in single-phase organic solvents [51–53]. Recent proposals suggested that water enhances rates of H-assisted CO dissociation via H_2O-mediated hydrogen shuttling [39].

The positive effects of organic solvents on FT rate were discussed in chapter 2 in light of single-site and dual-site mechanistic proposals. In the former, organic solvent molecules disrupt dense adlayers of CO, prevalent at high CO pressures, and decreased CO dissociation barriers [68]. In the latter, organic solvents help keep Ru surfaces clean by facilitating the removal of hydrocarbon products from chain-growth active sites [70]. Interestingly, FT reactions on a catalyst with higher oil wettability increased the magnitude of the rate enhancements by the organic phase (Chapter 2). It was suggested that the location of the catalyst particle at the decalin/water interface plays a role in increasing catalytic activity.

In this chapter, a systematic study of catalyst hydrophobicity on FT rates and selectivities is carried out. Ru supported on silica (Ru/SiO_2) of varying hydrophobicity are prepared, characterized and tested in liquid-phase FT in biphasic decalin/water.

Catalyst hydrophobization is carried out by SiO_2 surface silylation [74]. Organosilanes of different hydrocarbon chain lengths at varying concentrations are used to obtain different degrees of hydrophobicity and the effects on FT rates and selectivities are measured and discussed.

3.2. Experimental

3.2.1. Catalyst preparation and characterization

Silica gel Davisil 646 (Sigma-Aldrich), labeled here "SiO_2", was used as received. Ruthenium supported on SiO_2 (Ru/SiO_2) catalysts were prepared by conventional incipient wetness impregnation with ruthenium (III) nitrosyl nitrate (Alfa-Aesar) as the Ru metal precursor. In a typical preparation, the appropriate volume of metal precursor was dissolved in deionized water and added dropwise onto the SiO_2 support. Next, the catalyst was dried, first at room temperature for 6 hours, then at 80 °C for 12 hours in a vacuum oven. After preparation, the catalyst was treated in flowing hydrogen. The temperature was ramped, first at 2 °C/min to 120 °C and held for 1 hour to assure complete drying. Following, the temperature was ramped at 2 °C/min to 400 °C and held for 3 h to eliminate nitrosyl nitrate ions.

Hydrophobic Ru/SiO_2 catalysts were prepared by a silylation method previously described [74]. Alkyl trichlorosilanes of different hydrocarbon chain lengths (Alfa Aesar) were used to achieve different degrees of hydrophobicity. Briefly, 1 g of the

parent Ru/SiO_2 catalyst was dispersed in 20 ml of toluene by sonication at 25% amplitude with a Horn Sonicator (Fischer Scientific Model 505C). Then the Ru/SiO_2 suspension was added to a 50 ml solution of the alkyl trichlorosilanes in toluene (0.5 – 3.0 mmol/g catalyst). The final suspension was stirred for 24 h at 500 rpm. The functionalized material was recovered by filtration, washed thoroughly with methanol, and dried at 80 °C in a vacuum oven.

TGA was evaluated using a Netzsch STA-449 F1 Jupiter equipped with a type S thermocouple. A sample of hydrophobic Ru/SiO_2 (30-70mg) was placed in a crucible in the TGA cell under constant flow of Ar (20 ml/min) and air (40 ml/min). After pre-heating to 40°C the temperature was ramped at 2°C/min to the final 750°C. Weight losses were recorded with a nanobalance in single furnace configuration. N_2 physisorption was performed using a micromeritics ASAP 2000 unit. Prior to analysis, the samples were degassed in situ at 180°C for 6 h. For transmission electron microscopy (TEM), the catalyst sample was pre-reduced at 400 ºC in flowing H_2 for 3 h. Following, a few milligrams of the solid were dispersed in 2-propanol by horn sonication (Fischer Scientific Model 505C) before deposition onto a lacey carbon coated copper grid. TEM images were obtained on a JEOL 2100 field emission system operated at 200 kV. Particle size distribution and dispersion were estimated by measuring particle diameters for 100 particles. Contact angle measurements were

carried out in an optical tensiometer Attension Theta Lite. A 6.5 µl water droplet was placed on the surface of disc-shaped catalyst pellet. Contact angle measurements were recorded as a function of time for 60 seconds.

3.2.2. Fischer-Tropsch catalytic activity measurements

Fischer-Tropsch (FT) catalytic activity tests were carried out in a 300-ml stainless steel autoclave reactor (Parr instruments 4560) operating in batch mode. The temperature inside the reactor was controlled with a CAL 9500P controller (CAL Controls Ltd.) while the pressure was monitored with an Ashcroft 2074 digital industrial pressure gauge. In a typical run, 50 mg of catalyst were dispersed in 70 ml of decalin (mix. cis + trans, anhydrous ≥99.9%, Sigma-Aldrich) by horn sonication (50% amplitude). Following, 10 ml of deionized water (18 MΩ) were added and the final mixture sonicated by horn sonication (50% amplitude). After sealing and purging with N_2, the reactor was pressurized with H_2 to 500 psi and heated to 250 °C for a reduction period of 1 h with a stirring speed of 300 rpm. After the reduction, the reactor was cooled down and the H_2 pressure released. Following, the reactor was purged and pressurized to 800 psi with the reactants H_2/CO (ratio 4/1). After equilibration of the pressure reading, the temperature was raised to 220 °C while stirring at 300 rpm to start the reaction. After completion of the reaction period, the reactor was quickly cooled down to room temperature and a high-pressure gas sample was taken.

Concentrations of H_2, CO, and CO_2 in the gas phase were analyzed by gas chromatography with a thermal conductivity detector (GC-TCD, Carle 400 AGC). Light hydrocarbons present in the gas phase (C1-C7) were analyzed by gas chromatography-mass spectrometry (GC-MS, Agilent 7820A, MS 5975 Series MSD) equipped with a

capillary, bonded polystyrene-divinylbenzene (DVB) column (HP-PLOT/Q) of 30 m x 0.320 mm x 20.0 μm. After releasing the reactor pressure, the liquids were separated from the solid catalyst by centrifugation followed by filtration with 0.22 μm PTFE filter forming two immiscible layers of clear liquid. The two phases were analyzed by GC-FID and GC-MS. An Agilent GC-FID 7890B equipped with a capillary, low polarity column (Phenomenex ZB-5), 60.0 m x 0.25mm x 0.25 μm, was used for product quantification, while a Shimadzu QP2010 GC–MS equipped with a mid-polarity (Phenomenex ZB-1701) capillary column, 60.0 m x 0.25 mm x 0.25 μm nominal, was used for product identification. Standards available commercially were used to confirm product identity and to determine FID response factors. Phenol was used as an internal standard to help close mass balances. Turnover frequencies (TOF) based on CO consumption and yields and selectivities based on moles of C were calculated as follows:

$$TOF\ (h^{-1}) = \frac{mol\ CO\ reacted}{mol\ Ru\ exposed \cdot h}$$

$$\%\ Yield = \frac{Total\ mol\ C\ in\ product}{mol\ of\ C\ in\ CO\ (initial)}\ x\ 100$$

$$\%\ Selectivity = \frac{mol\ of\ C\ in\ product}{Total\ mol\ of\ C\ in\ all\ products} \times 100$$

3.2.3 Hydrogenation of 2-butene-1,4 diol and 1-dodecene

The hydrogenation of 2-butene-1,4 diol and 1-dodecene was used to determine the location of catalyst particles during FT in biphasic decalin/water. 2-butene-1,4 diol dissolves preferentially in water while 1-dodecene is highly soluble in organic solvents. Rates of hydrogenation for these compounds in biphasic mixtures was used to

determine the preferential location of Ru/SiO_2 catalysts of various hydrophobicity during reaction. In a typical biphasic run, 20 mg of catalyst were added to the reactor and dispersed in 30 ml of decalin by horn sonication (50% amplitude). Next, 30 ml of water were added and the final mixture sonicated again by horn sonicator (50% amplitude). After sealing and purging, the reactor was pressurized to 500 psi with H_2 for a reduction period at 250 °C for 1 h. Following, the H_2 pressure was reduced to 80 psi and the temperature raised to 40 °C. At that moment, a mixture of 10 ml of water and 10 ml of decalin containing the reactants was injected from a pressurized cylinder. The final pressure was adjusted to 200 psi with additional H_2. The zero reaction time was taken as the moment when the desired reaction temperature and pressure were reached after the reactants were injected. For pure solvent reactions, the catalyst was dispersed initially in 60 ml of pure decalin or water and the appropriate reactant was injected in 20 ml of the same solvent from the pressurized cylinder. At the end of the reaction period, the reactor was quickly cooled down to room temperature and depressurized and the products filtered and analyzed by gas chromatography. An Agilent GC-FID 7890B equipped with a capillary, low polarity column (Phenomenex ZB-5) 60.0 m x 0.25mm x 0.25 μm was used for product quantification, while a Shimadzu QP2010 GC–MS equipped with a mid-polarity (Phenomenex ZB-1701) capillary column, 60.0 m x 0.25 mm x 0.25 μm nominal, was used for product identification. Standards available commercially were used to confirm product identity and to determine FID response factors. Phenol was used as an internal standard to help close mass balances.

3.3. Results

3.3.1. Catalyst preparation and characterization

Table 4 summarizes catalyst samples prepared in the present study. SiO_2 (Davisil 646) was decorated with Ru metal particles to prepare Ru/SiO_2 and then functionalized with various trichloro(Alkyl) silanes. Three different samples of Ru/SiO_2 were functionalized to varying extents with trichloro(ethyl)silane (ETS) and were labeled Ru/SiO_2-ETS-A, Ru/SiO_2-ETS-B, and Ru/SiO_2-ETS-C, respectively, in order of increasing density of silane groups. Additional samples of Ru/SiO_2 functionalized with trichloro(hexyl)silane (HTS), trichloro(dodecyl)silane (DTS), and trichloro(octadecyl)silane (OTS), were labeled Ru/SiO_2-HTS, Ru/SiO_2-DTS, and Ru/SiO_2-OTS, respectively (Table 4).

Table 4. 7%Ru/SiO_2 functionalized with trichloro(alkyl)silanes of different alkyl chain length.

Sample	Silane precursor	No. of carbons
SiO_2 (Davisil 646)	-	-
Ru/SiO_2	-	-
Ru/SiO_2-ETS-A*	Trichloro(Ethyl)silane	2
Ru/SiO_2-ETS-B*	Trichloro(Ethyl)silane	2
Ru/SiO_2-ETS-C*	Trichloro(Ethyl)silane	2
Ru/SiO_2-HTS	Trichloro(Hexyl)silane	6
Ru/SiO_2-DTS	Trichloro(Dodecyl)silane	12
Ru/SiO_2-OTS	Trichloro(Octadecyl)silane	18

*ETS-A, ETS-B, and ETS-C were prepared with increasing density of silanes per gram of SiO_2

Figure 17 shows the results of thermogravimetric analysis (TGA) in flowing air for all Ru/SiO_2 catalyst functionalized with trichloro(alkyl)silanes. Weight losses from 0 to 150 °C correspond mainly to the removal of water. At temperatures higher than 150 °C the alkyl groups attached to SiO_2 surfaces start oxidizing to CO_2 and H_2O, causing steep weight losses in the TGA profiles. In the range 300-350 °C, rates of weight loss decreased drastically, suggesting that the oxidation of alkyl groups ended. Continued weight loss at temperatures higher than 300-350 °C may be associated with dehydroxylation of SiO_2. Table 5 shows weight percent of silanes from TGA analysis. The values were corrected for the oxidation of Ru metal to Ru oxides that cause weight increase. BET surface area and silane density in molecules/nm^2 is also shown in Table 5. As expected, Ru/SiO_2-ETS-A, Ru/SiO_2-ETS-B, and Ru/SiO_2-ETS-C contain increasing amounts of ETS groups per nm^2 of SiO_2. BET surface area decreased with increasing density of silanes for ETS functionalized catalysts, while increasing alkyl chain also decreased the surface area. Reduced BET surface area after surface silylation has been observed before [75,76] and was attributed to the blockage of pores that decreased the access to catalyst surfaces. This is consistent with results in Table 5 as higher concentration of silanes and higher-molecular weight silanes are more likely to block access to a greater fraction of pores.

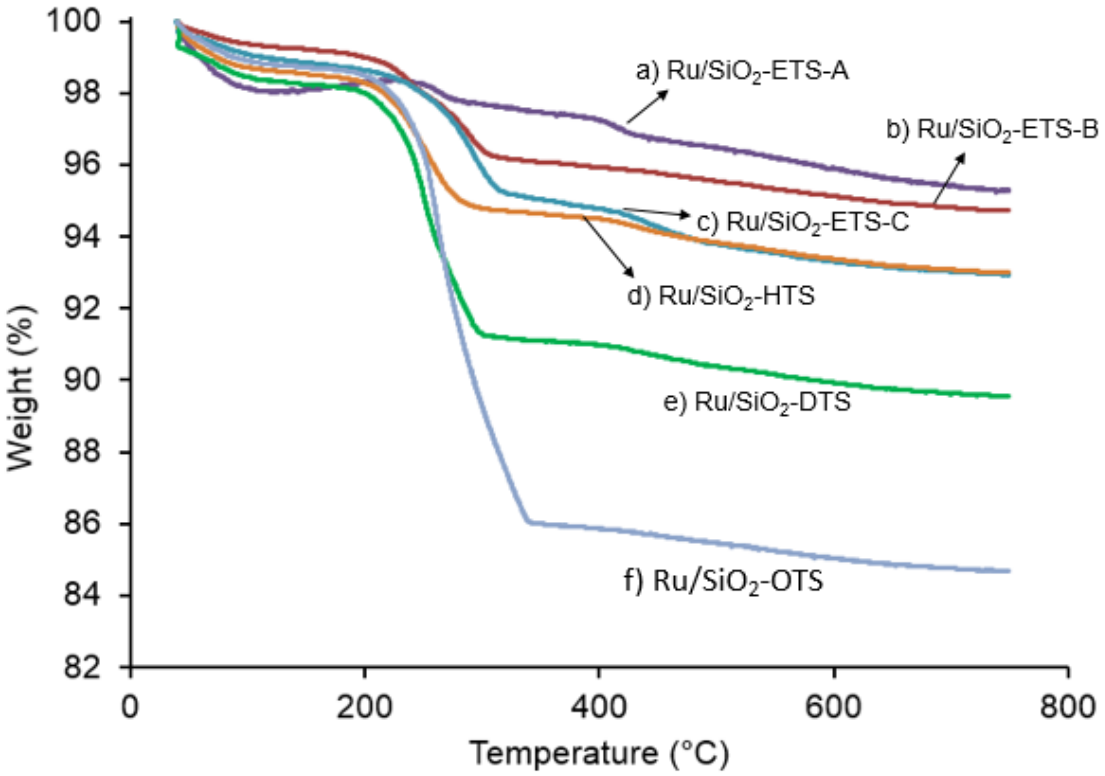

Figure 17. Thermogravimetric analysis (TGA) of Ru/SiO2 catalysts functionalized with trichloro(alkyl)silanes (ATS) of different chain length and different density of silanes per surface area. a) Ru/SiO2-ETS-A b) Ru/SiO2-ETS-B , c) Ru/SiO2-ETS-C, d) Ru/SiO2-HTS , e) Ru/SiO2-DTS, f) Ru/SiO2-OTS.

Table 5. Ru/SiO2 functionalized with trichloro(alkyl)silanes of different alkyl chain length: Weight percent of silane, BET surface area, density of silanes per surface area.

Sample	Weight % silane	BET Area ($m^2/g\ SiO_2$)	Silane molecules/nm^2
SiO_2 (Davisil 646)	-	283.2	-
Ru/SiO2-ETS-A	4.8	286.6	0.70
Ru/SiO2-ETS-B	7.3	289.7	1.10
Ru/SiO2-ETS-C	7.9	277.8	1.20
Ru/SiO2-HTS	8.1	300.8	0.91
Ru/SiO2-DTS	11.4	282.6	0.97
Ru/SiO2-OTS	17.1	248.6	1.21

Figure 18 and Figure 19 show TEM images of Ru/SiO_2 before and after functionalization with trichloro(alkyl)silanes. Average particle diameter for Ru/SiO_2 was 2.76 nm while dispersion was 42.8 %. TEM images in Figure 18 show that after functionalization with increasing concentrations of ETS particle size and dispersion of Ru/SiO_2 catalysts were not significantly altered. Similarly, TEM images in Figure 19 show that particle sizes and dispersion of Ru/SiO_2 catalysts before and after functionalization with HTS, DTS, and OTS did not vary noticeably.

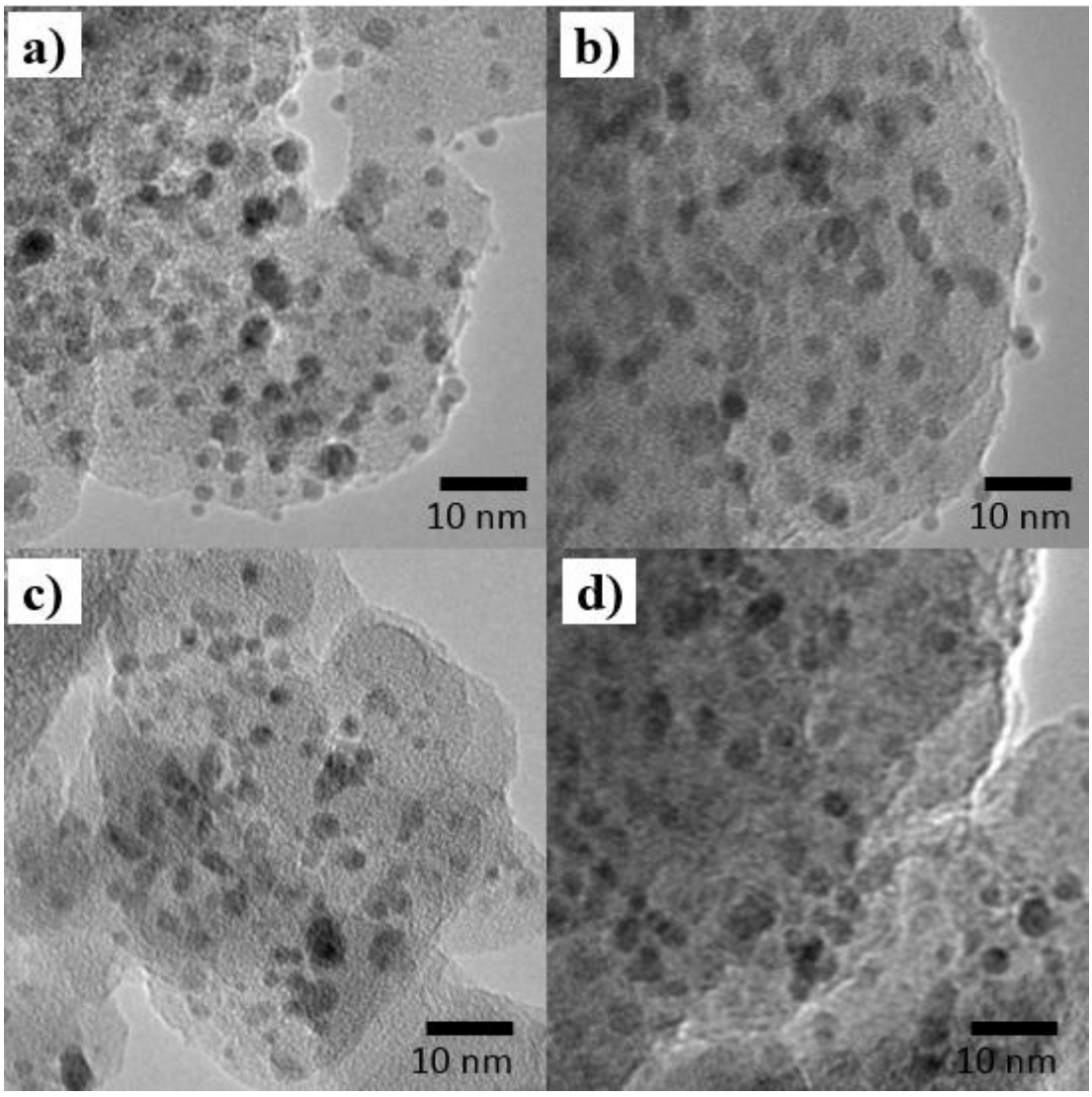

Figure 18. Transmission Electron Microscopy (TEM) images of Ru/SiO_2 catalysts functionalized with trichloro(ethyl)silanes (ETS) of different density of silanes per surface area. a) Ru/SiO2 (without functionalization) b) Ru/SiO_2-ETS-A (0.69 silanes/nm^2), c) Ru/SiO_2-ETS-B (1.07 silanes/nm^2), d) Ru/SiO_2-ETS-C (1.22 silanes/nm^2).

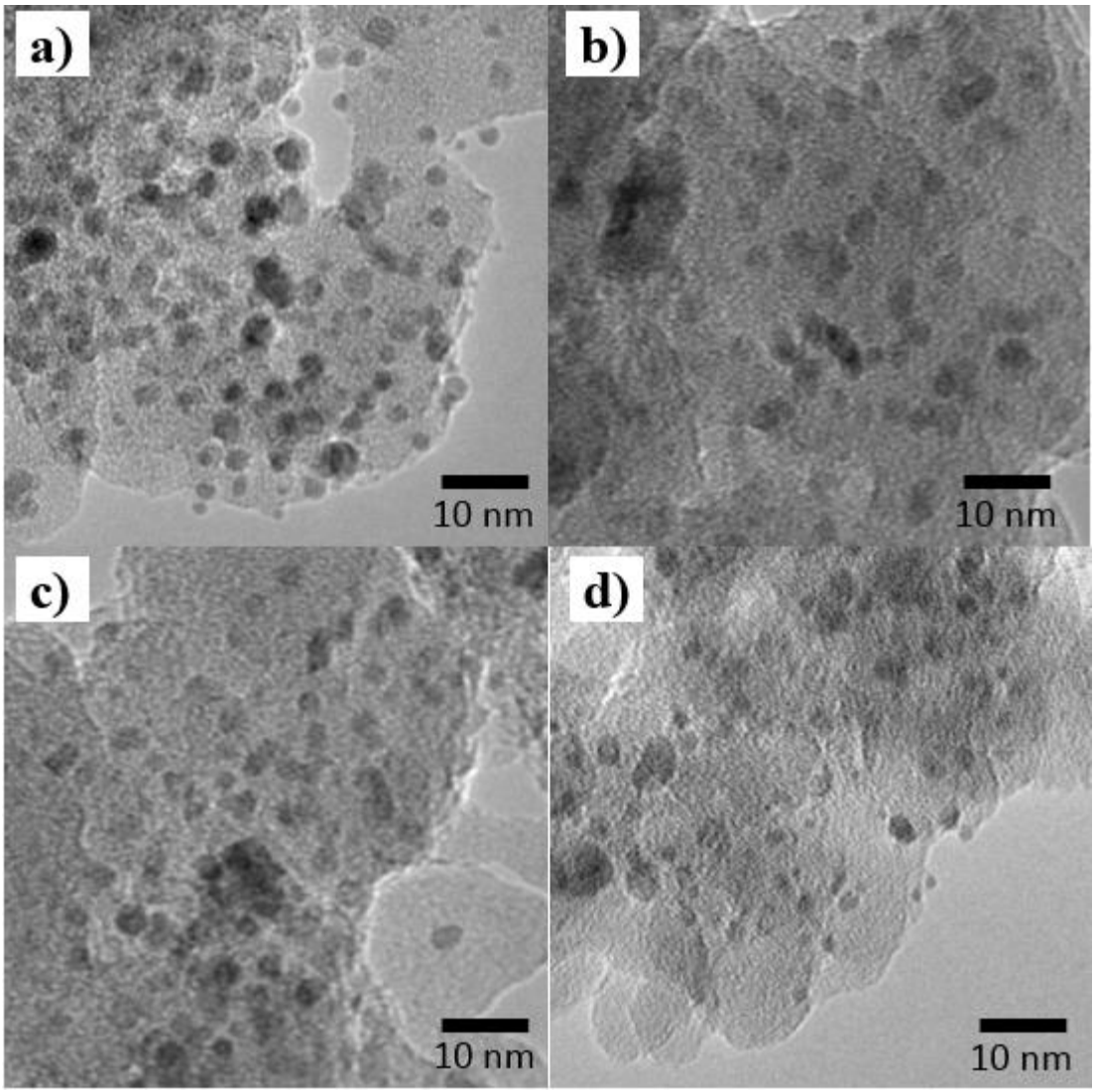

Figure 19. Transmission Electron Microscopy (TEM) images of Ru/SiO_2 catalysts functionalized with trichloro(alkyl)silanes of different alkyl chain length and different density of silanes per nm^2 surface area. a) Ru/SiO2 (without functionalization) b) Ru/SiO_2-HTS (0.86 silanes/nm^2), c) Ru/SiO_2-DTS (0.97 silanes/nm^2), d) Ru/SiO_2-OTS (1.38 silanes/nm^2).

Figure 20 shows the water-air contact angle for functionalized Ru/SiO_2 catalysts as a function of time. Water droplets placed on the surface of catalyst pellets absorbed into the bulk of the pellet because of the porosity of SiO_2 particles. Moreover, rates of absorption were proportional to the hydrophobicity of SiO_2 particles. For example, for

Ru/SiO_2 functionalized with ETS, increasing density of ETS molecules per nm^2 increased the initial contact angle and slowed down the decrease in contact angle with time (Figure 20b). Similarly, increasing the length of the alkyl chain in HTS, DTS and OTS increased the initial contact angle and slowed down its decrease as a function of time (Figure 20a).

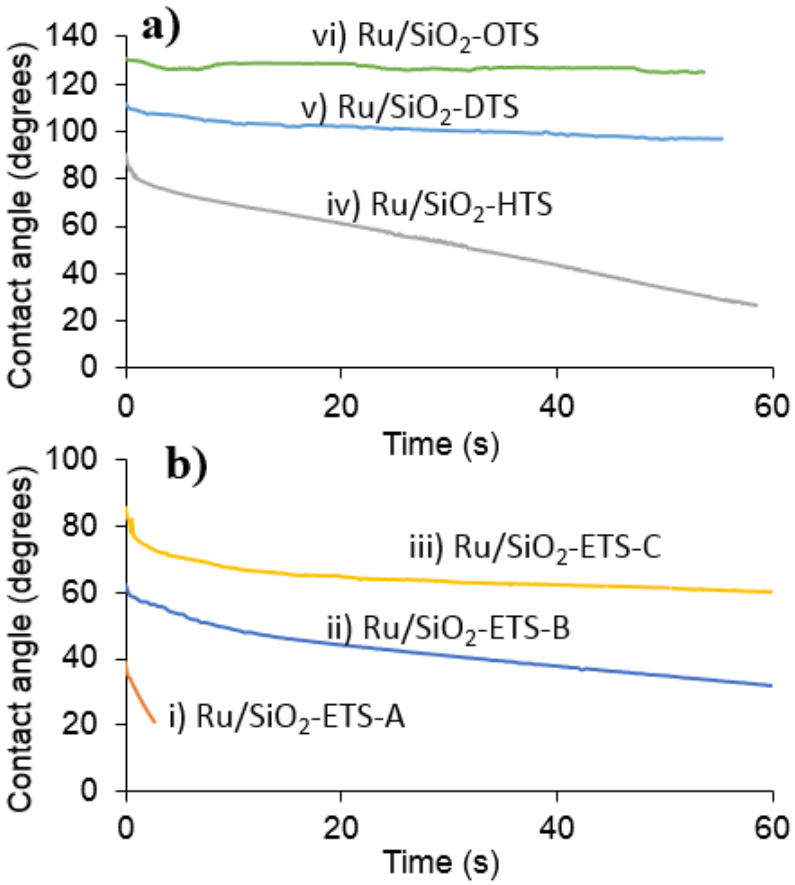

Figure 20. Water-air contact angle as a function of time for Ru/SiO2 catalysts functionalized with trichloro(alkyl)silanes (ATS) of different alkyl chain length and different density of silanes per surface area. i) Ru/SiO2-ETS-A (0.69 silanes/nm2), ii) Ru/SiO2-ETS-B (1.07 silanes/nm2), iii) Ru/SiO2-ETS-C (1.22 silanes/nm2), iv) Ru/SiO2-HTS (0.86 silanes/nm2), v) Ru/SiO2-DTS (0.97 silanes/nm2), vi) Ru/SiO2-OTS (1.38 silanes/nm2).

Table 6 summarizes the contact angle measured at time 0 and after 60 seconds for all functionalized Ru/SiO_2 catalysts. At time 0, the contact angle of the catalysts increased with increasing density of silanes and alkyl chain length. For example, Ru/SiO_2-ETS-A had the lowest contact angle followed by Ru/SiO_2-ETS-B and Ru/SiO_2-ETS-C in order of increasing density of silanes. Even though Ru/SiO_2-HTS and Ru/SiO_2-DTS had lower density of silanes than ETS-B and ETS-C, they showed higher initial contact angles than catalysts functionalized with ETS. This shows that longer alkyl chains make Ru/SiO_2 more hydrophobic at similar silane densities. Ru/SiO_2-OTS had the longest alkyl chain and the highest density of silanes of all samples and, as a result, showed the highest hydrophobicity.

Table 6. Air-water contact angle at time 0 and after 60 seconds for Ru/SiO_2 functionalized with trichloro(alkyl)silanes of different alkyl chain length.

	Silane molecules/nm^2	Water-air contact angle	
Sample	-	0 s	60 s
Ru/SiO_2-ETS-A	0.70	38.8°	0°
Ru/SiO_2-ETS-B	1.10	62.5°	31.8°
Ru/SiO_2-ETS-C	1.20	85.7°	60.3°
Ru/SiO_2-HTS	0.91	90.8°	26.3°
Ru/SiO_2-DTS	0.97	111.4°	96.5°
Ru/SiO_2-OTS	1.21	131.1°	125.4°

After 60 seconds, the contact angle for all catalysts decreased to different extents. Ru/SiO_2-ETS-A was completely absorbed into the catalyst pellet after less than 20 seconds. The contact angles of Ru/SiO_2-OTS and Ru/SiO_2-DTS decreased the least while that of Ru/SiO_2-HTS decreased the most. Thus, after 60 s, Ru/SiO_2-HTS showed lower contact angle than Ru/SiO_2-ETS-B and Ru/SiO_2-ETS-C, suggesting that Ru/SiO_2-HTS has less resistance to water penetration than Ru/SiO_2-ETS-B and Ru/SiO_2-ETS-C even though Ru/SiO_2-HTS showed initial higher contact angle. This rapid decrease in contact angle for HTS may be related to its low silane density. At 0.91 silane molecules/nm^2 and 6 carbons in the chain, HTS catalysts allow the penetration of water faster than ETS catalysts which had higher density of silanes. Figure 21 and Figure 22 show, respectively, images of the measured initial contact angles (after a few seconds) and final contact angles (after 60 s).

Figure 23 plots the initial measured contact angles as a function of the density of silanes per SiO_2 surface area. For Ru/SiO_2 catalysts functionalized with ETS, the initial contact angle increased proportionally with increasing density of silanes per surface area. For Ru/SiO_2 catalysts functionalized with HTS, DTS, and OTS, the initial contact angle also increased with increasing density of silanes, but the values did not fall in the same trendline as the catalysts functionalized with ETS. This is expected since longer

hydrocarbon chains should make the catalyst surface more hydrophobic at similar silane surface density.

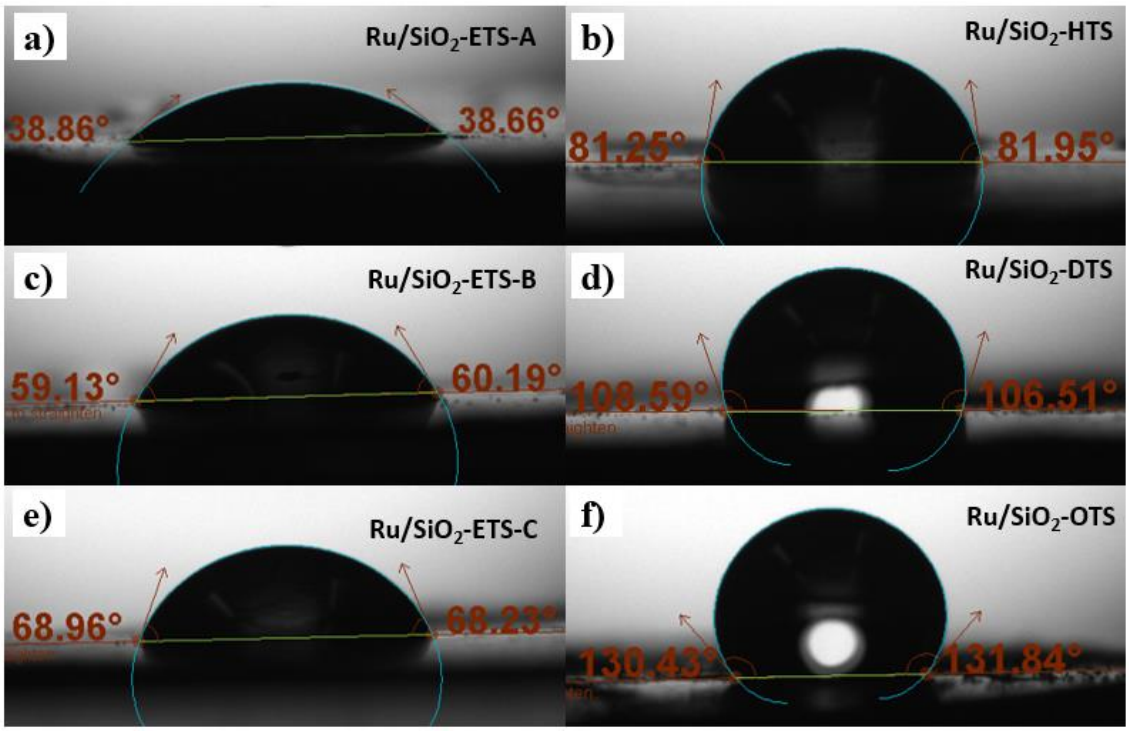

Figure 21. Water-air contact angle (after a few seconds) of Ru/SiO_2 catalysts functionalized with trichloro(alkyl)silanes (ATS) of different alkyl chain length and different density of silanes per surface area. a) Ru/SiO_2-ETS-A (0.69 silanes/nm^2), b) Ru/SiO_2-ETS-B (1.07 silanes/nm^2), c) Ru/SiO_2-ETS-C (1.22 silanes/nm^2), d) Ru/SiO_2-HTS (0.86 silanes/nm^2), e) Ru/SiO_2-DTS (0.97 silanes/nm^2), f) Ru/SiO_2-OTS (1.38 silanes/nm^2).

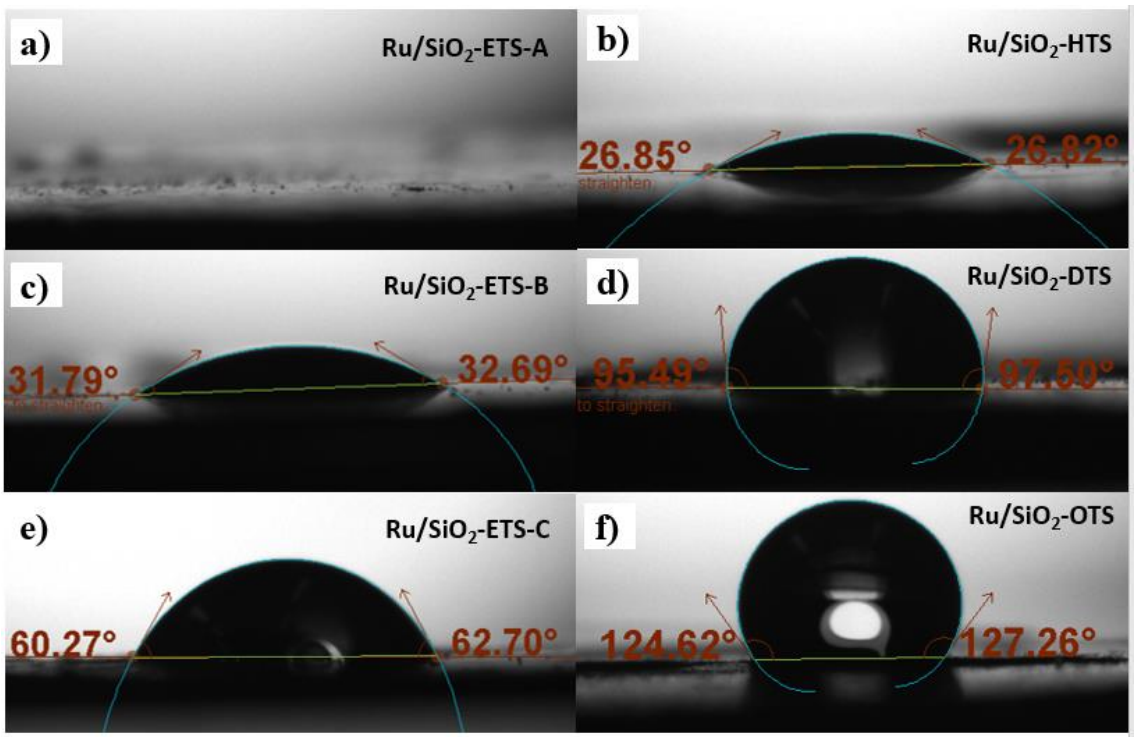

Figure 22. Water-air contact angle (After 60s) of Ru/SiO_2 catalysts functionalized with trichloro(alkyl)silanes (ATS) of different alkyl chain length and different density of silanes per surface area. a) Ru/SiO_2-ETS-A (0.69 silanes/nm^2), b) Ru/SiO_2-ETS-B (1.07 silanes/nm^2), c) Ru/SiO_2-ETS-C (1.22 silanes/nm^2), d) Ru/SiO_2-HTS (0.86 silanes/nm^2), e) Ru/SiO_2-DTS (0.97 silanes/nm^2), f) Ru/SiO_2-OTS (1.38 silanes/nm^2).

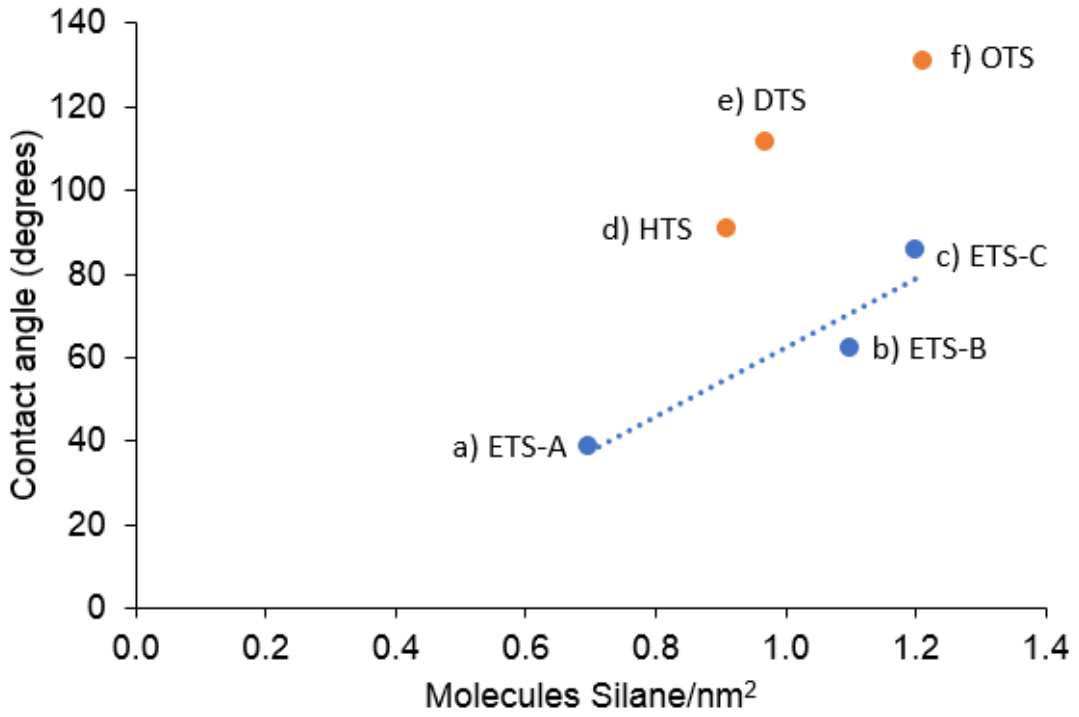

Figure 23. Initial water-air contact angle as a function of density of silanes per nm^2 for Ru/SiO_2 catalysts functionalized with trichloro(alkyl)silanes (ATS) of different alkyl chain length. a) Ru/SiO_2-ETS-A, b) Ru/SiO_2-ETS-B, c) Ru/SiO_2-ETS-C, d) Ru/SiO_2-HTS, e) Ru/SiO_2-DTS, f) Ru/SiO_2-OTS.

3.3.2. Fischer-Tropsch catalytic activity tests

Figure 24 plots CO consumption TOF as a function of silane density. ETS-A and ETS-B catalysts showed small rate enhancements compared to the hydrophilic catalysts even though silane densities were 0.70 and 1.10 silanes/nm^2, respectively. Interestingly, for ETS-C, with slightly higher silane density (1.20 silanes/nm^2) the activity almost doubled (~1077 h^{-1}) compared to the hydrophilic catalyst (569 h^{-1}). This suggests that a minimum concentration of ETS on catalyst surfaces might be required to observe significant rate enhancements. On the other hand, samples functionalized with

organosilanes with longer carbon chains seem to require lower density of silanes to achieve high rates. For example, HTS and DTS showed higher FT rates than all ETS catalysts even though density of silanes was only 0.91 and 0.97 silanes/nm^2, respectively, which was lower than ETS-B but higher than ETS-A. OTS catalysts were prepared with the highest density of silanes (1.21 silanes/nm^2) and resulted in the highest FT rates (1455 h^{-1}).

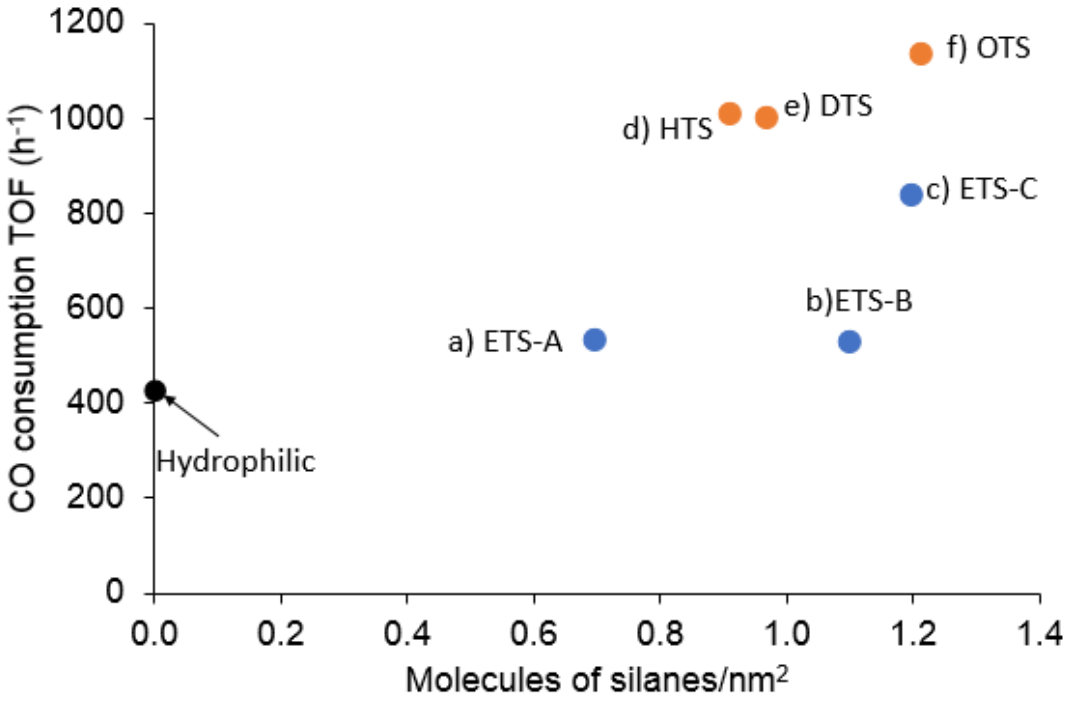

Figure 24. Fischer-Tropsch CO consumption TOF in biphasic decalin/water (13% water) as a function of density of silanes per nm2 in Ru/SiO2. Catalysts are functionalized with trichloro(alkyl)silanes (ATS) of different alkyl chain length. a) Ru/SiO_2-ETS-A, b) Ru/SiO_2-ETS-B, c) Ru/SiO_2-ETS-C, d) Ru/SiO_2-HTS, e) Ru/SiO_2-DTS, f) Ru/SiO_2-OTS . Reaction conditions: Batch reactor; solvents: decalin 70 ml, water 10 ml; 220 °C, 800 psi H2/CO (2/1), 300 rpm, 1h.

As seen in Figure 23, catalysts functionalized with organosilanes of longer carbon chain showed higher hydrophobicity (as measured by contact angles) at similar silane density. Therefore, higher rates in HTS, DTS, and OTS (Figure 24) may be due to higher hydrophobicity. This suggests that contact angle, rather than density of silanes, may be a better descriptor of FT rates in biphasic decalin/water when comparing organosilanes of different carbon chain length.

Figure 25 plots CO consumption TOF as a function of water-air contact angles. ETS-A and ETS-B showed small increases in FT rates compared to hydrophilic catalysts at water-air contact angles of 39° and 62°, respectively. ETS-C showed greater FT rate enhancements at a contact angle of 86° while HTS, DTS and OTS showed the greatest rate values with respective contact angles greater than 90°. FT rate trends in Figure 25 suggest that there are two distinct activity regimes with varying hydrophobicity. That is, at low contact angles (<62°) rates remained at relatively low values close to rates of hydrophilic catalysts (569 to 699 h^{-1}). Meanwhile, higher contact angles (>90°) led to higher values of FT rates (1338 - 1510 h^{-1}). The transition between the two reaction rate regimes occurred between 62° and 90° as exemplified by ETS-C (86°) which showed intermediate reaction FT rates (1115 h^{-1}).

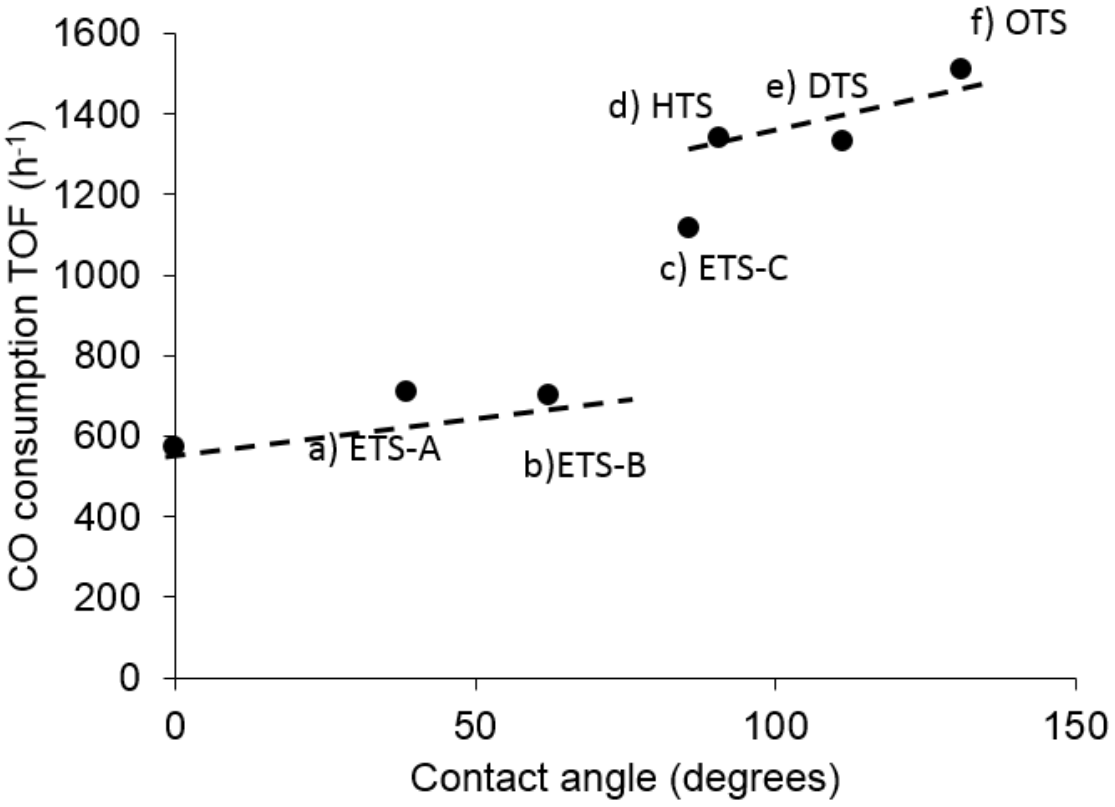

Figure 25. Fischer-Tropsch CO consumption TOF as a function of catalyst hydrophobicity measured by the air-water contact angle. Catalysts are Ru/SiO_2 functionalized with trichloro(alkyl)silanes (ATS) of different alkyl chain length. a) Ru/SiO_2-ETS-A, b) Ru/SiO_2-ETS-B, c) Ru/SiO_2-ETS-C, d) Ru/SiO_2-HTS, e) Ru/SiO_2-DTS, f) Ru/SiO_2-OTS. Reaction conditions: Batch reactor; solvents: decalin 70ml, water 10ml; 220 °C, 800 psi H_2/CO (2/1), 300 rpm, 1h.

Figure 26 plots hydrocarbon selectivity as a function of water-air contact angles. Even though CO consumption turnover frequencies increased significantly at high hydrophobicity (Figure 25), selectivities to hydrocarbons changed only slightly (Figure 26). Selectivity to C6+ hydrocarbons increased from ~80% for the hydrophilic catalyst to ~86% for the most hydrophobic catalyst, while C2-C5 decreased from 13.5% to 11.3%, and CH_4 selectivity decreased from 6.9% to 2.7% for the most hydrophobic

catalyst. This suggests that the positive effect of higher hydrophobicity affects rate-determining steps without significantly modifying chain growth rates. Interestingly, CO_2 formation rates also decreased as a function of hydrophobicity (Figure 27), from ~30h^{-1} for the hydrophilic catalyst to ~5.8 h^{-1} for the most hydrophobic catalyst (OTS).

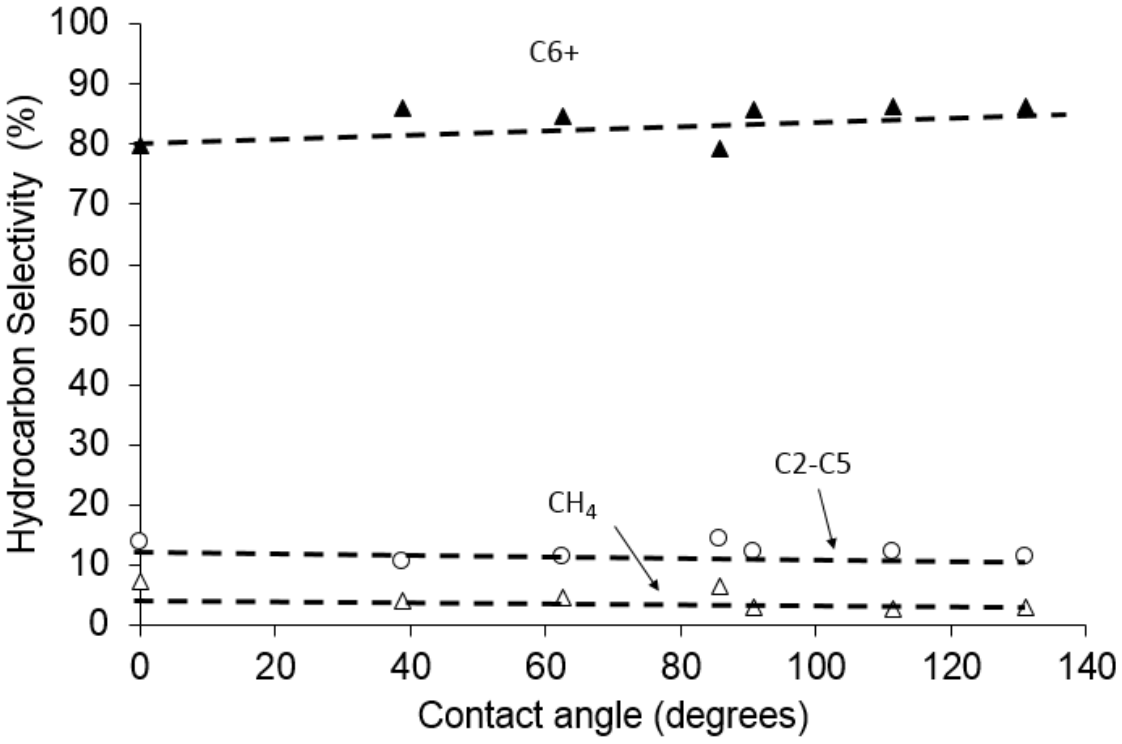

Figure 26. Fischer-Tropsch product selectivity as a function of catalyst hydrophobicity measured by the air-water contact angle. Catalysts are Ru/SiO_2 functionalized with trichloro(alkyl)silanes (ATS) of different alkyl chain length. a) Ru/SiO_2-ETS-A, b) Ru/SiO_2-ETS-B, c) Ru/SiO_2-ETS-C, d) Ru/SiO_2-HTS, e) Ru/SiO_2-DTS, f) Ru/SiO_2-OTS. Reaction conditions: Batch reactor; solvents: decalin 70ml, water 10ml; 220 °C, 800 psi H_2/CO (2/1), 300 rpm, 1h.

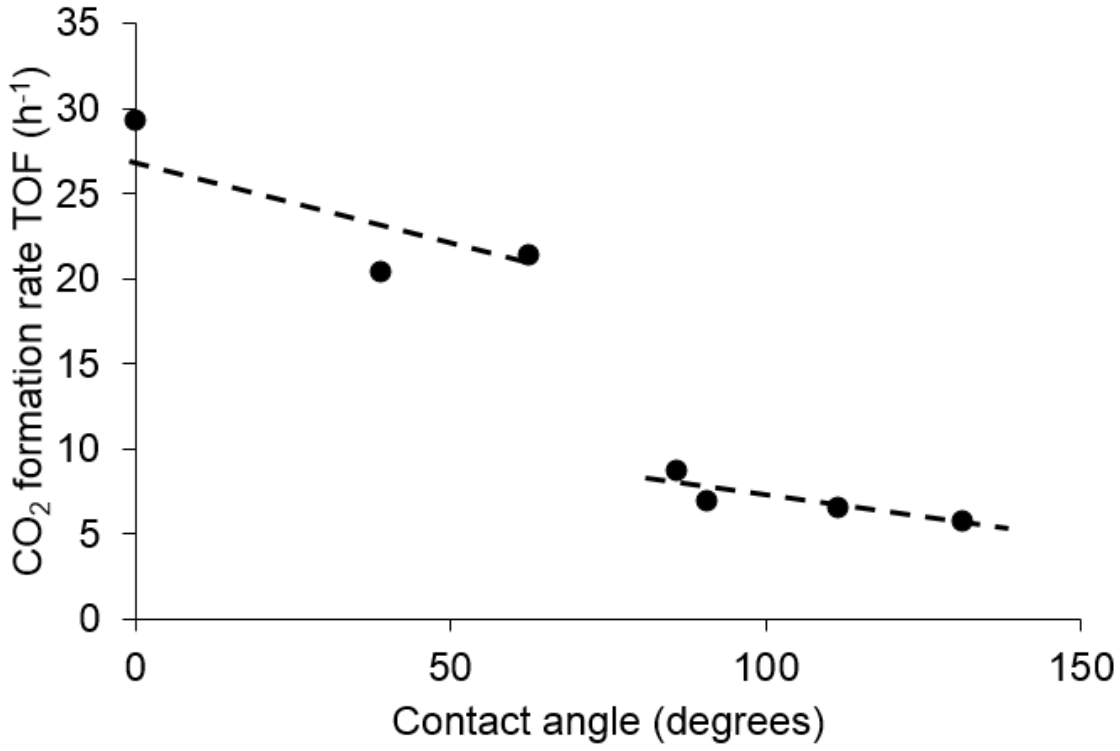

Figure 27. CO_2 formation rate as a function of catalyst hydrophobicity measured by the air-water contact angle. Catalysts are Ru/SiO2 functionalized with trichloro(alkyl)silanes (ATS) of different alkyl chain length. a) Ru/SiO2-ETS-A, b) Ru/SiO2-ETS-B, c) Ru/SiO2-ETS-C, d) Ru/SiO2-HTS, e) Ru/SiO2-DTS, f) Ru/SiO2-OTS. Reaction conditions: Batch reactor; solvents: decalin 70ml, water 10ml; 220 °C, 800 psi H2/CO (2/1), 300 rpm, 1h.

3.4. Discussion

Improved rates on highly hydrophobic Ru/SiO_2 in biphasic FT is consistent with positive effects on activity by organic solvents discussed in chapter 2 of this dissertation. In chapter 2, organic solvents increased FT rates on Ru supported on carbon nanotubes and higher catalyst hydrophobicity improved activity enhancements (Figure 10). However, only two catalysts with different oil wettability were tested as the main goal of that section was to investigate the effect of organic solvents in biphasic media. In this chapter, the effect of hydrophobicity of the catalyst in biphasic FT was systematically investigated on Ru/SiO_2. SiO_2, as catalyst support, is a convenient and

simple material to investigate the effects of oil wettability since hydrophobicity can be easily adjusted and characterized by functionalization with organosilanes.

3.4.1. FT rates in pure decalin, decalin/water, and pure water

Figure 28 compares Ru/SiO_2 (hydrophilic) and Ru/SiO_2-OTS (hydrophobic) in three different solvent systems: pure decalin, water/decalin, and pure water. Both catalysts were tested in pure decalin and decalin/water whereas only the hydrophilic catalyst was tested in pure water. Hydrophobic Ru/SiO_2 does not disperse effectively in pure water solvents but floats on the surface and sticks to the walls of the reactor as it is rejected from the water phase. Therefore, measured rates in pure water for hydrophobic catalysts would contain significant error and, thus, were not performed.

Rates observed for the hydrophilic and hydrophobic catalyst in different solvent systems (Figure 28) are consistent with results for Ru supported on carbon nanotubes of different oil wettability reported in chapter 2 and for Ru supported on carbon nanotube nanohybrids reported elsewhere [52,53]. That is, for hydrophilic catalysts (Ru/SiO_2), catalytic activity increased in biphasic compared to pure decalin and was slightly higher in pure water (Figure 28). On the other hand, hydrophobic catalysts (Ru/SiO_2-OTS) in pure decalin showed higher CO consumption rates than the hydrophilic catalyst in the same solvent. In decalin/water, the hydrophobic catalyst showed significantly higher rates than the hydrophilic in biphasic mixtures or the hydrophilic in pure water.

These results are consistent with high catalyst hydrophobicity as enabler of the positive effects of organic solvents in FT rates both in single-organic and biphasic media. High hydrophobicity might enhance the contact of Ru metal surfaces with organic phases in biphasic and single-phases that in turn enhances FT rates. In the following section, the

phase selective hydrogenation of water-soluble and oil-soluble reactants was carried out in biphasic media to investigate whether, in fact, hydrophobic Ru/SiO_2 catalysts interact preferentially with organic solvents in biphasic decalin/water during FT experiments.

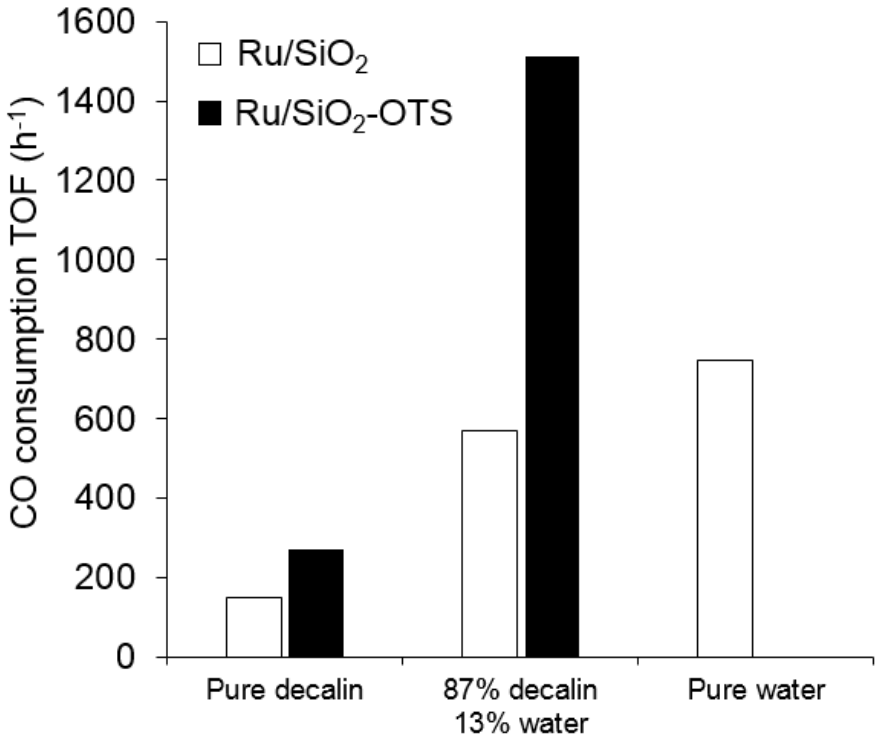

Figure 28. Fischer-Tropsch CO consumption TOF in pure decalin, biphasic decalin/water (13% water), and pure water with two different catalysts: Ru/SiO_2 and Ru/SiO_2-OTS. Reaction conditions: Batch reactor; 80ml solvent, 50mg cat, 220 °C, 800 psi H_2/CO (2/1), 300 rpm, 1h.

3.4.2. Location of catalyst particles in biphasic decalin/water experiments

The hydrogenation of decalin-soluble 1-dodecene and water-soluble 2-butene-1,4-diol was used to determine which phase preferentially wets catalyst particles during biphasic decalin/water reactions (Figure 29). First, the rate of hydrogenation of reactants in pure water and pure decalin was determined. 2-butene-1,4-diol in pure water in the presence of hydrophilic Ru/SiO_2 reacted at a rate of ~1050 h^{-1} while 1-dodecene in pure decalin

in the presence of hydrophobic Ru/SiO_2-HTS reacted at rate of ~1860 h^{-1}. When both molecules were reacted in biphasic decalin/water with only the hydrophilic catalyst the water-soluble reactant was consumed at a higher rate (~610 h^{-1}) than the decalin soluble reactant (~107 h^{-1}). Conversely, when both molecules were reacted in biphasic decalin/water with only the hydrophobic catalyst (Ru/SiO_2-HTS), the decalin-soluble reactant was consumed at a higher rate (~1150 h^{-1}) than the water-soluble reactant (~430 h^{-1}).

These results show that during reaction in biphasic media, hydrophobic catalysts are wetted preferentially by decalin while hydrophilic catalysts are wetted preferentially by water. This very important result confirms that, in fact, during FT in biphasic decalin/water on hydrophobic catalysts, Ru surfaces are wetted preferentially by organic phases and, as a result, FT rates increased (Figure 28). Positive effects on activity by organic phases were discussed before in light of single-site and dual-site mechanistic paths (chapter 2). In single-site mechanistic paths, organic molecules may adsorb on Ru surfaces and disrupt dense CO monolayers, prevalent at high CO pressures, reducing CO-dissociation barriers[68]. In the dual-site mechanism, decalin may play a role in effectively removing hydrocarbon product molecules from Ru surfaces which increase the number of active chain-growth which increases overall rates of reaction.

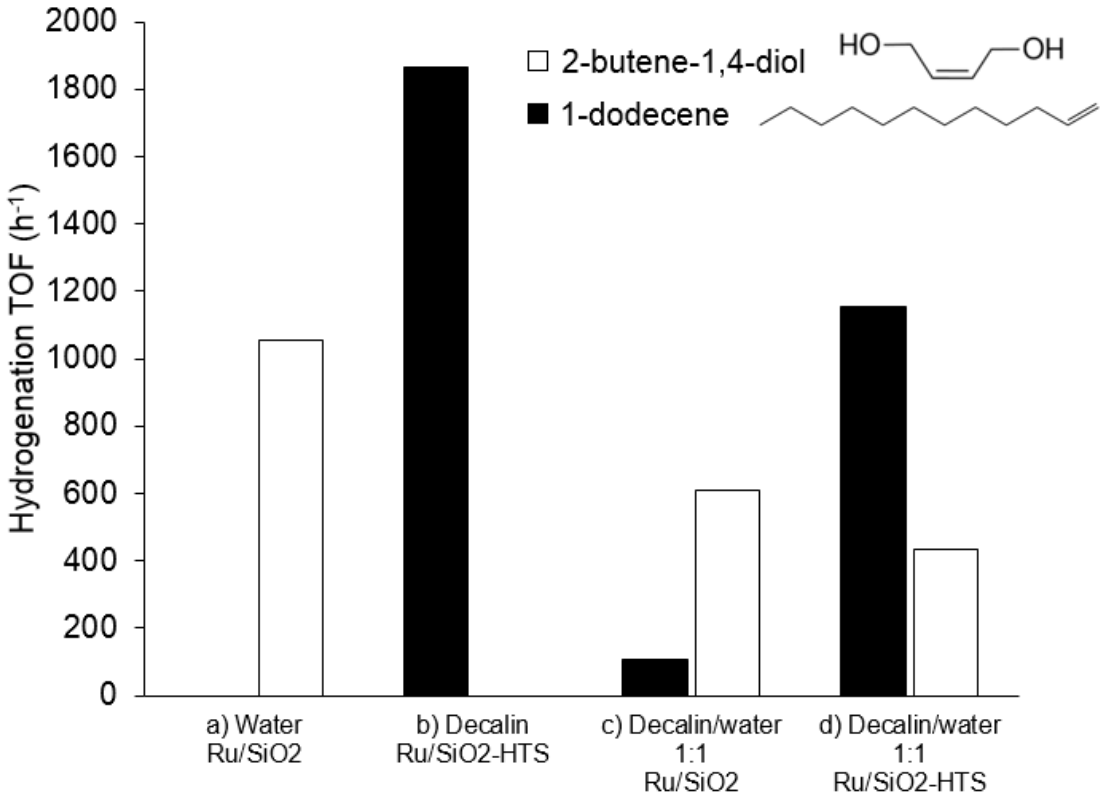

Figure 29. Hydrogenation TOF of water-soluble 2-butene-1,4-diol and decalin-soluble 1-dodecene with a hydrophobic and a hydrophilic catalyst in different solvent systems: a) 2-butene-1,4-diol in pure water with Ru/SiO_2; b) 1-dodecene in pure decalin with Ru/SiO_2-HTS; c) mixed 2-butene-1,4-diol and 1-dodecene in biphasic decalin/water (50% water) with Ru/SiO_2; and d) mixed 2-butene-1,4-diol and 1-dodecene in biphasic decalin/water (50% water) with Ru/SiO_2-HTS. Reaction conditions: 40 °C, 200 psi H_2, 300rpm, 1h. Catalyst amount = 50mg. 2-butene-1,4 diol concentration in water = 0.2M; 1-dodecane concentration in decalin = 0.2M.

3.4.3. FT rates as a function of catalyst hydrophobicity

Hydrophobic Ru/SiO_2 samples obtained by surface silylation showed increasingly higher FT rates with higher hydrophobicity in biphasic decalin/water (Figure 25). Interestingly, Figure 25 suggests that a minimum level of hydrophobicity is required to observe large enhancements in FT rates. At low contact angles (<62°), rates increased only slightly with increasing contact angles, then a steep rate increase took place at

contact angles near 90°. Finally, after reaching higher reaction rates, at contact angles greater than 90°, rates continued increasing only slowly with increasing hydrophobicity. These results suggest that a minimum degree of hydrophobicity is required for catalysts to effectively interact with the organic solvent in oil/water mixtures. Moreover, CO_2 formation from water-gas shift also showed two distinct activity regimes consistent with CO consumption rate trends. When FT rates were low at low contact angles (<62°), CO_2 rates from water-gas shift were high (Figure 27), and when FT rates were high at high contact angles (>90°), CO_2 rates were low, suggesting that high contact with organic phases leads to concomitant reduced contact with water phases that reduced the rate of water-gas shift in biphasic decalin/water.

Surface-anchored alkane moieties, most especially longer-carbon chains, can interact strongly with molecules of organic solvents via van der Waals interactions. When SiO_2 surfaces are significantly covered with organosilanes, strong van der Waals interactions may attract molecules of the organic solvent forming oil films near surfaces which increases hydrophobicity and FT rates (Figure 25). Conversely, when organosilane density is low, oil films may not consistently form on SiO_2 surfaces due to poor van der Waals forces. As a result, catalyst hydrophobicity and FT rates in the presence of organic solvents would be more similar to non-functionalized Ru/SiO_2 (Figure 25). Similar behavior was observed before for multiwall carbon nanotubes (Chapter 2). Hydrophilic defects on carbon nanotube surfaces enabled them to easily disperse in pure water solvents. Nevertheless, when the same carbon nanotubes where placed in biphasic decalin/water, van deer Waals interactions between hydrophobic carbon nanotube surfaces and decalin molecules significantly increased carbon nanotube hydrophobicity

and FT rates. As a result of the increased hydrophobicity, carbon nanotube particles did not disperse in the water phase anymore. Thus, for Ru/SiO_2 functionalized with organosilanes, a minimum surface coverage of organic moieties seems necessary to stabilize a consistent network of organic solvent molecules near catalyst surfaces that effectively increases hydrophobicity and FT rates in biphasic decalin/water.

Consistent with these observations, organosilanes of short carbon chain lengths (ETS) might require higher silane densities than long-carbon-chain silanes (HTS, DTS, OTS) to interact strongly with organic solvents and form oil films on catalyst surfaces that increase FT rates. For example, ETS-B and DTS had similar silane densities, but FT rates were significantly higher on Ru/SiO_2-DTS (Figure 24). Even though ETS-B and DTS molecules on SiO_2 surfaces are separated by similar distances between molecules, the longer 12-carbon DTS chains experience greater van der Waals interactions with organic solvents and neighboring DTS molecules that would enable the formation of organic solvent molecule networks near SiO_2 surfaces. On the other hand, shorter ETS molecules on SiO_2 surfaces, with only 2 carbons per molecule, may not experience very strong van der Waals interactions with organic solvents molecules. As a result, at low surface silane densities, networks of organic solvent molecule cannot consistently form near SiO_2 surfaces and oil wettability might be similar to the non-functionalized Ru/SiO_2. Consistently, ETS-functionalized catalysts required a higher density of silanes (>1.2 silanes/nm^2) to strongly interact with organic solvents and achieve FT rates in the range of the high activity regime (ETS-C, Figure 24).

Finally, largely unchanged selectivities as a function of contact angle in Figure 26 are consistent with effects of organic solvents on FT discussed in Chapter 2. Even though

the contact of catalyst surface with organic solvents was enhanced at higher hydrophobicity, selectivities did not change simply because organic solvents only improve FT rates (Chapter 2). Based on single-site mechanistic paths, organic solvents increase the rate of chain initiation by disrupting dense CO adlayers, prevalent at high CO pressures, which reduces energy barriers for CO-dissociation. Chain growth does not increase because growing hydrocarbon chains have the ability to self-disrupt CO adlayers so there is no added benefit from disruption of the CO monolayers by organic solvents. Based on the dual-site mechanism, the presence of organic solvents increases the number of available chain-growth sites by efficiently removing hydrocarbon products from the surface. This cleaning effect does not affect chain-growth rates, and therefore, should not affect product distributions.

3.5. Conclusions

High hydrophobicity of Ru/SiO_2 catalysts led to higher FT rates in single-decalin and biphasic decalin/water media. Both hydrophilic and hydrophobic Ru/SiO_2 catalysts showed higher FT rates and improved selectivities to long-chain hydrocarbons, in the presence of water, consistent with previous reports. Moreover, FT rates on hydrophobic Ru/SiO_2 catalysts in the presence of organic solvents (decalin) were up to two times higher than hydrophilic Ru/SiO_2. These results are consistent with hydrophobic supports as enablers of positive effects of organic solvents on FT rates on ruthenium metals. Positive effects of organic solvents on FT rates are consistent with single-site and dual-site FT mechanistic paths. In single-site mechanism, organic solvent molecules disrupt dense CO adlayers reducing barriers for CO-dissociation, while in dual-site

mechanistic proposals, organic solvents help effectively clean Ru surfaces and keep the activity of chain-growth sites.

Enhanced contact of hydrophobic catalyst particles with organic phases was proposed to bring about the positive effect of organic solvents on FT rates in biphasic media. To investigate the location of catalyst particles during biphasic experiments, the hydrogenation of water-soluble (2-butene-1,4-diol) and oil-soluble (1-dodecene) reactants was carried out. Hydrophobic Ru/SiO_2 showed higher consumption rates of oil-soluble molecules when both reactants were present, showing that, in fact, during biphasic decalin/water reactions, hydrophobic Ru/SiO_2 particles are wetted preferentially by the organic phase. On the other hand, non-functionalized hydrophilic Ru/SiO_2 showed higher rates of consumption of water-soluble reactants consistent with preferential contact with the aqueous phase during biphasic experiments.

It was proposed that strong van der Waals interactions between surface-anchored alkane moieties and organic solvents might stabilize networks of organic solvent molecules near SiO_2 surfaces which increased catalyst hydrophobicity and FT rates. Thus, when hydrophobicity was low, poor van der Waals interactions led to rates similar to non-functionalized hydrophilic catalysts. Consistently, experiments with varying catalyst hydrophobicity suggest that a minimum level of hydrophobicity was required to observe significant rate enhancements. Distinct high and low activity regimes were observed with varying hydrophobicity measured by the water-air contact angle. Low contact angles (<62°) resulted in FT rates close to non-functionalized hydrophilic Ru/SiO_2 catalysts (569 to 699 h^{-1}), while high contact angles (>90 °) led to high FT activity (1338 - 1510 h^{-1}). Moreover, alkyl silanes of shorter carbon chain length (ETS) required

higher surface silane density than silanes with longer alkyl chains (HTS, DTS, OTS) to observe rates in the high activity regime.

Chapter 4: Ruthenium Particle Size Effects in Fischer-Tropsch Synthesis on Hydrophobic Ru/SiO_2 Catalysts in Biphasic Media

Abstract

Hydrophobic catalysts led to higher FT rates than the hydrophilic counterparts at similar average Ru particle size. Moreover, it appears that introducing hydrophobicity by surface silylation enhances FT rates in the same proportion regardless of the average metal particle size. Ru supported on SiO_2 of varying average metal particle sizes were prepared, characterized and tested in biphasic Fischer-Tropsch (H2:CO = 2:1, 220 °C, 800 psi). Additionally, catalysts with varying Ru particle size were functionalized with organosilanes of different alkyl chain length. Preliminary results for hydrophilic Ru/SiO_2 catalysts with Ru particle sizes in the range 2.44 – 4.78 nm showed FT rate and selectivity trends consistent with reported results in gas phase and aqueous phase. Finally, highly hydrophobic catalysts showed significantly higher TOFs and normalized activity at similar particle sizes.

4.1. Introduction

Fischer-Tropsch converts mixtures of CO and H_2 to hydrocarbons at high pressures and temperatures [27]. Since its discovery in the 1920's, Fischer-Tropsch has attracted enormous industrial and academic interest [5]. From a fundamental perspective, the mechanism of Fischer-Tropsch synthesis has occupied the mind and work of the greatest researches in the last century, and still the nature of the dominant elementary steps remains disputed. It is generally accepted that FT synthesis is a family of surface-polymerization type reactions in which hydrocarbon chains are initiated by the

activation of CO, followed by rapid incorporation of CO-derived monomers, before final desorption as alkanes, alkenes or oxygenated hydrocarbons [77].

FT synthesis is known to be a structure-sensitive reaction [40,77]. Particle sizes smaller than 6-10 nm led to lower FT rates in Co [15] and Ru [16,64]. Conversely, at particle sizes greater than 10 nm, FT rates remained unchanged [15,16]. Conflicting explanations have been given in the literature for the behavior of FT rates as a function of metal particle size. It has been suggested that highly-coordinated, low-index planes, prevalent on larger metal particles, are responsible for FT activity [21,67,68]. In this proposal, H-assisted CO dissociation paths were shown to be the dominant path on Co an Ru catalysts [20]. Alternatively, it was proposed that low-coordination step-edge sites are responsible for FT activity [17,18]. These low-coordination step-edge sites are not stable in small particles but rather in large particles in the so called "open corners" [78]. In this proposal, direct CO dissociation was found to be the preferred path.

While several studies have investigated the effect of particle size on Ru-catalyzed FT in gas phase [16,79] and aqueous phase [51,80,81], no reports have been published on the effect of Ru particle size on FT rates in biphasic media. Here, a series of hydrophilic Ru/SiO_2 catalysts with varying Ru particle sizes were prepared, characterized and tested in biphasic FT. Moreover, hydrophobicity is introduced to catalysts of different particle sizes by surface silylation with organosilanes of different hydrocarbon lengths. Preliminary results obtained are discussed based on proposed explanations for the structure insensitivity of the Fischer-Tropsch reaction.

4.2. Experimental

4.2.1. Catalyst preparation and characterization

Ru supported on silica catalysts were prepared by conventional incipient wetness impregnation (IWI). Silica gel Davisil 646 (Sigma Aldrich) was used as received and labeled "SiO_2". In a typical preparation procedure, the appropriate amount of ruthenium (III) nitrosyl nitrate (Alfa-Aesar), used as metal precursor, was dissolved in deionized water and added dropwise onto 1 g of SiO_2 support. Following, the catalyst was dried, first at room temperature for 6 hours, then at 80 °C in a vacuum oven for 12 hours. After preparation, catalysts were treated in flowing hydrogen at high temperatures to remove nitrosyl nitrate ions and reduce Ru to its metal form. First, the temperature was ramped at 2 °C/min to 120 °C and held for 60 min to assure complete removal of water. Next, the temperature was ramped at 2 °C/min from 120 to 400 °C and held for 3 h before cooling down to room temperature. Post-synthesis treatments were varied to obtain different Ru cluster sizes. For example, heating to 120 °C was omitted for some samples, while ramping rate, final temperature, and holding time were varied to obtain variations in particle size distributions. Table 7 lists details of all catalysts prepared with varying Ru loadings and varying post-synthesis treatment conditions.

Hydrophobicity of Ru/SiO_2 catalysts was modified by surface silylation following a method previously described [74]. In a typical preparation procedure, 1 g of the parent Ru/SiO_2 was dispersed in 20 ml of toluene by horn sonicator at 25% amplitude (Fischer Scientific Model 505C). Next, the suspension was added to a 50 ml solution of the desired alkyl trichlorosilane in toluene. The final suspension was stirred at 500 rpm for 24 h at room temperature. At the end of the treatment period, the material was

recovered by filtration, washed thoroughly with methanol, and dried at 80 °C in a vacuum oven.

Table 7. Summary of Ru/SiO_2 catalysts prepared with varying Ru loading and varying post-synthesis conditions.

Catalyst	Label	Heating rate °C /min	Post-synthesis treatment conditions (H_2 flow)
1%Ru/SiO_2	1$RuSiO_2$	2	1 h at 120 °C, 3 h at 400 °C
3%Ru/SiO_2	3$RuSiO_2$	2	1 h at 120 °C, 3 h at 400 °C
7%Ru/SiO_2-A	7$RuSiO_2$-A	2	1 h at 120 °C, 3 h at 400 °C
7%/$RuSiO_2$-B	7$RuSiO_2$-B	10	1h at 250 °C
7%/$RuSiO_2$-C	7$RuSiO_2$-C	10	1h at 500 °C
7%/$RuSiO_2$-D	7$RuSiO_2$-D	10	3h at 700 °C

Particle size average and distribution was determined from transmission electron microscopy (TEM). TEM images were obtained on a JEOL 2100 field emission system operated at 200 kV. For sample preparation, the sample was pre-reduced in hydrogen at 400 °C for 3 h. Next, a few milligrams of the solid were dispersed in 2-propanol (Sigma-Aldrich) by horn sonication (Fischer Scientific Model 505C) before deposition onto a lacey carbon copper grid. Particle size average and distribution was determined by measuring the diameter of 150 particles using the free software ImageJ. Finally, Ru dispersion (D) was calculated assuming half-sphere-shaped particles using the following equation:

$$D = \frac{\sum \frac{1}{2}\pi d_i^2 \rho_P}{\sum \frac{1}{12}\pi d_i^3 \rho_B}$$

where d_i is the measured diameter of particle i, ρ_P is the planar density for Ru(0001) in atoms/nm^2 and ρ_B is the atom bulk density in atoms/nm^3.

Thermogravimetric analysis (TGA) was used to measure the mass of functional groups attached to SiO_2 surfaces. TGA was completed using a Netzsch STA-449 F1 Jupiter equipped with a type S thermocouple and a nanobalance in single furnace configuration. In a typical test, a sample of hydrophobic Ru/SiO_2 was placed in the TGA cell under constant flow of argon (20 ml/min) and air (40 ml/min). After pre-heating to 40 °C, the temperature in the cell was ramped at 2° C/min to 750 °C. N_2 physisorption was performed using a micromeritics ASAP 2000 unit. Prior to analysis the samples were degassed in situ at 180 ºC for 6 h.

4.2.2. Fischer-Tropsch catalytic activity tests

Fischer-Tropsch activity measurements were carried out in a 300-ml autoclave Parr reactor (Parr Inst. 4560) operating in batch mode. The temperature inside the reactor was controlled with a CAL 9500P controller (CAL controls Ltd) while pressure was monitored with an industrial digital pressure gauge (Ashcroft 2074). In a typical run, 50-200 mg of catalyst were dispersed in 70 ml of decalin (mix cis + trans, Sigma Aldrich) by horn sonicator at 50% amplitude (Fischer Scientific Model 505C). Next, 10 ml of deionized water (18 MΩ) were added and the final mixture sonicated again at 50% amplitude. Next, the reactor was sealed and purged, first with N_2 and then with H_2, before pressurizing to 500 psi with H_2 for in-situ catalyst reduction at 250 °C for 1 h. After completing the reduction step, the reactor was cooled down and depressurized, before purging and pressurizing again to 800 psi with H_2/CO (ratio 2/1) for reaction, while stirring at 300 rpm. After stabilization of the pressure reading, the reactor was heated to the reaction temperature (220 °C) and held for the desired reaction time,

typically 1-3 h. When the reaction period ended the reactor was quickly cooled down to room temperature and a high-pressure gas sample was taken.

Gas samples were analyzed with GC-TCD and GC-MS to quantify CO, H_2, light hydrocarbons, and CO_2. GC-TCD (Carle 400 AGC) was used to measure concentrations of CO, H_2 and CO_2 while light hydrocarbons (C1-C7) were detected and measured with a GC-MS (GC Agilent 7820A, MS 5975 Series MSD) equipped with a capillary, bonded polystyrene-divinylbenzene (DVB) column (HP-PLOT/Q) of 30 m x 0.320 mm x 20.0 μm. Liquid products were separated from solid catalyst particles by centrifugation followed by filtration with a 0.22 μm PTFE filter forming two immiscible layers of clear liquid. Both phases were analyzed by GC-MS and GC-FID. For product identification, a Shimadzu QP2010 GC–MS equipped with a mid-polarity (Phenomenex ZB-1701) capillary column, 60.0 m x 0.25 mm x 0.25 μm nominal, was used, while product quantification was performed with an Agilent GC-FID 7890B equipped with a capillary, low polarity column (Phenomenex ZB-5) 60.0 m x 0.25mm x 0.25 μm. Standards were used where possible to determine FID response factors and phenol was used as an internal standard to help close mass balances. Turnover frequencies (TOF) based on CO consumption and yields and selectivities based on moles of C were calculated as follows:

$$TOF\ (h^{-1}) = \frac{mol\ CO\ reacted}{mol\ Ru\ exposed \cdot h}$$

$$\%\ Yield = \frac{Total\ mol\ C\ in\ product}{mol\ of\ C\ in\ CO\ (initial)}\ x\ 100$$

$$\%\ Selectivity = \frac{mol\ of\ C\ in\ product}{Total\ mol\ of\ C\ in\ all\ products} \times 100$$

4.3. Preliminary results and discussion

4.3.1. Catalyst preparation and characterization

Figure 30 through Figure 32 show TEM images and particle size distributions for all catalysts prepared. Catalysts with increasing Ru metal particle size were successfully synthesized, with average particle sizes ranging from 2.44 nm to 4.78 nm. Increasing Ru loading from 1% to 7% ($1RuSiO_2$, $3RuSiO_2$, $7RuSiO_2$-A) without changes in post-synthesis treatment conditions (Table 7) resulted in particle sizes ranging from 2.44 to 2.76 nm, while varying post-synthesis treatments conditions for catalysts with 7% Ru ($7RuSiO_2$ A to D) led to Ru metal particle sizes ranging from 2.76 to 4.78 nm. Interestingly, particle size distributions were narrower for smaller particle sizes (Figure 30 and Figure 31) and wider for catalysts with larger Ru metal particles (Figure 32). Dispersions for all catalysts were calculated based on TEM images and reported in Table 8 in order of increasing average particle size. Consistently, and despite variations in widths of size distributions, metal dispersions decreased with increasing average metal particle size.

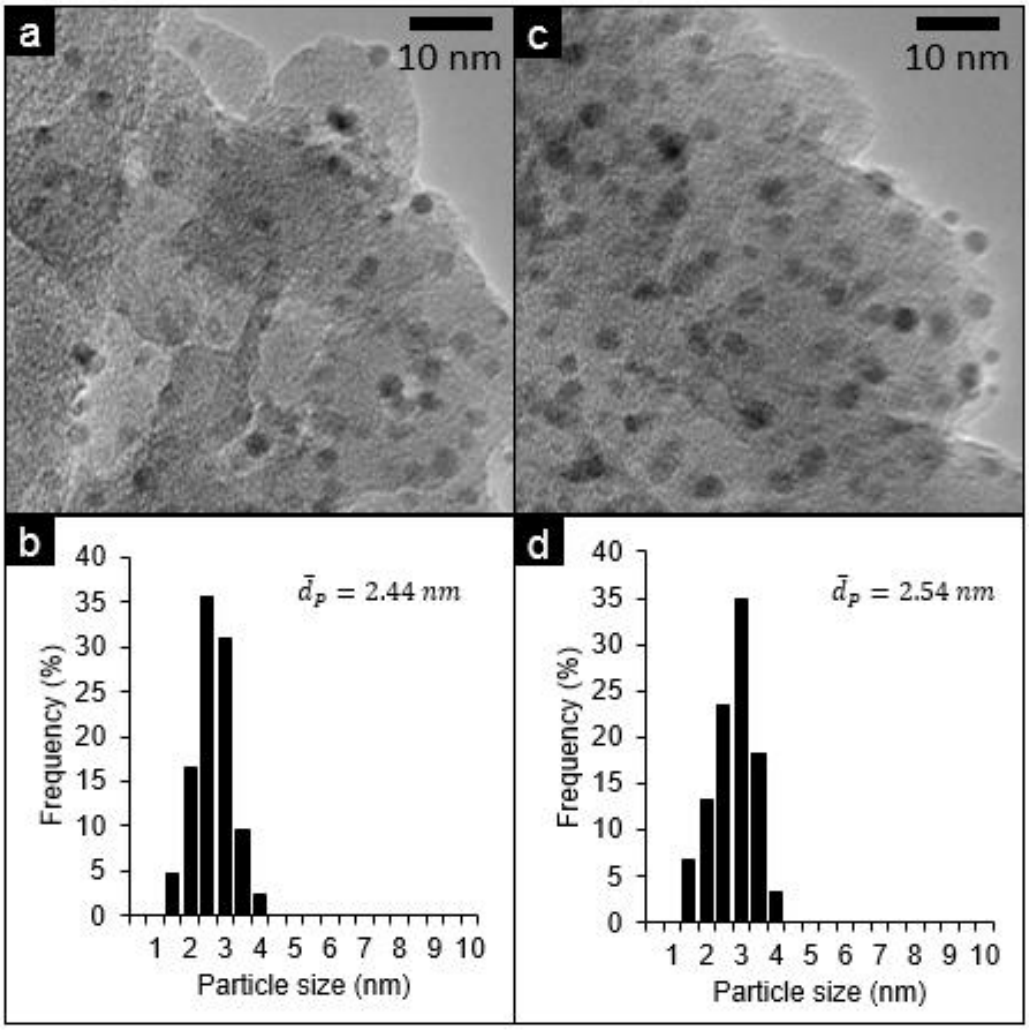

Figure 30. Transmission Electron Microscopy (TEM) images of Ru/SiO_2 catalysts and their corresponding particle size distributions. a) and b) $3RuSiO_2$. c) and d) $1RuSiO_2$.

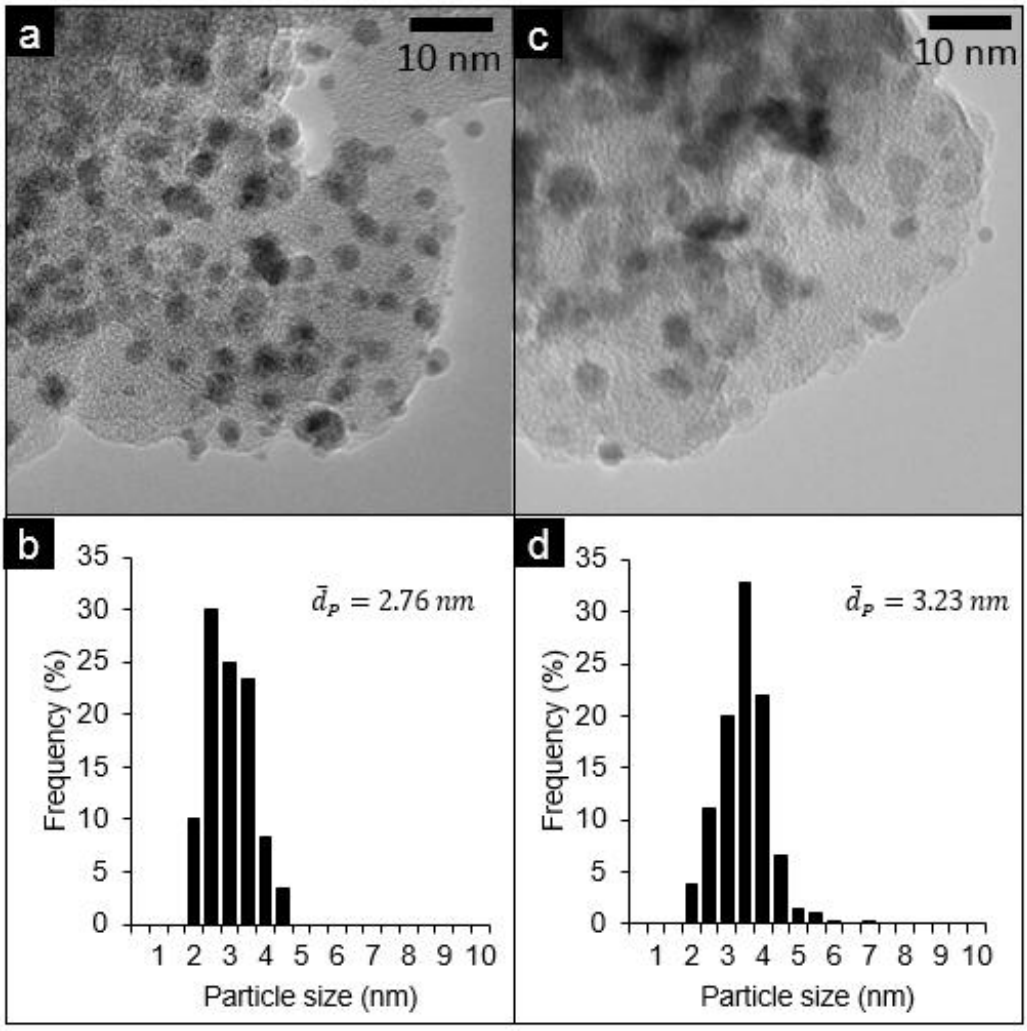

Figure 31. Transmission Electron Microscopy (TEM) images of Ru/SiO_2 catalysts and their corresponding particle size distributions. a) and b) $7RuSiO_2$-A c) and d) $7RuSiO_2$-B.

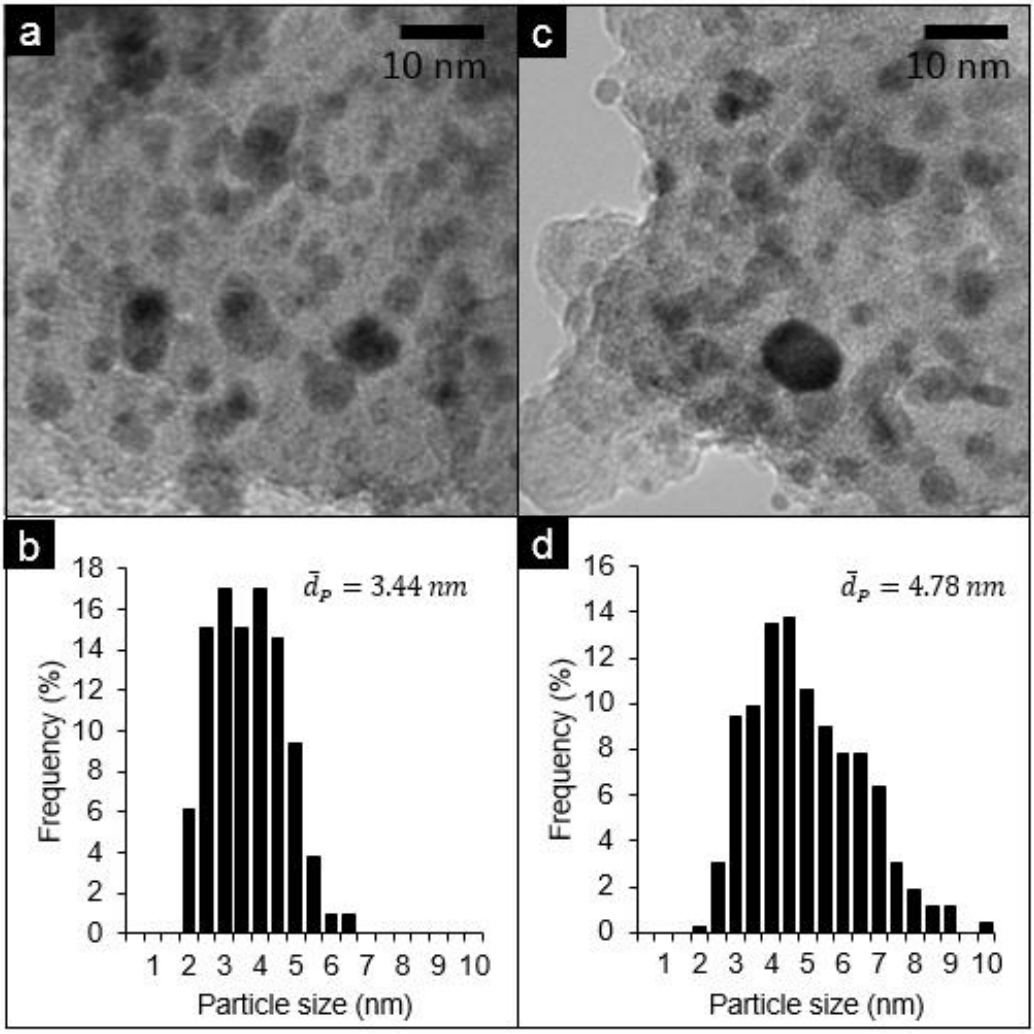

Figure 32. Transmission Electron Microscopy (TEM) images of Ru/SiO_2 catalysts and their corresponding particle size distributions. a) and b) $7RuSiO_2$-C c) and d) $7RuSiO_2$-D.

Table 8. Summary of average metal particle size and dispersion for Ru/SiO_2 catalysts based on TEM analysis.

Catalyst	$\overline{dp}$	D
$3RuSiO_2$	2.44	48.8
$1RuSiO_2$	2.54	46.2
$7RuSiO_2$-A	2.76	42.8
$7RuSiO_2$-B	3.23	36.5
$7RuSiO_2$-C	3.44	32.5
$7RuSiO_2$-D	4.78	22.1

Table 9 lists hydrophobic Ru/SiO_2 catalysts prepared in this study. Samples of parent $3RuSiO_2$ and $7RuSiO_2$-A were functionalized with trichloro(ethyl)silane (ETS) of similar concentrations while a sample of parent $7RuSiO_2$-A was also functionalized with trichloro(octadecyl)silane (OTS) at higher concentration. Data for $3RuSiO_2$-ETS is not available in Table 9 but values are expected to be similar to $7RuSiO_2$-A-ETS as preparation procedures were identical. Weight percent of silanes in Table 9, calculated from TGA weight loss showed that $7RuSiO_2$-A-OTS had a higher silane content than samples functionalized with ETS. Consistently, BET surface area for OTS-functionalized catalysts was significantly lower as higher concentrations of the bulkier octadecyl moieties are likely to block pores and decrease access to surfaces. Silane density was calculated based on silane mass and BET surface area and reported in Table 9. Higher silane density for OTS-functionalized catalysts (1.21 molecules/nm^2) led to higher catalyst hydrophobicity as suggested by measured water-air contact angles. Finally, Ru particle sizes were found to be unchanged after silane functionalization as confirmed by TEM imaging.

Table 9. Ru/SiO_2 functionalized with trichloro(alkyl)silanes of different alkyl chain length: Weight percent of silane, BET surface area, density of silanes per surface area.

Sample	Weight % silane†	BET Area (m^2/g SiO_2)	Silane density molecules/nm^2	Water-air contact angle
SiO_2 (Davisil 646)	-	283.2	-	-
$3RuSiO_2$-ETS	NA	NA	NA	NA
$7RuSiO_2$-A-ETS	4.8	286.6	0.70	38.8 °
$7RuSiO_2$-A-OTS	17.1	248.6	1.21	131.1 °

† Calculated based on TGA measurements.

4.3.2. Fischer-Tropsch as a function of Ru particle size

Figure 33 shows CO consumption turnover frequencies (TOF) as a function of Ru average metal particle size for hydrophilic and hydrophobic Ru/SiO_2 catalysts in biphasic decalin/water. Under the conditions of this study, CO consumption TOF increased with increasing Ru particle size for non-functionalized Ru/SiO_2 catalysts in the range 2.44 to 4.78 nm. These results are consistent with previous reports for aqueous and gas phase FT where CO consumption TOF as a function of Ru particle size was found to increase at particle sizes beyond 5 nm [16,51,80,81]. Carballo *et. al.* [16] found that, at 250 °C, CO consumption TOF increased with Ru particle size and reached a plateau at Ru particle diameters close to 10 nm, while Kang et. al. [80], operating at 150 °C, showed that FT TOF stopped increasing at particle diameters close to 6 nm. ETS-functionalized catalysts showed higher FT rates than hydrophilic catalysts at the same Ru particle size (Figure 33). Interestingly, both 3RuSiO2-ETS and 7RuSiO2-A-ETS increased FT rates to similar extents compared to their non-functionalized counterparts. That is, FT rates in hydrophobic catalysts increased approximately 1.2-1.4 times compared the hydrophilic homologue. This suggests that hydrophobic catalysts in biphasic decalin/water enhance the rate of the active sites in the same proportion regardless of Ru particle size. Nevertheless, additional experiments with hydrophobic Ru/SiO_2 of different Ru particle size need to be performed to confirm that these observations are true for all Ru particle sizes in this study.

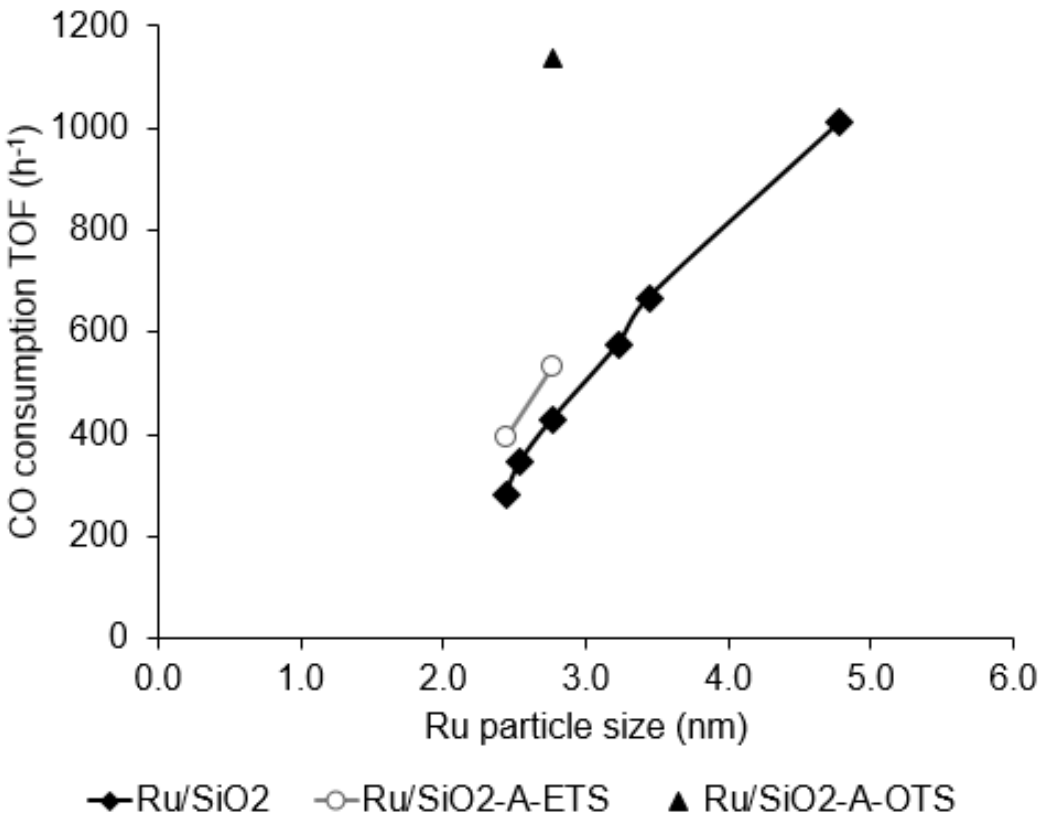

Figure 33. Fischer-Tropsch CO consumption TOF as a function of Ru metal particle size for hydrophilic and ETS functionalized Ru/SiO_2 catalysts. Reaction conditions: Decalin 70ml, water 10ml, 220 °C, 800 psi H_2/CO (2/1), 300 rpm, 1h. In situ reduction: 250 °C, 500 psi H_2, 1h).

FT rates for 7RuSiO_2-OTS at 2.76 nm are also plotted in Figure 33. Increasing hydrophobicity at low Ru particle size (2.76 nm) increased TOFs (1135.7 h^{-1}) beyond the FT rates observed for hydrophilic catalysts with the largest particle size (4.78 nm, 1012.9h^{-1}). Moreover, FT activity per gram of Ru catalyst increased significantly as shown in Figure 34. For hydrophilic catalysts, FT activity increased initially with increasing Ru particle size and reached a plateau at around 3.44 nm (Figure 34). ETS-functionalized Ru/SiO_2 seems to follow similar trends and would be expected to reach the plateau at a higher FT activity level when more data points are added at bigger

particle sizes. It is evident, however, that 7RuSiO$_2$-OTS reached significantly higher FT-specific activities than all other catalysts even at smaller particle sizes (Figure 34). Thus, FT rates for OTS-functionalized Ru/SiO$_2$ at higher Ru particle sizes (4.78 nm) are expected to be significantly higher than hydrophilic catalysts.

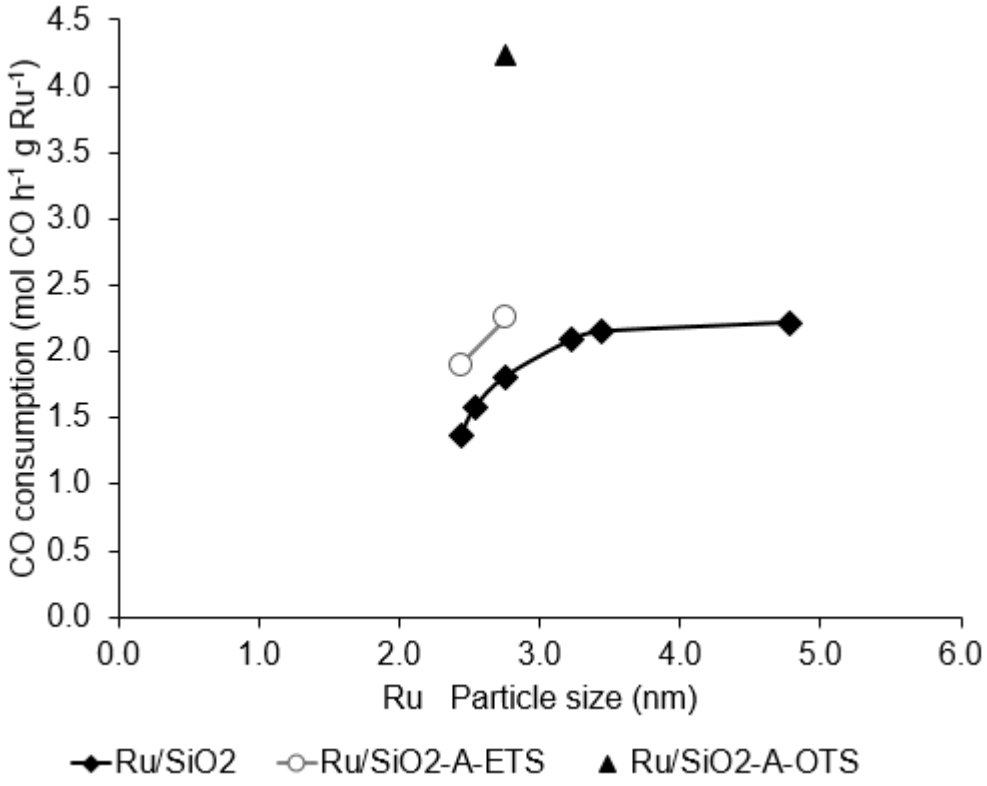

Figure 34. Fischer-Tropsch specific activity normalized by Ru loading for hydrophilic and ETS functionalized Ru/SiO$_2$ catalysts. Reaction conditions: Decalin 70ml, water 10ml, 220 °C, 800 psi H$_2$/CO (2/1), 300 rpm, 1h. In situ reduction: 250 °C, 500 psi H$_2$, 1h.

Figure 35 shows product selectivity as a function of particle size for hydrophilic Ru/SiO$_2$ catalysts. As average Ru metal particle size increased, selectivity to long-chain hydrocarbons increased slightly (C6+), while selectivity to light hydrocarbons showed a small decline (CH_4, C2-C5). This is consistent with work by Kellner and Bell [79] that showed that FT chain-growths remained largely unchanged as a function of Ru particle

size at dispersions lower than 0.7. Similarly, Carballo et. al. [16] observed only slight changes in selectivity with Ru particle sizes up to 25 nm.

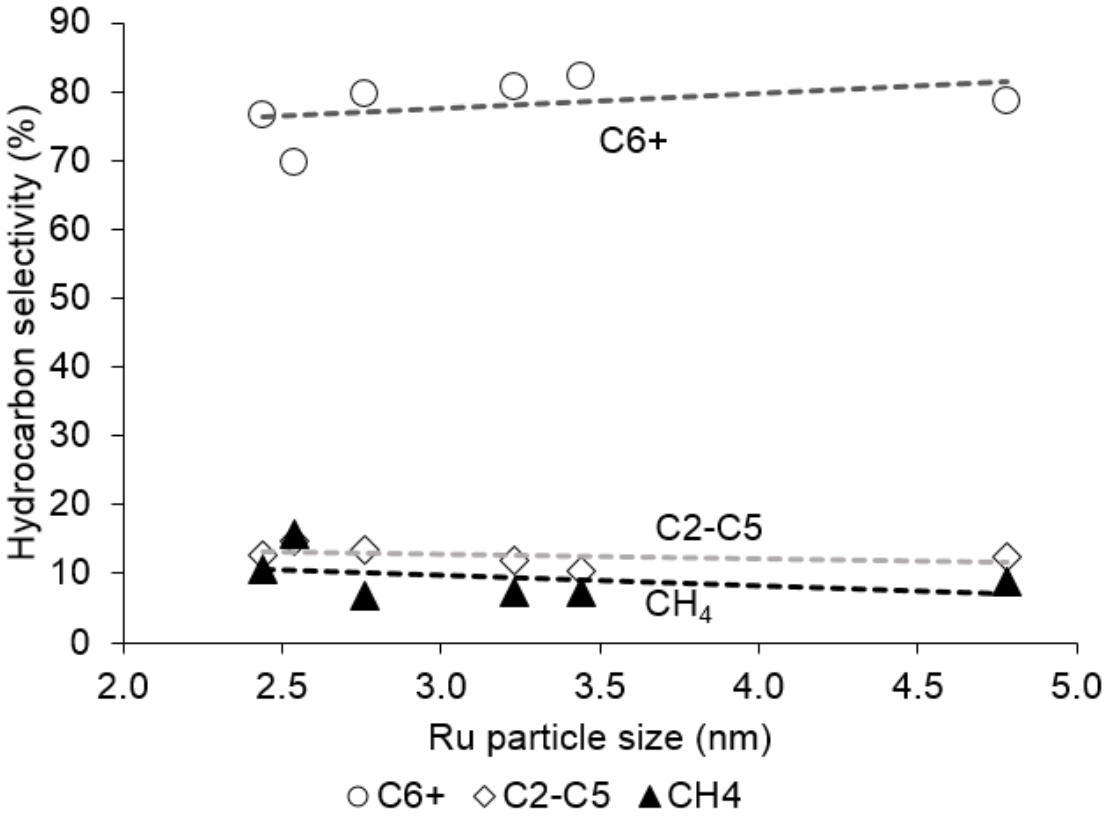

Figure 35. Fischer-Tropsch selectivity as a function of Ru metal particle sized for hydrophilic and ETS functionalized Ru/SiO_2 catalysts. Reaction conditions: Decalin 70ml, water 10ml, 220 °C, 800 psi H_2/CO (2/1), 300 rpm, 1h. In situ reduction: 250 °C, 500 psi H_2, 1h.

Table 10 compares FT selectivities for hydrophilic and hydrophobic Ru/SiO_2 catalysts of similar particle size and varying hydrophobicity in biphasic decalin/water. Selectivity to long-chain hydrocarbons (C6+) increased to 86% for the most hydrophobic $7RuSiO_2$-A-OTS, which is greater than the highest C6+ selectivity observed with varying particle sizes for hydrophilic Ru/SiO_2 (~82%). This suggests that while chain-growth rate increases slightly with increasing particle size, hydrophobic catalysts bring about greater increases in chain-growth.

Table 10. Preliminary results of activity and selectivity for hydrophilic and hydrophobic Ru/SiO_2 catalysts as Decalin 70ml, water 10ml, 220 °C, 800 psi H_2/CO (2/1), 300 rpm, 1h. Conversion ~10%.

Sample	dp	TOF	Activity	Selectivity (%)		
	nm	h^{-1}	mol CO/ h g Ru	CH_4	C2-C5	C6+
7RuSiO2	2.76	428.0	1.81	6.9	13.5	79.7
7RuSiO2-ETS	2.76	531.5	2.25	4.1	10.3	85.7
7RuSiO2-OTS	2.76	1135.7	4.24	2.7	11.3	86.0

4.4. Conclusions

Higher turnover frequencies with increasing Ru average particle sizes in the range 2.44-4.78 nm for hydrophilic Ru./SiO_2 catalysts is consistent with previous reports on the effect of Ru particle size in gas phase and aqueous phase. As discussed in Chapter 3 of the present dissertation, hydrophilic Ru/SiO_2 catalysts in biphasic media showed similar FT rates and selectivities than pure aqueous solvents. Therefore, their performance as a function of particle size in biphasic media was expected to be similar to aqueous phase experiments. Moreover, hydrocarbon selectivity as a function of average Ru particle size remain largely unchanged which is consistent with previous observations that chain-growth probabilities are not significantly affected by particle size. Interestingly, hydrophobization with ETS led to increased FT rates in a similar proportion regardless of the particle size. However, further experiments with ETS-functionalized catalysts with varying particle sizes are required to confirm these observations. Finally, the most hydrophobic OTS-functionalized Ru/SiO_2 with a relatively small Ru particle size (2.76 nm) showed the greatest increase in TOF and normalized rates even beyond the largest average Ru particle size for hydrophilic catalysts.

Appendix A: Supporting Information Chapter 2

A.1. Ethylene hydrogenation experiments

Low temperature ethylene hydrogenation is a classical structure-insensitive reaction used to probe the exposed metal surface area of catalysts [82]. While ethylene hydrogenation is structure-insensitive, ethane hydrogenolysis is not [83]. Therefore, higher temperatures may lead to a variety of surface species [84]. We were careful to confirm that, at the low-temperature conditions of these experiments, no hydrogenolysis products were observed. Following, Ru particle sizes for Ru/CNT and Ru/CNT-Ox were determined based on known rates of ethylene hydrogenation measured on Ru/TiO_2 catalysts of known Ru particle size.

First, ethylene hydrogenation rates at 5% conversion were measured in a fully characterized Ru/TiO_2 catalyst (Table A1). Ru particle sizes in Ru/TiO_2 were determined by TEM; BET surface area by N_2 physisorption; and Ru weight percent was confirmed by Inductively Coupled Plasma (ICP). Additionally, no measurable ethylene conversion was observed on TiO_2 alone. Next, ethylene hydrogenation rate at 5% conversion on Ru/CNT and Ru/CNT-Ox was measured and the average Ru particle size determined by assuming ethylene hydrogenation TOFs remained unchanged (Table A2).

Table A1. Ru/TiO_2 catalyst properties.

Catalyst	ICP (wt %)	BET Surface Area (m^2/g)	Average Particle size (nm)
Ru/TiO_2	4.4	55	3.17

Table A2. Measured rates and calculated particle size and dispersions for Ru/CNT and Ru CNT-Ox

Catalyst	ICP (wt %)	Rate (mol/mol Ru s)	Dispersion (%)	Particle Size (nm)
Ru/CNT-Ox	8.66	4.38	48.07	2.98
Ru/CNT	9.03	4.88	50.46	2.84

A.2. Comparison of FT rates in the present work with values reported in the literature.

Table A3. FT rates in the present work compared to values reported in the literature.

	Particle size	Temperature	CO/H_2 ratio	System	Water	Specific CO consumption rate	CO consumption TOF
	nm	T(°C)				Mole CO/mole Ru h	h^{-1}
Liu et al. 2017 †	1.9	160	2/1	Liquid phase	Pure H_2O	12	16
Liu et al. 2017	6.8	160	2/1	Liquid phase	Pure H_2O	7.8	37
Hibbitts et al. 2013 ‡	7	190	4.5/1	Vapor Phase	No H_2O	31	165
Hibbitts et al 2013	7	190	4.5/1	Vapor Phase	Vapor H_2O	68	350
Carballo et al. 2011 *	12.5	250	10/1	Vapor phase	No H_2O	51	464
Present Work	2.8	160	4/1	Liquid Phase	Decalin/H_2O	16	32
Present Work	2.8	190	4/1	Liquid phase	Pure water	35	71
Present work	2.8	190	4/1	Liquid phase	Decalin/H_2O	81	162
Present work	2.8	220	4/1	Liquid phase	Pure water	168	335.1
Present work	2.8	220	4/1	Liquid phase	Decalin/H_2O	313	626.8

† Liu *et al.* 2017 [85]
‡ Hibbitts *et al.* 2013[39]
* Carballo *et al.* 2011 [16]

A.3. FT activity of Ru/SiO2-OTS catalysts.

Table A4. Activity of Ru/SiO2 catalysts compared to most active run for Ru/CNT (220 C, 800 psi H2/CO (4/1)).

Catalyst	Rate h^{-1}	Rate mol CO/g cat h
Ru/CNT	608.4	0.27
Ru/SiO_2-OTS	841.4	0.40

References

[1] G.P. Van Der Laan, A.A.C.M. Beenackers, Kinetics and Selectivity of the Fischer–Tropsch Synthesis: A Literature Review, Catal. Rev. 41 (1999) 255–318. doi:10.1081/CR-100101170.

[2] R. Guettel, U. Kunz, T. Turek, Reactors for Fischer-Tropsch Synthesis, Chem. Eng. Technol. 31 (2008) 746–754. doi:10.1002/ceat.200800023.

[3] R.D. (Burns and R.S.C. (US)) Srivastava, V.U.S. Rao, G. Cinquegrane, G.J. (Pittsburgh E.T.C. Stiegel, Catalysts for Fischer-Tropsch, Hydrocarb. Process. USA. 69:2 (1990). https://www.osti.gov/scitech/biblio/6987043 (accessed March 16, 2017).

[4] V.U.S. Rao, G.J. Stiegel, G.J. Cinquegrane, R.D. Srivastava, Iron-based catalysts for slurry-phase Fischer-Tropsch process: Technology review, Fuel Process. Technol. 30 (1992) 83–107. doi:10.1016/0378-3820(92)90077-4.

[5] M.E. Dry, The Fischer–Tropsch process: 1950–2000, Fisch.-Tropsch Synth. Eve XXI Century. 71 (2002) 227–241. doi:10.1016/S0920-5861(01)00453-9.

[6] S.N. Khadzhiev, A.S. Lyadov, M.V. Krylova, A.Y. Krylova, Fischer-Tropsch synthesis in a three-phase system with iron catalyst nanoparticles, Pet. Chem. 51 (2011) 24–31. doi:10.1134/S0965544111010075.

[7] H. Kölbel, M. Ralek, The Fischer-Tropsch Synthesis in the Liquid Phase, Catal. Rev. 21 (1980) 225–274. doi:10.1080/03602458008067534.

[8] M.E. Dry, T. Shingles, L.J. Boshoff, G.J. Oosthuizen, Heats of chemisorption on promoted iron surfaces and the role of alkali in Fischer-Tropsch synthesis, J. Catal. 15 (1969) 190–199. doi:10.1016/0021-9517(69)90023-2.

[9] M.A. Vannice, The catalytic synthesis of hydrocarbons from H2CO mixtures over the group VIII metals, J. Catal. 37 (1975) 449–461. doi:10.1016/0021-9517(75)90181-5.

[10] B. Jager, R. Espinoza, Advances in low temperature Fischer-Tropsch synthesis, Catal. Today. 23 (1995) 17–28. doi:10.1016/0920-5861(94)00136-P.

[11] S.T. Sie, M.M.G. Senden, H.M.H. Van Wechem, Conversion of natural gas to transportation fuels via the shell middle distillate synthesis process (SMDS), Catal. Today. 8 (1991) 371–394. doi:10.1016/0920-5861(91)80058-H.

[12] E. Iglesia, S.C. Reyes, R.J. Madon, S.L. Soled, Selectivity Control and Catalyst Design in the Fischer-Tropsch, Adv. Catal. 39 (1993) 221.

[13] H. Pichler, H. Buffleb, Brennst. Chem. 21 (1940) 273.

[14] J.-Y. Park, Y.-J. Lee, P.K. Khanna, K.-W. Jun, J.W. Bae, Y.H. Kim, Alumina-supported iron oxide nanoparticles as Fischer–Tropsch catalysts: Effect of particle size of iron oxide, J. Mol. Catal. Chem. 323 (2010) 84–90. doi:10.1016/j.molcata.2010.03.025.

[15] G.L. Bezemer, J.H. Bitter, H.P.C.E. Kuipers, H. Oosterbeek, J.E. Holewijn, X. Xu, F. Kapteijn, A.J. van Dillen, K.P. de Jong, Cobalt Particle Size Effects in the Fischer−Tropsch Reaction Studied with Carbon Nanofiber Supported Catalysts, J. Am. Chem. Soc. 128 (2006) 3956–3964. doi:10.1021/ja058282w.

[16] J.M.G. Carballo, J. Yang, A. Holmen, S. García-Rodríguez, S. Rojas, M. Ojeda, J.L.G. Fierro, Catalytic effects of ruthenium particle size on the Fischer–Tropsch Synthesis, J. Catal. 284 (2011) 102–108. doi:10.1016/j.jcat.2011.09.008.

[17] S. Shetty, A.P.J. Jansen, R.A. van Santen, Direct versus Hydrogen-Assisted CO Dissociation, J. Am. Chem. Soc. 131 (2009) 12874–12875. doi:10.1021/ja9044482.
[18] I.M. Ciobica, R.A. van Santen, Carbon Monoxide Dissociation on Planar and Stepped Ru(0001) Surfaces, J. Phys. Chem. B. 107 (2003) 3808–3812. doi:10.1021/jp030010x.
[19] I.A.W. Filot, R.A. van Santen, E.J.M. Hensen, The Optimally Performing Fischer-Tropsch Catalyst, Angew. Chem. 126 (2014) 12960–12964. doi:10.1002/ange.201406521.
[20] M. Ojeda, R. Nabar, A.U. Nilekar, A. Ishikawa, M. Mavrikakis, E. Iglesia, CO activation pathways and the mechanism of Fischer–Tropsch synthesis, J. Catal. 272 (2010) 287–297. doi:10.1016/j.jcat.2010.04.012.
[21] M. Ojeda, A. Li, R. Nabar, A.U. Nilekar, M. Mavrikakis, E. Iglesia, Kinetically Relevant Steps and H2/D2 Isotope Effects in Fischer−Tropsch Synthesis on Fe and Co Catalysts, J. Phys. Chem. C. 114 (2010) 19761–19770. doi:10.1021/jp1073076.
[22] B.T. Loveless, C. Buda, M. Neurock, E. Iglesia, CO Chemisorption and Dissociation at High Coverages during CO Hydrogenation on Ru Catalysts, J. Am. Chem. Soc. 135 (2013) 6107–6121. doi:10.1021/ja311848e.
[23] R.B. Anderson, R.A. Friedel, H.H. Storch, Fischer-Tropsch Reaction Mechanism Involving Stepwise Growth of Carbon Chain, J. Chem. Phys. 19 (1951) 313. doi:10.1063/1.1748201.
[24] H. Schulz, Short history and present trends of Fischer–Tropsch synthesis, Appl. Catal. Gen. 186 (1999) 3–12.
[25] R.A. van Santen, I.M. Ciobîcă, E. van Steen, M.M. Ghouri, Mechanistic Issues in Fischer–Tropsch Catalysis, in: Adv. Catal., Elsevier, 2011: pp. 127–187. http://linkinghub.elsevier.com/retrieve/pii/B9780123877727000034 (accessed July 15, 2015).
[26] R.A. van Santen, A.J. Markvoort, I.A.W. Filot, M.M. Ghouri, E.J.M. Hensen, Mechanism and microkinetics of the Fischer–Tropsch reaction, Phys. Chem. Chem. Phys. 15 (2013) 17038. doi:10.1039/c3cp52506f.
[27] F. Fischer, H. Tropsch, Synthesis of Petroleum from Gasification Products of Coal a t Normal Pressure, Brennst.-Chem. 7 (1926) 97–116.
[28] H.H. Storch, N. Golumbic, R.B. Anderson, The Fischer–Tropsch and Related Syntheses, Wiley, New York, 1951.
[29] A.T. Bell, Catalytic Synthesis of Hydrocarbons over Group VIII Metals. A Discussion of the Reaction Mechanism, Catal. Rev. 23 (1981) 203–232. doi:10.1080/03602458108068076.
[30] A. Erdohelyi, F. Solymosi, Effects of the support on the adsorption and dissociation of CO and on the reactivity of surface carbon on Rh catalysts, J. Catal. 84 (1983) 446–460. doi:10.1016/0021-9517(83)90015-5.
[31] V. Ponec, Active centres for synthesis gas reactions, Catal. Today. 12 (1992) 227–254. doi:10.1016/0920-5861(92)85043-L.
[32] M.E. Dry, Practical and theoretical aspects of the catalytic Fischer-Tropsch process, Appl. Catal. Gen. 138 (1996) 319–344. doi:10.1016/0926-860X(95)00306-1.

[33] A.A. Adesina, Hydrocarbon synthesis via Fischer-Tropsch reaction: travails and triumphs, Appl. Catal. Gen. 138 (1996) 345–367. doi:10.1016/0926-860X(95)00307-X.
[34] S.A. Eliason, C.H. Bartholomew, Reaction and deactivation kinetics for Fischer–Tropsch synthesis on unpromoted and potassium-promoted iron catalysts, Appl. Catal. Gen. 186 (1999) 229–243. doi:10.1016/S0926-860X(99)00146-5.
[35] B.H. Davis, Fischer–Tropsch Synthesis: Reaction mechanisms for iron catalysts, Catal. Today. 141 (2009) 25–33. doi:10.1016/j.cattod.2008.03.005.
[36] G.P. van der Laan, A.A.C.M. Beenackers, Intrinsic kinetics of the gas–solid Fischer–Tropsch and water gas shift reactions over a precipitated iron catalyst, Appl. Catal. Gen. 193 (2000) 39–53. doi:10.1016/S0926-860X(99)00412-3.
[37] S. Storsæter, D. Chen, A. Holmen, Microkinetic modelling of the formation of C1 and C2 products in the Fischer–Tropsch synthesis over cobalt catalysts, Surf. Sci. 600 (2006) 2051–2063. doi:10.1016/j.susc.2006.02.048.
[38] W.K. Hall, R.J. Kokes, P.H. Emmett, Mechanism studies of the Fischer-Tropsch synthesis: the incorporation of radioactive ethylene, propionaldehyde and propanol, J. Am. Chem. Soc. 82 (1960) 1027–1037.
[39] D.D. Hibbitts, B.T. Loveless, M. Neurock, E. Iglesia, Mechanistic Role of Water on the Rate and Selectivity of Fischer-Tropsch Synthesis on Ruthenium Catalysts, Angew. Chem. Int. Ed. 52 (2013) 12273–12278. doi:10.1002/anie.201304610.
[40] S. Shetty, R.A. van Santen, CO dissociation on Ru and Co surfaces: The initial step in the Fischer–Tropsch synthesis, Catal. Today. 171 (2011) 168–173. doi:10.1016/j.cattod.2011.04.006.
[41] R.C. Brady, R. Pettit, Mechanism of the Fischer-Tropsch reaction. The chain propagation step, J. Am. Chem. Soc. 103 (1981) 1287–1289. doi:10.1021/ja00395a081.
[42] P.J. Flory, Molecular Size Distribution in Linear Condensation Polymers1, J. Am. Chem. Soc. 58 (1936) 1877–1885. doi:10.1021/ja01301a016.
[43] G.V. Schulz, Phys. Chem. B. 43 (1939) 25.
[44] G. Henrici-Olivé, S. Olive, The Fischer-Tropsch Synthesis: Molecular Weight Distribution of Primary Products and Reaction Mechanism, Angew. Chem. Int. Ed. Engl. 15 (1976) 136–141.
[45] H. Schulz, E. vein Steen, M. Claeys, Selectivity and mechanism of Fischer-Tropsch synthesis with iron and cobalt catalysts, in: H.E.C.-H. and R.F. Howe (Ed.), Stud. Surf. Sci. Catal., Elsevier, 1994: pp. 455–460. doi:10.1016/S0167-2991(08)63911-7.
[46] J. Li, X. Zhan, Y. Zhang, G. Jacobs, T. Das, B.H. Davis, Fischer–Tropsch synthesis: effect of water on the deactivation of Pt promoted Co/Al2O3 catalysts, Appl. Catal. Gen. 228 (2002) 203–212. doi:10.1016/S0926-860X(01)00977-2.
[47] M. Claeys, E. van Steen, On the effect of water during Fischer–Tropsch synthesis with a ruthenium catalyst, Catal. Today. 71 (2002) 419–427. doi:10.1016/S0920-5861(01)00469-2.
[48] A.M. Hilmen, D. Schanke, K.F. Hanssen, A. Holmen, Study of the effect of water on alumina supported cobalt Fischer–Tropsch catalysts, Appl. Catal. Gen. 186 (1999) 169–188. doi:10.1016/S0926-860X(99)00171-4.

[49] I.C. Yates, C.N. Satterfield, Intrinsic kinetics of the Fischer-Tropsch synthesis on a cobalt catalyst, Energy Fuels. 5 (1991) 168–173. doi:10.1021/ef00025a029.
[50] E. Iglesia, Design, synthesis, and use of cobalt-based Fischer-Tropsch synthesis catalysts, Appl. Catal. Gen. 161 (1997) 59–78. doi:10.1016/S0926-860X(97)00186-5.
[51] C. Xiao, Z. Cai, T. Wang, Y. Kou, N. Yan, Aqueous-Phase Fischer–Tropsch Synthesis with a Ruthenium Nanocluster Catalyst, Angew. Chem. 120 (2008) 758–761. doi:10.1002/ange.200703481.
[52] D. Shi, J.A. Faria Albanese, T.N. Pham, D.E. Resasco, Enhanced Activity and Selectivity of Fischer-Tropsch Synthesis Catalysts in Water/Oil Emulsions, ACS Catal. (2014). http://pubs.acs.org/doi/abs/10.1021/cs500040n (accessed January 12, 2015).
[53] D. Shi, J.A. Faria, A.A. Rownaghi, R.L. Huhnke, D.E. Resasco, Fischer–Tropsch Synthesis Catalyzed by Solid Nanoparticles at the Water/Oil Interface in an Emulsion System, Energy Fuels. 27 (2013) 6118–6124. doi:10.1021/ef401198m.
[54] B.H. Davis, Overview of reactors for liquid phase Fischer–Tropsch synthesis, Catal. Today. 71 (2002) 249–300. doi:10.1016/S0920-5861(01)00455-2.
[55] M.A. Vannice, The Catalytic Synthesis of Hydrocarbons from Carbon Monoxide and Hydrogen, Catal. Rev. 14 (1976) 153–191. doi:10.1080/03602457608073410.
[56] C.A. Mims, L.E. McCandlish, Evidence for rapid chain growth in the Fischer-Tropsch synthesis over Iron and Cobalt catalysts, J. Phys. Chem. 91 (1987) 929–937.
[57] M.S.P. Shaffer, X. Fan, A.H. Windle, Dispersion and packing of carbon nanotubes, Carbon. 36 (1998) 1603–1612. doi:10.1016/S0008-6223(98)00130-4.
[58] K. Esumi, M. Ishigami, A. Nakajima, K. Sawada, H. Honda, Chemical treatment of carbon nanotubes, Carbon. 34 (1996) 279–281. doi:10.1016/0008-6223(96)83349-5.
[59] C. Bower, A. Kleinhammes, Y. Wu, O. Zhou, Intercalation and partial exfoliation of single-walled carbon nanotubes by nitric acid, Chem. Phys. Lett. 288 (1998) 481–486. doi:10.1016/S0009-2614(98)00278-4.
[60] N.M. Briggs, J.S. Weston, B. Li, D. Venkataramani, C.P. Aichele, J.H. Harwell, S.P. Crossley, Multiwalled Carbon Nanotubes at the Interface of Pickering Emulsions, Langmuir. 31 (2015) 13077–13084. doi:10.1021/acs.langmuir.5b03189.
[61] N. Briggs, A.K.Y. Raman, L. Barrett, C. Brown, B. Li, D. Leavitt, C.P. Aichele, S. Crossley, Stable pickering emulsions using multi-walled carbon nanotubes of varying wettability, Colloids Surf. Physicochem. Eng. Asp. 537 (2018) 227–235. doi:10.1016/j.colsurfa.2017.10.010.
[62] B.E. Poling, J.M. Prausnitz, J.P. O'Connell, The properties of gases and liquids, McGraw-Hill, 2001.
[63] R.S. Albal, Y.T. Shah, N.L. Carr, A.T. Bell, Mass transfer coefficients and solubilities for hydrogen and carbon monoxide under Fischer-Tropsch conditions, Chem. Eng. Sci. 39 (1984) 905–907. doi:10.1016/0009-2509(84)85060-5.
[64] C.S. Kellner, A.T. Bell, Infrared studies of carbon monoxide hydrogenation over alumina-supported ruthenium, J. Catal. 71 (1981) 296–307. doi:10.1016/0021-9517(81)90232-3.

[65] X. Liu, W. Linghu, X. Li, K. Asami, K. Fujimoto, Effects of solvent on Fischer–Tropsch synthesis, Appl. Catal. Gen. 303 (2006) 251–257. doi:10.1016/j.apcata.2006.02.009.
[66] C.N. Satterfield, H.G. Stenger, Effect of liquid composition on the slurry Fischer-Tropsch synthesis. 1. Rate of reaction, Ind. Eng. Chem. Process Des. Dev. 24 (1985) 407–411. doi:10.1021/i200029a032.
[67] J. Liu, D. Hibbitts, E. Iglesia, Dense CO Adlayers as Enablers of CO Hydrogenation Turnovers on Ru Surfaces, J. Am. Chem. Soc. 139 (2017) 11789–11802. doi:10.1021/jacs.7b04606.
[68] D. Hibbitts, E. Dybeck, T. Lawlor, M. Neurock, E. Iglesia, Preferential activation of CO near hydrocarbon chains during Fischer–Tropsch synthesis on Ru, J. Catal. 337 (2016) 91–101. doi:10.1016/j.jcat.2016.01.010.
[69] Z. Zhao, Kinetics and Solvent Effects on Supported Metal Catalysts for Biomass Conversion, University of Oklahoma, 2018.
[70] S.G. Shetty, I.M. Ciobîcă, E.J.M. Hensen, R.A. van Santen, Site regeneration in the Fischer–Tropsch synthesis reaction: a synchronized CO dissociation and C–C coupling pathway, Chem. Commun. 47 (2011) 9822. doi:10.1039/c1cc11499a.
[71] A.J. Markvoort, R.A. van Santen, P.A.J. Hilbers, E.J.M. Hensen, Kinetics of the Fischer-Tropsch Reaction, Angew. Chem. Int. Ed. 51 (2012) 9015–9019. doi:10.1002/anie.201203282.
[72] J.M.G. Carballo, E. Finocchio, S. García-Rodriguez, M. Ojeda, J.L.G. Fierro, G. Busca, S. Rojas, Insights into the deactivation and reactivation of Ru/TiO2 during Fischer–Tropsch synthesis, Catal. Today. 214 (2013) 2–11. doi:10.1016/j.cattod.2012.09.018.
[73] F. Anaya, D.E. Resasco, unpublished work, (n.d.).
[74] R. Singh, P.K. Dutta, Use of surface-modified zeolite Y for extraction of metal ions from aqueous to organic phase, Microporous Mesoporous Mater. 32 (1999) 29–35. doi:10.1016/S1387-1811(99)00085-2.
[75] P.A. Zapata, J. Faria, M.P. Ruiz, R.E. Jentoft, D.E. Resasco, Hydrophobic Zeolites for Biofuel Upgrading Reactions at the Liquid–Liquid Interface in Water/Oil Emulsions, J. Am. Chem. Soc. 134 (2012) 8570–8578. doi:10.1021/ja3015082.
[76] P.A. Zapata, Y. Huang, M.A. Gonzalez-Borja, D.E. Resasco, Silylated hydrophobic zeolites with enhanced tolerance to hot liquid water, J. Catal. 308 (2013) 82–97. doi:10.1016/j.jcat.2013.05.024.
[77] R.A. Van Santen, Complementary Structure Sensitive and Insensitive Catalytic Relationships, Acc. Chem. Res. 42 (2009) 57–66. doi:10.1021/ar800022m.
[78] X.-Q. Zhang, R.A. van Santen, E.J.M. Hensen, Carbon-Induced Surface Transformations of Cobalt, ACS Catal. 5 (2015) 596–601. doi:10.1021/cs501484c.
[79] C.S. Kellner, A.T. Bell, Effects of dispersion on the activity and selectivity of alumina-supported ruthenium catalysts for carbon monoxide hydrogenation, J. Catal. 75 (1982) 251–261.
[80] J. Kang, S. Zhang, Q. Zhang, Y. Wang, Ruthenium Nanoparticles Supported on Carbon Nanotubes as Efficient Catalysts for Selective Conversion of Synthesis Gas to Diesel Fuel, Angew. Chem. 121 (2009) 2603–2606. doi:10.1002/ange.200805715.

[81] X.-Y. Quek, R. Pestman, R.A. van Santen, E.J.M. Hensen, Structure sensitivity in the ruthenium nanoparticle catalyzed aqueous-phase Fischer–Tropsch reaction, Catal Sci Technol. 4 (2014) 3510–3523. doi:10.1039/C4CY00709C.
[82] J.N. Kuhn, C.-K. Tsung, W. Huang, G.A. Somorjai, Effect of organic capping layers over monodisperse platinum nanoparticles upon activity for ethylene hydrogenation and carbon monoxide oxidation, J. Catal. 265 (2009) 209–215. doi:10.1016/j.jcat.2009.05.001.
[83] D.E. Resasco, G.L. Haller, A model of metal-oxide support interaction for Rh on TiO2, J. Catal. 82 (1983) 279–288. doi:10.1016/0021-9517(83)90194-X.
[84] D.S. Jordan, A.T. Bell, Influence of ethylene on the hydrogenation of carbon monoxide over ruthenium, J. Phys. Chem. 90 (1986) 4797–4805. doi:10.1021/j100411a018.
[85] W.-Z. Li, J.-X. Liu, J. Gu, W. Zhou, S. Yao, R. Si, Y. Guo, H.-Y. Su, C.-H. Yan, W.-X. Li, Y.-W. Zhang, D. Ma, Chemical Insights into the Design and Development of Face-centered cubic Ruthenium Catalysts for Fischer-Tropsch Synthesis, J. Am. Chem. Soc. (2017). doi:10.1021/jacs.6b10375.